© Copyright 2025
David Alonso Villalobos Chaves

From the ground to the skies: Ecomorphological predictors of diet and trophic diversification in small Neotropical mammals

David Alonso Villalobos Chaves

A dissertation

submitted in partial fulfillment of the

requirements for the degree of

Doctor of Philosophy

University of Washington

2025

Reading committee:

Sharlene E. Santana, Chair

George J. Kenagy

Greg Wilson

Program Authorized to Offer Degree:
Biology

University of Washington

Abstract

From the ground to the skies: Ecomorphological predictors of diet and trophic diversification in small Neotropical mammals

David Alonso Villalobos Chaves

Chair of the Supervisory Committee:
Sharlene E. Santana
Biology

During the evolution and dietary diversification of vertebrates, astounding morphological, physiological and behavioral adaptations evolved to procure and efficiently process their preferred food resources. These adaptations affect how well each species obtains energy, survives and reproduces in their environment, and are directly related to resource partitioning and diversification patterns.

This dissertation seeks to elucidate patterns of morphological and functional adaptations on small Neotropical mammals related to selective pressures exerted by their dietary ecology. I used myomorph rodents and bats as model taxa to develop my research, as these animals show exceptionally high taxonomic and ecological diversity, which makes them ideal for understanding ecomorphological trends in the evolution of feeding

structures. Through my three chapters, I tested the hypothesis that evolved differences in size and shape of morphological structures are directly associated with differences in the feeding ecology of the species. Moreover, by linking these adaptations to variations in performance among tasks of vital importance for energy acquisition during feeding (e.g., biting, chewing), I also explored how functional adaptations might have allowed subsequent functional dietary specialization on some taxa and, ultimately, trophic segregation among Neotropical mammal communities.

In chapter 1, I coupled data on functional mandibular measurements and dental topography metrics with dietary information under a phylogenetic framework to investigate the functional correlates of mandibular and molar diversity among Akodontine rodents. Here, both mandibular and dental morphologies seem to have evolved to facilitate the efficient processing of specific food items with unique mechanical properties (e.g., arthropod exoskeleton vs plant materials). Both mandibular and dental traits show strong dietary signals towards processing specific food resources, with herbivory and insectivory dietary regimes shaping the most extreme morphologies. Altogether, our study gives insight into the strong relationship between rodent's feeding structures and dietary ecology, highlighting the traits that are, potentially, under stronger selective forces and that might have facilitated the trophic diversification and specialization in the Akodontine tribe.

In chapter 2, I used morphological and performance traits to investigate the influence of feeding ecology on the form-function relationships of feeding structures in rodents, and explored the potential implications of these differences on morphological specialization and resource partitioning among sympatric members of a community in

Costa Rica. I found a strong dietary signal on multiple external, mandibular and dental traits, with shape differences being more extreme in specialized feeding ecologies. I also found multiple trade-offs between the morphology and performance of the feeding apparatus of these rodents, highlighting the compromise that usually is detected when extreme morphologies evolve. Our data give insight into form-function-performance relationships of rodent feeding structures and provide clues on potential mechanisms that have allowed trophic diversification among sympatric species.

In chapter 3, I investigated the functional relationship among size, shape and feeding performance in a community of Neotropical Free-tailed bats in Costa Rica. Specifically, we evaluated how the size of cranial structures and the shape of molar teeth correlate and influence food processing. We found strong connections of morphological and functional specialization with performance outcomes, highlighting mechanisms of trophic resource partitioning among members of the community. These, in turn, might be influenced by adaptations to the mechanical properties of different food resources. Altogether, our study successfully connected morphology and performance with dietary ecology, setting an example on how to couple these data to better understand ecological patterns and trade-offs of trophic specialization.

TABLE OF CONTENTS

LIST OF FIGURES

LIST OF TABLES

ACKNOWLEDGMENTS

You know who you all are. My heart is filled with love and gratitude towards you and all the support that I have had to finish this project. While writing this, I am thinking about you, about your love and care, about how important you are for me, about how much I love you and about how fortunate I am to have met you and to have you in my life. I would not be here without you, this research would not exist without you. Gracias desde el fondo de mi corazón.

DEDICATION

To love, connection, and all the people and things that give meaning to my life experience. My deepest gratitude will always be with you.

CHAPTER 1

Chew on this! — Functional correlates of mandibulo-dental morphology and the trophic diversification of akodontine rodents

Drawing of a Brazilian shrew mouse, *Blarinomys breviceps*.
Art based on a photo by R. Stumpp.

1.1 ABSTRACT

The shape and size of the vertebrate feeding apparatus is highly informative about what an animal is adapted to eat. In mammals, this dietary signal is particularly strong in the mandible and the molars, as the main function of these structures is to acquire and process food items for further digestion. This ecomorphological relationship has been key to understanding the diversification of multiple clades, including highly taxonomic and ecologically diverse lineages such as bats and rodents. Here, we quantified functional traits of the mandible and the molars of a speciose clade of rodents (tribe Akodontini, Subfamily Sigmodontinae) in order to elucidate functional correlates between the morphological diversity and the trophic diversification of these Neotropical rodents. We found that diet has had a strong influence on the shape of the mandible and the molars, with extreme dietary regimes showing the most specialized morphologies. Specifically, herbivores and insectivores species show contrasting jaw morphologies, with shapes that functionally differ in the amount of area available for masticatory muscle attachment. Most molar topography metrics, on the other hand, seem to converge in herbivores and insectivores, suggesting functional advantages of molars with sharp and numerous breakage sites for processing n different food items. Finally, omnivorous species show a high variation in the measured traits, which suggests potential advantages of generalized morphologies for processing food items with multiple and contrasting mechanical properties. Overall, our data revealed morpho-functional adaptations and potential trade-offs in the evolution of rodent feeding structures, highlighting mechanisms that might have facilitated trophic segregation and specialization in Akodontine rodents.

Key words: diet, jaw, molars, mechanical advantage, resource partitioning.

1.2 INTRODUCTION

In ecomorphological studies, trophic ecology has been frequently highlighted as one of the main drivers of morphological evolution of feeding structures (Martin & Wainwright 2011; Dumont et al., 2012). Within the skull of vertebrates, for example, structures such as the mandible and teeth have been strongly correlated with diet, as these parts of the feeding apparatus are mostly responsible for the controlled movements to acquire and carefully process the food items for further digestion.

The mandible, on one side, serves as an insertion area for the muscles that open and close the jaw during biting and mastication (Greaves 2012), therefore, it is expected that selective forces have been shaping mandibular forms to morphologies adapted to generate the precise forces and speeds (e.g., mechanical advantage — Grossnickle 2020 , Navalón et al., 2019; Westneat 2003) necessary to efficiently process food items that can vary in a myriad ways (e.g., size, shape, hardness, etc). On the other hand, food-tooth interaction has been proposed to be one of the major drivers of tooth morphology, and especially of molar topography (Lucas 1979; Bergqvist 2002), as natural selection will favor the evolution of shapes that are efficient at processing food items of specific mechanical properties (e.g., hard vs soft objects—Spears & Crompton 1996; Lucas 2004; Berthaume 2016a). Altogether, understanding the functional relationship between feeding structures and dietary ecology is utterly crucial as these interactions underlie ecological and evolutionary processes including dietary niche partitioning and trophic radiations (Lucas 1979; Yamaoka 1983; among others), which are ultimately linked to increases in

phenotypic and functional diversity (Hulsey & Wainwright 2002; Konow et al., 2008; Mehta 2009).

In highly diverse groups such as bats, mandibulo-dental disparity has been directly linked to invasion of new diet-affiliated adaptive zones (Dumont et al., 2012; Grossnickle 2023) and to variations in feeding performance among coexisting species (Santana et al., 2011; Villalobos-Chaves & Santana 2021). Moreover, in other highly diverse taxa such as rodents, where members have independently and repeatedly evolved different dietary specializations (Evans et al., 2007), mandibular and molar disparity have been hypothesized as the major drivers of phenotypic diversity (Martin et al., 2016; Maestri et al., 2017; Grossnickle 2020; Missagia et al., 2020), by facilitating diversification through food niche partitioning processes, for example, functional variation that is translated into performance differences (Bezzobs & Sanson 1997). However, among rodent lineages, the morphofunctional relationships between mandibulo-dental shape and dietary ecology have been mostly explored in murine rodents (Muridae) (Misonne 1969; Martin et al., 2016; Evans et al., 2007), with a few insights into the mandibular morphology of other lineages (Evans et al., 2007; Maestri et al., 2017; Missagia et al. 2020).

Here, we investigated the relationship between dietary ecology and the morphological diversification of mandibular and dental traits among a representative sample of Neotropical Akodontine rodents (Tribe Akodontini — Cricetidae: Sigmodontinae). The Akodontini tribe represents a taxonomically diverse (88 species — Paradiñas et al., 2017; Steppan & Schenk 2017) group of Neotropical sigmodontine rodents that are characterized by a successful radiation in South America (D'Elía &

Pardiñas 2015; Maestri et al., 2017). Akodontini rodents show a mesmerizing diversity of life history strategies, with species morphotypes that are linked to contrasting ecological niches (e.g., substrate and diet — Hershkovitz 1966; Reig 1980; D'Elía & Pardiñas 2015; Missagia et al., 2020; Pardiñas et al., 2020). Morphological adaptations in akodontines seem to have evolved independently of phylogenetic relatedness among clades, and the presence of several lineages in Akodontini that seem to be specialized on specific food resources (e.g., insects, vegetation) makes this group of rodents ideal to investigate ecomorphological patterns and functional tradeoffs of specialized morphologies (Missagia et al., 2020).

Specifically, we tested the hypothesis that evolved differences in mandibular morphology and molar topography reflect functional dietary specializations towards food resources with different mechanical properties. As the variation in shape, size, function and performance of mammalian feeding structures are strongly tied to the challenges of processing specific food items, we predicted that species with more specialized diets (e.g., high plant matter content or high animal matter content) evolved more extreme morphologies due to the advantages of those shapes for processing foods with specific mechanical properties. Conversely, due to the potential trade-offs of having generalized morphologies, we predicted that omnivorous species will show less extreme morphologies that allow them to process food items of highly variable material properties (e.g., stiff and pliant materials).

1. 3 MATERIALS AND METHODS

1.3.1 Taxonomic sample & data collection

We collected micro-computed tomography (µCT) scans of the skull of voucher specimens belonging to the Neotropical rodent tribe Akodontine (Supporting information file 1 — Table S1) using a Skyscan 1172 µCT Scanner (Bruker MicroCT, Belgium). All scans were performed at an 13.03 um image voxel size while keeping other scanning parameters consistent (Supporting information file 1 — Table S1). After scanning, we used NRecon (Microphotonics) to convert CT shadow images into image stacks ('slices'), which we imported into Mimics v. 22.0 (Materialise, Leuven, Belgium) to produce 3D surface (*.stl) files (i.e., mesh models). Raw stl files were then imported into Geomagic Studio v. 2019 (Geomagic Inc., Research Triangle Park, NC, USA) for further processing and isolation of the structures of interest for the analysis.

Voucher specimens were sourced from the following museums: American Museum of Natural History, New York (AMNH), Burke Museum of Natural History and Culture, University of Washington, Seattle (UWBM), Field Museum of Natural History, Chicago (FMNH), Natural History Museum of Los Angeles County, Los Angeles (LACM), Museum of Vertebrate Zoology, University of California, Berkeley (MVZ), National Museum of Natural History (NMNH), and the Smithsonian National Museum of Natural History, Washington D.C. (USNM). Our unprocessed data set comprises 144 specimens from a phylogenetically diverse sample with 45 species spanning 15 genera (Supporting information file 1 — Table S1).

1.3.2 Morphological data

Mandibular traits —We collected 11 linear measurements and one angle (Fig.1.1; Supplementary information file 1 — Table S2) from scaled, hemi-mandible (lateral view) pictures that were obtained using our 3D mesh models and the software 3D Slicer (Fedorov et al., 2012; http://www.slicer.org). Scaled pictures were taken while only using the right hemi-mandible, both from the lingual and the labial views (see Fig. 1.1). Measurements were obtained with the help of ImageJ (National Institutes of Health, Bethesda, MD, USA).

To control for size variation among the mandibular measurements, we transformed raw measurements to log-shape ratios (Mosimann 1970) by dividing them by the geometric mean of all 11 linear measurements (i.e., a proxy for jaw size). The resulting ratio was then log10-transformed for further analysis (Claude 2013; Price et al. 2019). As measurement 12 (i.e., the JAPr angle — Grossnickle 2020) is not a linear measurement, we only applied a log10-transformation to this metric. This size correction method has the advantage of preserving the variation related with allometry (Grossnickle 2020), hence the results presented here are mainly based using log-shape ratios.

In addition to log-shape ratios, we employed an alternative size correction method to further account for morphological variation associated with both size and allometry (Mosimann 1970; Grossnickle 2020) while incorporating the phylogenetic relationships and phylogenetic signal into the size correction process (Revell 2009; Price et al. 2019). Here, we obtained the residuals by regressing log10- transformed measurements against log10-transformed jaw length (measurement 2) using phylogenetic generalized least squares (PGLS) regressions (Martins & Hansen 1997) via the caper package (Orme et al.,

2023) in the R software (R Core Team 2024). For this method, the JAPr angle was equally treated as the other linear measurements, and the residuals from each regression were saved and then used in all subsequent comparative analyses (see Table S1.4).

Dental traits — To collect data on molar topography, we first visually filtered our 3D mesh models based on tooth wear. This was done because wear can affect topography metrics. Out of 5 tooth wear categories (i.e., from 4 = highly worn molars to 0 = unworn molars), we only analyzed mesh models with values between 0 and 3 (Supplementary information file 1 — Table S3).

Next, we isolated the entire tooth crown (i.e., above the enameled cervix) of the selected mandibular right tooth rows (i.e., molars) (Boyer 2008) and oriented them following Pampush et al. (2016), that is, with the occlusal plane parallel to the X-axis (which pointed anteriorly), the Y-axis perpendicular to the occlusal plane, and the Z-axis pointing in the lingual direction (see Fig. S3.2 of Chapter 3). Curated and oriented models were then simplified (25,000 faces), smoothed (20 smoothing iterations, lambda of 0.6) and saved (as PLY file) with the help of Avizo Lite 9.2.0 (FEI Visualization Sciences Group, Berlin, Germany) for further calculation of dental topography metrics. For the latter, we used the package molaR (Pampush et al., 2023) and its incorporated function, molaR_Batch, to collect data on the following metrics: the Dirichlet normal energy (hereafter: DNE), the convex portion of the Dirichlet normal energy (hereafter: Convex DNE), the concave portion of the Dirichlet normal energy (hereafter: Concave DNE), the concave and the convex area, the 2D area, the Relief index (hereafter: RFI), the Orientation patch count rotated (hereafter: OPCR), the Orientation patch count

(hereafter: OPC), and the Slope (Pampush et al., 2016) (Supplementary information file 1 — Table S3 and Table S4).

For RFI calculations, we used an alpha value of 0.075, as this was the minimum value that allowed us to keep the subscript inside the bounds (see details in Pampush et al., 2016). We performed OPCR calculations with a minimum of 3 faces and 8 steps, with a step size of 5.62, to make these comparable with previous studies. Further comparative analyses were performed using only a subset of all dental topography metrics (see details in the data analysis section and Fig. 1.1), which were selected after conducting Spearman correlations to evaluate redundancy among the variables. As dental topography metrics are not influenced by size differences (Berthaume et al., 2020), no size correction is needed for these traits.

1.3.3 Dietary information

We gathered quantitative and qualitative dietary data for the Akodontine species used in this study through an intensive literature review (Supporting information file 2 — Table S5, Table S6, Table S7a and Table S7b) following a modified approach based on Barbero et al. (2021) and Verde Arregoitia & D'Elía (2021). Accordingly, rodent species were classified into (1) one quantitative, continuous, dietary scheme based on the available and/or estimated amount of plant material in their diet, and (2) one qualitative dietary scheme of three categories (i.e., insectivores, omnivores, and herbivores). We defined insectivores as species with diets consisting of 80–100% animal prey (or 0–20% plant material — n = 16), omnivores as 20–85% plant material (n = 28), and herbivores as 85–100% plant material (n = 1) (Supporting information file 2 — Table S8). Although

these categories were based on state of the art information available, any diet classification for a Neotropical rodent species is probably an oversimplification; proposed thresholds are based on previous studies of diet in mammals (Verde Arregoitia & D'Elía 2021; Grossnickle 2020; Barbero et al., 2023) and my own subjective criteria based on behavioral observations described for some species or genera.

1.3.4 Phylogenetic relationships

Taxonomic and genetic sampling — We included 44 ingroup taxa (i.e., Akodontine species), 26 species from sister subfamilies and tribes within Cricetidae, and one outgroup belonging to Muridae (i.e., *Rattus norvegicus*) (Supporting information file 3 — Table S9, Table S10 and Table S11) in our analyses. The expanded set of outgroup terminals was deliberately selected not only to robustly test the monophyly of Akodontini but to allow the incorporation of key fossil evidence in our divergence time analyses (see below). To maximize both taxonomic and molecular coverage while minimizing missing data in the alignment matrix, we sourced DNA sequence data from GeneBank, prioritizing specimens with the greatest number of sequenced fragments from a curated list of nine loci commonly represented across our taxonomic sample (Supporting information file 3 — Table S11). Selection of specimens also considered geographic origin, with preference given to individuals collected near each species' type locality, to ensure taxonomic accuracy. In most cases, species were represented by multiple mitochondrial and nuclear loci. The final alignments included 51 sequences for *Acp5*, 71 for *Cytb*, 37 for *DMP1*, 56 for *GHR*, 60 for *Rbp3*, 58 for *RAG1*, 18 for *THY*, 33 for *COI*, and 24 for a long mitochondrial segment encompassing *tRNA-Thr*, *tRNA-Pro*, the control

region (D-loop), *tRNA-Phe*, *12S*, and *tRNA-Val* (hereafter referred to as the "Thr-Val block"; see Table S1.1 for details on coverage and variability). The taxonomy of all included species and subspecies was individually verified against available synonym lists (e.g., Wilson & Reeder, 2005; Paradiñas et al., 2017), the accepted species in the IUCN Red List (2024), and the geographic provenance of voucher specimens.

Phylogenetic Inference and Molecular Dating — To construct individual alignments, we used the MAFFT v.7 algorithm (Katoh & Standley 2013) in the Geneious v.9.1.8 platform (Biomatters, www.geneious.com). The alignments were performed with the 200 PAM (k=2) scoring matrix, a gap opening cost of 1.53, and an offset of 0.123. The 'auto' function was used to select the most appropriate alignment strategy based on sequence length and complexity. We concatenated the resulting alignments using a custom Python script that leveraged the Nexus module from Biopython's Bio.Nexus library. The resulting concatenated dataset contained 11,873 aligned characters, with 6,707 conserved sites, 4,910 variable sites, 3,161 parsimony-informative characters, and 1,670 singletons. Summary statistics for individual mitochondrial and nuclear loci are presented in Table S1.1.

To define an appropriate calibration strategy for divergence dating, we first generated maximum likelihood trees from the concatenated dataset using IQ-TREE 2 (Minh et al., 2020). We applied ModelFinder (Kalyaanamoorthy et al., 2017) to determine the most appropriate models of nucleotide substitution and partitioning schemes. We analyzed introns (if present) and exons from the same gene as separate data blocks. Once optimal partitioning and model schemes were identified, we conducted

maximum likelihood searches and evaluated clade support using 1,000 ultrafast bootstrap replicates (Hoang et al., 2018) and SH-like approximate likelihood ratio tests (Guindon et al., 2010). Each analysis was repeated ten times to ensure stability, and the top-scoring tree was retained. All resulting trees are included in the (Supplemental Material File 00). We estimated divergence times within a Bayesian framework using BEAST v1. 10.4 (Suchard et al. 2018), incorporating sequence data from all loci previously analyzed in IQ-TREE 2. Fossil calibrations were implemented as lognormal prior distributions, based on fossils 3–9 and 14 from Steppan & Schenk (2017: Table 1), which are grounded in the fossil age justifications detailed by Shenk et al. (2013) and references therein. Topological constraints (Fig. S1.1) were applied to enable the placement of calibration points using the best maximum likelihood topology generated with IQ-TREE2 as a reference. We applied the GTR+Γ model for nucleotide substitution and selected a birth–death speciation model as the tree prior, suitable for datasets with incomplete and uneven taxon sampling. To ensure robustness, three independent Markov chain Monte Carlo (MCMC) analyses were run, each initialized with a unique random seed. Each run was conducted for 900 million generations, with sampling every 90,000 steps. We evaluated convergence and effective sample sizes (ESS ≥ 200) using Tracer v1.7.2 (Rambaut et al., 2018). The first 10% of samples from each run were discarded as burn-in, and the remaining samples were combined using LogCombiner v1.10 (Drummond & Rambaut 2007). A summary tree with median node heights was generated using TreeAnnotator v1.10 (Drummond & Rambaut 2007). The XML input file, all BEAST outputs, and the resulting maximum clade credibility tree are provided in the Supplemental Material File 01.

1.3.5 Data analysis

We first mapped the dietary, dental and mandibular data on the reconstructed Akodontine phylogeny to visualize their variation across the tree's topology (Fig. 1.2, Fig. S1.5 and Fig. S1.6). In addition, we estimated the phylogenetic signal for the dental and mandibular traits by calculating Blomberg's K (Blomberg et al., 2003) and comparing our estimates to a null distribution (no signal) with the help of p-values obtained from 9999 random permutations of the tip values (Table S1.1 — Blomberg et al., 2003; Adams 2014). Both analyses were performed using the 'contMap' and the 'phylosig' function, respectively, from the 'phytools' package (Revell 2024). Next, we performed Principal Component Analysis (hereafter: PCA) on species' averages for the mandibular traits and for the dental topography metrics using the 'prcomp' function from the 'stats' package (R Core Team 2024). The first two components of each PCA, in addition to the reconstructed phylogeny of Akodontine, were then employed to generate a morphospace distribution of each dataset on a phylomorphospace (Fig. 1.3 and Fig. 1.4) by using the 'phytools' and 'ggpubr' packages (Kassambara 2023; Revell 2024).

Finally, following these exploratory analyses, and because means of traits for species can not be considered as statistically independent data points due to differing amounts of shared phylogenetic history (Felsenstein 1985), we then used the reconstructed phylogeny of Akodontine to explore the relationship between dietary ecology and morphological traits under a phylogenetic context. We performed phylogenetic generalized least squares regressions (hereafter: PGLS — Martins & Hansen 1997) via the caper package (Orme et al., 2023) for R software (R Core Team 2024) using the dietary information (i.e., arcsine-transformed proportion of dietary plant

material), the dental topography metrics, and the size-corrected jaw measurements. We examined univariate traits rather than performing analyses with multiple predictor variables because identifying specific morphological correlates of diet is especially valuable to functional and evolutionary analyses, and paleontological studies (Grossnickle 2020). Altogether, we performed three different PGLS regression analyses using (1) the log-shape ratios of all the data available (i.e., all the species and dietary groups), (2) the log-shape ratios removing *Kunsia tomentosus* (i.e., the only herbivore in the data set) to investigate the effects of this outlier, and (3) the residuals from the PGLS regressions using jaw length to control for size (see Mandibular traits section).

1.4 RESULTS

We found that, among both the dental and mandibular trait datasets, several dental topography metrics as well as mandibular measurements are significantly associated with diet (Table 1.1, Table S1.4, Fig. 1.3 and Fig. 1.4). Graphical representation of the best performing metrics can be found in Fig. 1.3, Fig. 1.4, Fig. S1.3 and Fig. S1.4.

The PCA of mandibular traits supported traits such as the jaw length and the JAPr angle as the main drivers of the separation along PC1 (46.43% of variance explained), and traits such as the coronoid process (CPr) and joint elevation as the main contributors of the variation in PC2 (17.84% of variance explained) (Fig. 1.3 and Table S1.3). Here, patterns on mandibular morphology indicate that insectivore species have longer jaws and smaller JAPr angles than omnivores and herbivores, respectively (Fig. 1.3), whereas traits such as the coronoid process and joint elevation show high variation among dietary groups (Fig. 1.3).

In the PCA based on dental (molar) topography metrics, the first two axes account for 92.18% of the variation (Fig. 1.4, Table S1.3) with variables such as the convex portion of the DNE and the OPC as the main drivers separating dietary ecologies in PC1, and the RFI as the main trait influencing PC2 (Table S1.3). In this morphospace, herbivorous and insectivorous species tend to have molars with more complex and sharper surfaces (ie., high Convex DNE and OPC) but lower occlusal areas (i.e., low RFI). Omnivores, on the other hand, show molars with low convex DNE and OPC, in addition to intermediate RFI values (Table 1.1, Fig. 1.4 and Fig. S1.4). Specifically, it seems most of the variation is being driven by the herbivore *K. tomentosus*, in addition to a few species of insect-eating Akodontine, which are located towards the more positive values of the PC1 (Fig. 1.4).

When both data sets (i.e., mandibular and dental) are included in the PCA , we find more morphological differentiation among dietary groups (as seen in Fig. S1.2). In this analysis, both PC axes show a clear separation among dietary categories, mainly with mandible traits (35.68% of variance explained) and dental traits (18.15% of variance explained) driving the variation in PC1 and PC2, respectively (Fig. S1.2). Correspondingly, this mandibulo-dental PCA indicates that herbivore species show larger JAPr angles and more complex and sharper molars, but reduced occlusal area and shorter jaws than insectivores and omnivores, respectively (Fig. S1.2).

Furthermore, the results from the PGLS regression analyses indicate that the best performing metrics associated with diet correspond to dental traits such as the concave portion of the DNE and the RFI (Table 1.1), and mandibular measurements related to the overall length of the jaw (i.e., the jaw length, the m1 to posterior jaw length and the jaw

joint to m1 length), in addition to the corpus depth, the JAPr ventral length and the JAPr angle (Table 1.1, Fig. 1.1 and Fig. S1.3). However, when the herbivore species (i.e., *K. tomentosus*) is excluded, our analysis highlights metrics such as the convex portion of the DNE, the corpus depth and the JAPr angle as the best performing traits associated with dietary differences (Table S1.5). Finally, by using regression residuals from size-corrected mandibular traits, the most predictive traits of the PGLS are the joint elevation and the JAPr angle (Table S1.4). Thus, in summary, the JAPr angle and DNE metrics are the most consistent predictors of dietary categories in our dataset across all the regressions performed.

1.5 DISCUSSION

Our results shed light on the influence of diet on the mandible and tooth morphology of rodents, whose masticatory features and jaw movements are unique among mammals (Cox & Baverstock 2016; Grossnickle 2020). In Akodontine rodents, we find that diet is strongly associated with morphological features such as the size of the angular process, thus predictors such as the JAPr distance measured to the ventral-most margin (measurement 11) and the JAPr angle (measurement 12) account for much of the differences between insectivores and herbivores (Table 1.1, Fig. 1.3, Fig. S1.2, Fig. S1.3), and between insectivores and omnivores (Table S1.4).

This positive correlation between JAPr metrics and the increase in plant matter in the rodents' diet (Fig. 1.3 and Fig. S1.3) is consistent with findings in other herbivorous rodents and other plant-consuming mammals (Maynard Smith & Savage 1959; Grossnickle & Polly 2013; Verde Arregoitia et al., 2017; Grossnickle 2020). Functionally,

larger JAPr distances and angles could provide larger attachment areas for two important masticatory muscles (i.e., the superficial masseter and the medial pterygoid) that facilitate fine control of transverse grinding occlusion movements (Maynard Smith & Savage 1959; Radinsky 1985; Crompton et al., 2010; Grossnickle 2017) and generate force vectors during orthal jaw closure (i.e., jaw pitch) (Maynard Smith & Savage 1959). In turn, enlarged (or depressed) angular processes are biomechanically advantageous for processing materials with more fiber contents, as these require more efficient grinding movements to be comminuted and then digested (Sanson 2006).

Among other mandibular traits that are strong predictors of diet in akodontine rodents, our analysis detected the length of the mandible (measurement 2), and more strongly, the length of the posterior portion of the mandible (measurement 3 and 8, Table 1.1. Fig. 1.3 and Fig. S1.3). These results indicate that insectivores possess, overall, more elongated mandibles, and that the jaw joint is relatively closer to the m1 in herbivores than in other dietary groups (Fig. 1.3 and Fig. S1.2). Previous studies have associated similar patterns to the mechanical advantage of the jaw, and interpreted them as adaptations to processing foods with contrasting material properties (Grossnickle 2020; Missagia et al., 2020). For example, as arthropod exoskeletons might offer, overall, less resistance than plant matter to being punctured by the incisors and grinded by the molars, the elongation of the mandible in Akodontine, could represent a trade-off between bite force and jaw closing speed (Samuels 2009; Fabre et al., 2017). That is, a longer mandible reduces the mechanical advantage of the main jaw adductor muscles (i.e., deep and superficial masseter and temporalis muscles) due to shorter in-levers and longer out-levers (Samuel 2009; Maestri et al., 2016; Missagia et al., 2020), while conferring a

faster closing speed (Samuels 2009; Fabre et al., 2017). Enhanced biting and chewing speed might be more advantageous than a high bite force in insectivorous species, as they might hunt for live prey that can escape if not secured rapidly (Fabre et al., 2017). On the other hand, a greater mechanical advantage due to shorter jaws (i.e., shorter outlever that results in higher bite forces) may be necessary and selected for in species that include more plant matter in their diet, as this would help to efficiently chew tough plant material with their cheek teeth (Grossnickle 2020; Missagia et al., 2020). Finally, herbivorous and omnivorous species also show a larger jaw corpus depth (measurement 7), which could reflect the evolution of increased incisor size for gnawing on more challenging food items (e.g., harder foods — Radinsky 1968; Grossnickle 2020).

Although our log-shape ratio analysis indicates that several mandibular traits are strongly associated with dietary categories in Akodontine rodents (Table 1.1), the strength of some of these associations is lost when the alternative size-correction method that involves PGLS regression residuals is used (Table S1.5; see Methods), or when *K. tomentosus* (the only herbivore in the sample) is removed from the analysis (Table S1.4). This suggests that the correlations between jaw length measurements and diet are partially caused by the overall jaw size (i.e., the geometric mean), which tends to increase with greater herbivory (Grossnickle 2020). These patterns are probably driven by the fact that the residuals do not contain variation associated with allometric relationships between mandibular traits and jaw length, in addition to the mathematical consequence of employing the geometric mean of the jaw as the denominator in the log-shape ratio analysis (i.e., larger jaw size values will generate smaller ratios for measurements that do

not tend to increase allometrically and with greater plant matter consumption) (Grossnickle 2020).

Akodontine rodents have also developed a diverse array of molar topographies that exhibit strong functional relationships to diet (Fig. 1.4, Fig. S1.2, Fig. S1.4 and Fig. S1.6). For instance, our PGLS analyses revealed a significant influence of the convex and concave portion of the DNE, in addition to the RFI, for trophic differentiation (Table 1.1, Table S1.4 and Fig. S1.4). Morphospace separation, on the other hand, is driven by the convex portion of the DNE, the OPC and the RFI. Here, although our analysis highlights both components of the DNE as significant, the lack of a explicit functional hypothesis to explain concave DNE values (Pampush et al., 2022), and the fact that our results are highly influenced by the extreme morphology of *K. tomentosus* (Table 1.1 vs Table S1.4), make us preferentially focus on the analysis of the more functionally relevant part of the metric (the convex portion — Pampush et al., 2022).

Considering the the convex portion of DNE, our data reveal that the occlusal sharpness and breakage sites (see van der Glas et al., 1992) are higher in herbivores and insectivorous species, suggesting that –independent of the food items being processed– functionally similar pressures may lead to morphologies with similar dental topography values. High values on these metrics have been previously documented in other taxa (Winchester et al., 2014), arguing that in animals that routinely chew on fibrous leaves or insect exoskeletons, an increase in the availability and sharpness of shearing surfaces can improve the grinding efficiency of the molars (Winchester et al., 2014). Ultimately, these morphologies allow for better access to the cytosol of plant cells for more rapid enzymatic hydrolysis in the gut of plant tissue consumers (Sanson 2006) or a more

efficient breakdown of the insect cuticle and internal tissues/organs for further digestion and energy extraction in the insect consumers (Jeuniaux 1961). Importantly, and independently of the inclusion or exclusion of herbivores in our sample, our data show that insectivorous rodents have evolved, overall, sharper and more complex occlusal surfaces (i.e, high convex DNE and OPC) than omnivorous species (Fig. 1.4, Fig. S1.2 and Fig. S1.4). This result suggests that processing insect exoskeleton does require specialized molar topographies in rodents and that (as similarly observed for omnivorous species) the large interspecific variation detected among single metrics (Fig. S1.4) within guilds might indicate variations in the mechanical properties of the food items being processed by the molars (e.g., soft-bodied vs hard-bodied insects — Strait 1993). Similar patterns have also been observed in the mandible of insectivorous Akodontine rodents, with for example, species of *Oxymycterus* having greater mechanical advantages of the deep masseter due to the consumption of potentially larger prey items that require greater bite forces (Missagia et al., 2020). Deeper knowledge of the natural history of these species might eventually lead to better understanding of the dietary ecology of these rodents, and how it relates to the trade-offs involved in the evolution of more generalized or specialized morphologies.

Considering the similar trends in DNE and OPC described above for all the dietary groups, the low values of relief index detected for the herbivore *K. tomentosus* suggests an intriguing compromise among the quantity and sharpness of breakage sites and the occlusal area (Fig. 1.4 and Fig. S1.4). Future research on *K. tomentosus* is needed to validate or disprove any assumption about how their dietary ecology specifically relates to these findings. However, interpretations of RFI values on other taxa (Boyer

2008; Berthaume et al., 2020; Villalobos-Chaves & Santana 2021; López-Aguirre et al., 2022) suggest that herbivorous species with low relief index values (i.e., species with brachydont molars) are better adapted to feed on less abrasive vegetation (i.e., plant matter with less cellulose and phytoliths) that minimize tooth wear (Williams & Kay 2001). This could give us hints of the potential diet and mechanical properties of the food items that selectively shaped the extreme molar topography of this species. Lastly, insectivorous and omnivorous Akodontine rodents seem to have evolved relatively taller-crowned teeth with more surface area for their size (i.e., more hypsodont teeth) than species of their tribe with more herbivorous diets (i.e., at least in the case of *K. tomentosus* — Fig. 1.4, Fig. S1.4 and Fig. S1.6). From a mechanical standpoint, this pattern might reflect the mechanical challenges of processing insect exoskeleton, or a combination of food items with a moderate to high presence of structural carbohydrates, which might be more efficiently comminuted with taller crowned/cusped molars applying lower stresses distributed over larger contact areas (Strait 1993).

In mammal feeding ecomorphology, mandibular and dental shapes exhibit strong dietary signals that mostly follow well established trends related to the mechanical challenges of processing specific and/or preferred foods (e.g., insects, leaves, fruits, etc. — Berthaume 2016b; Evans & Pineda-Munoz 2018; Grossnickle 2020, among many others). Here, we explored both mandibulo-dental adaptations in the diverse tribe of Neotropical akodontine rodents, providing compelling evidence of the correlational relationships between dietary ecology (as the proportion of dietary plant material) and the morphology of distinct parts of the feeding apparatus. Because the rodent feeding apparatus and mechanics are exceptionally different to other mammal taxa, and rodents

are among the most taxonomically diverse clade of vertebrates in the world (Wilson et al., 2016), our data bestow unique evidence that highlights functional traits likely derived from selective dietary pressures. Finally, as simple dietary categories or percentages may not completely explain functional variation in morphology due to differential and overlapping material properties and mechanical demands of different food items (Lucas 1979; Strait 1993; Lucas & Teaford 1994; Strait 1997), future steps should be focused on the acquisition and use of quantitative dietary data(e.g., mechanical properties) and feeding behavior of the species, as these traits may allow us to fully understand the taxonomic and trophic diversification of Akodontine rodents.

1.6 ACKNOWLEDGMENTS

We are really grateful to all natural history museums curators, managers and staff for their willingness to share voucher specimens for this research. DVC was supported by endowments from the Mammalogy Department at the Burke Museum of Natural History and Culture, the Department of Biology (WRF-Hall Fellowship) and the Graduate School (Boeing International Fellowship) from the University of Washington.

1.7 DATA AVAILABILITY STATEMENT

Curated data used for the analysis and scripts are archived here. 3D models (i.e., stl or ply files) will be available upon request.

1.8 TABLES AND FIGURES

Table 1.1 Summary statistics for bivariate phylogenetic generalized least squares (PGLS) regressions, which examine the relationship between diet (as arcsine-transformed proportion of dietary plant material) and mandibulo-dental traits in Akodontine rodents. Significance codes: 0 '***' 0.001 '**' 0.01 '*' 0.05 '.' 0.1 ' ' 1

Dental traits	Est.	SE	*t*-stat	*p*-value	AIC	delta	*w*
1) Convex portion of the DNE	0.00092211	0.00062991	1.4639	0.1517	11.701917	13.811115	0.0008949949
2) Concave portion of the DNE	0.00079128	0.00040097	1.9734	0.05595 .	11.057053	13.166250	0.0012355239
3) Orientation Patch Count	0.00054289	0.00112962	0.4806	0.6336	13.077893	15.187090	0.0004498123
4) Relief Index	-2.0441	1.0735	-1.9041	0.06470 .	9.964925	12.074122	0.0021330630
Jaw traits							
1) Diastema length	-0.77744	0.74718	-1.0405	0.3049	12.199272	14.308470	0.0006979452
2) Jaw length	-0.81261	0.24667	-3.2942	0.0021802 **	7.858089	9.967287	0.0061164189
3) m1 to post. jaw	-1.14862	0.33418	-3.4371	0.0014683 **	7.082148	9.191346	0.0090155183
4) Joint elevation	-0.43673	1.13544	-0.3846	0.7027	13.161981	15.271179	0.0004312923
5) CPr elevation	-0.47728	0.83448	-0.5719	0.5708	12.957557	15.066754	0.0004777074
6) APr depth	1.35497	0.72292	1.8743	0.0688 .	9.771593	11.880790	0.0023495530
7) Corpus depth	3.03571	0.78009	3.8915	0.0004008 ***	4.508453	6.617650	0.0326483699
8) Jaw joint to m1	-1.16359	0.33605	-3.4625	0.0013675 **	6.942155	9.051353	0.0096691835
9) JCPr	0.75001	0.67009	1.1193	0.2702	12.013065	14.122262	0.0007660476
10) JAPr posterior length	-0.45593	1.25399	-0.3636	0.7182	13.153488	15.262685	0.0004331278
11) JAPr ventral length	2.64570	0.66844	3.9580	0.0003299 ***	4.119787	6.228985	0.0396514621
12) JAPr angle	4.48975	0.90181	4.9786	1.507e-05 ***	-2.109197	0.000000	0.8930299799

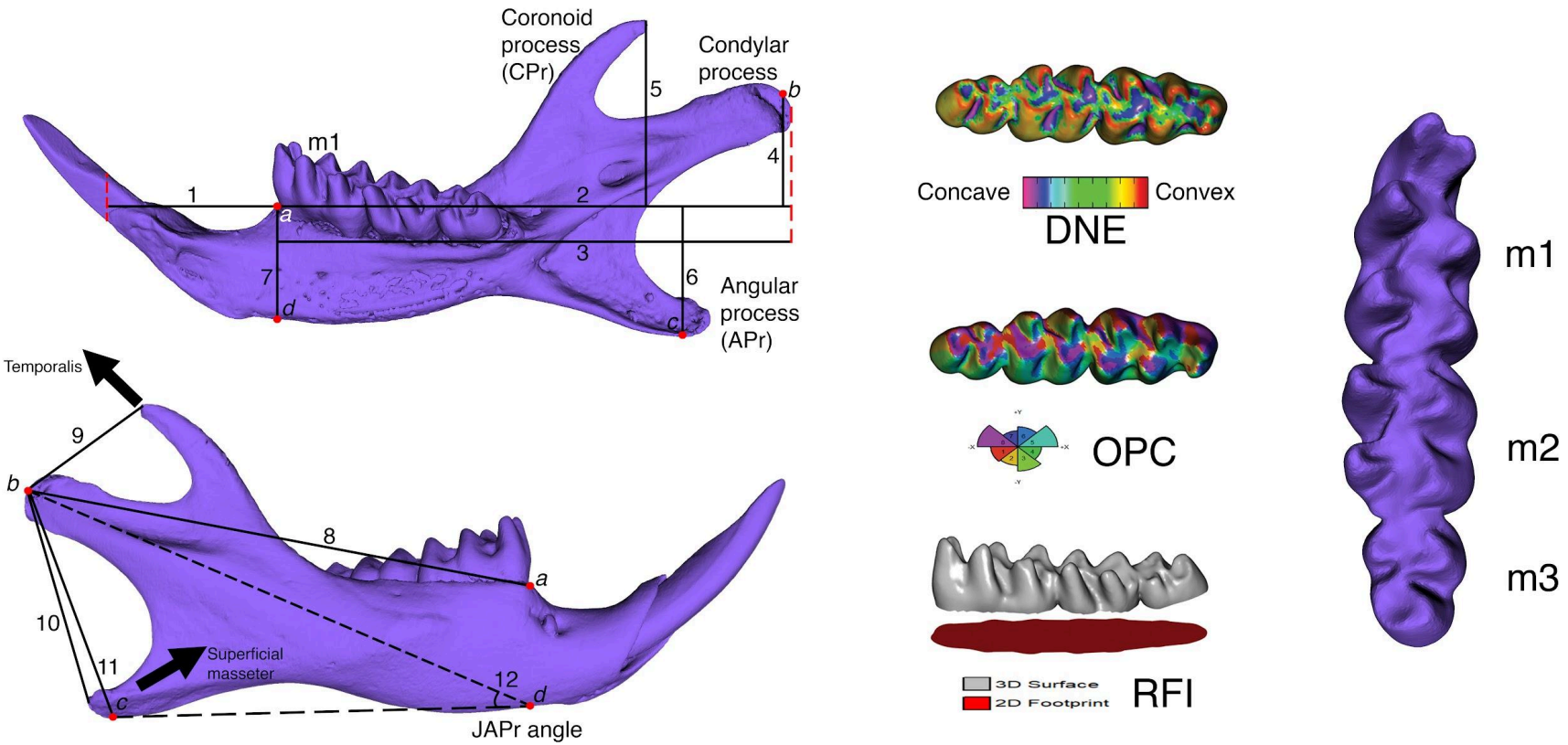

Figure 1.1. Mandibular and dental metrics collected from each voucher specimen. Measurements on the left view, top (lingual position) were taken perpendicular or parallel to the jaw length line (measurement 1 and 2) which passes along the alveolar margin. The bottom view (labial position) illustrates measurements involving the articulation surface of the condylar process (point b). Measurements 9 and 11 approximate the moment arm lengths for the force vectors of the temporalis muscle and superficial masseter muscle, respectively. Figure labels on the jaw correspond to: (1) diastema length, (2) jaw length, (3) M1 to

posterior jaw length, (4) joint elevation, (5) coronoid process (CPr) elevation, (6) angular process (APr) depth, (7) mandibular corpus depth, (8) jaw joint to m1 length, (9) jaw joint to coronoid process (JCPr) length, (10) jaw joint to the posterior-most point of the angular process (JAPr posterior) length, (11) jaw joint to the ventral-most point of the angular process (JAPr ventral) length, and (12) jaw joint to the angular process angle (JAPr angle). Measurements on the right view correspond to dental topography metrics extracted and analyzed from each mandibular right tooth row per specimen (m1, m2 and m3). DNE = Dirichlet Normal Energy; OPC = Orientation Patch Count, RFI = Relief Index. Detailed description of mandibular measurements are in Supporting information file 1, Table S2.

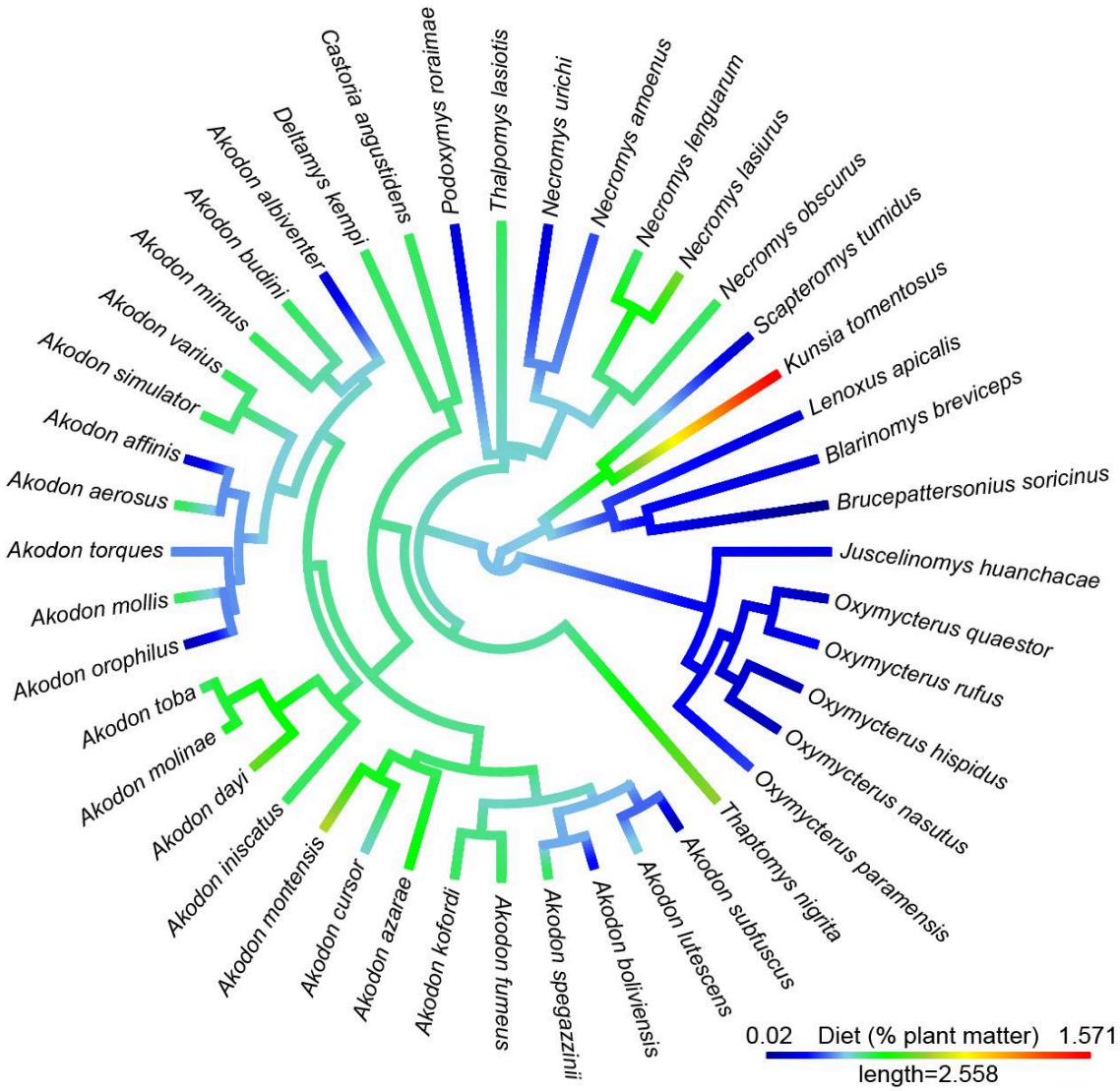

Figure 1.2. Dietary information (as arcsine-transformed proportion of percentage dietary plant material) mapped onto the phylogeny of akodontine rodents included in this study.

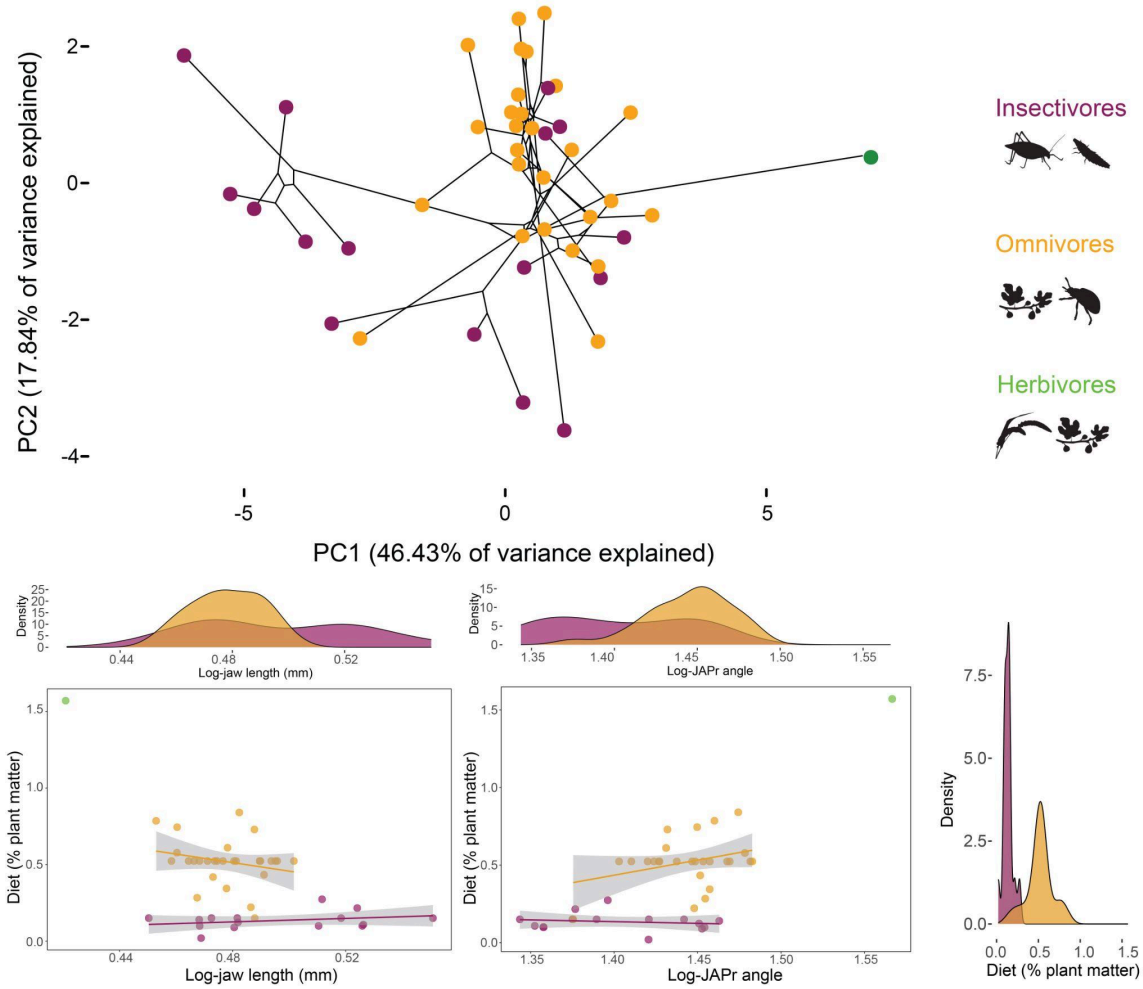

Figure 1.3. Phylomorphospace and descriptive plots depicting the morphospace distribution based on functional measurements of the jaw (top) and trends in the jaw length and jaw joint to the angular process angle (bottom) of Akodontini species with contrasting dietary ecologies.

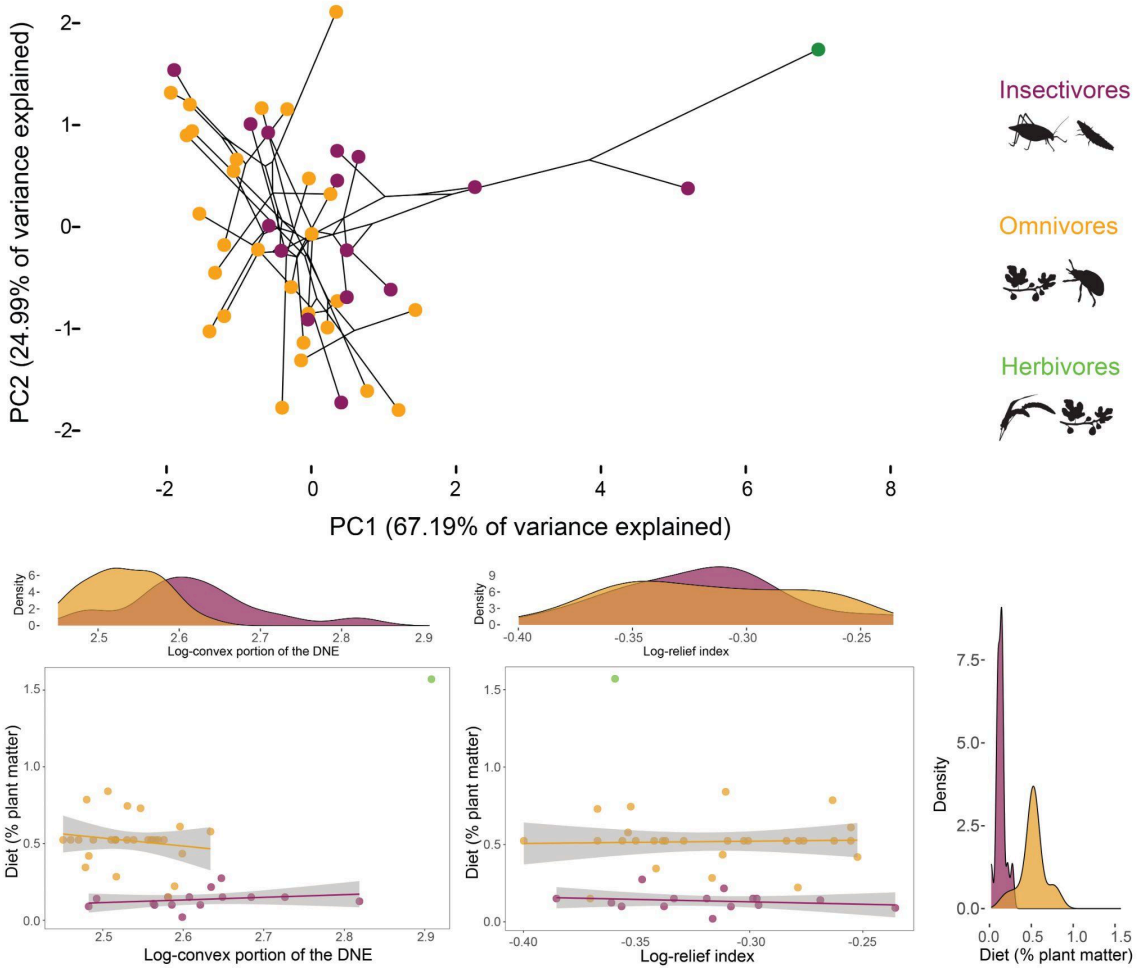

Figure 1.4. Phylomorphospace and descriptive plots depicting the morphospace distribution based on dental topography metrics (top), and trends in the convex DNE and relief index (bottom) of Akodontini species with contrasting dietary ecologies.

1.9 REFERENCES

Adams, D.C. 2014. A generalized K statistic for estimating phylogenetic signal from shape and other high-dimensional multivariate data. Systematic Biology, 63(5): 685–697.

Barbero, S., Teta, P., & Cassini, G.H. 2021. A comprehensive review of dietary strategies of sigmodontine rodents of central-eastern Argentina: linking diet, body mass, and stomach morphology. Canadian Journal of Zoology, 99(10): 885–901.

Barbero, S., Teta, P., & Cassini, G.H. 2023. An ecomorphological approach to the relationship between craniomandibular morphology and diet in sigmodontine rodents from central-eastern Argentina. Zoology, 156: 126066.

Bergqvist, L.P. 2002. The role of teeth in mammal history. Brazilian Journal of Oral Science, 2: 249–257.

Berthaume, M.A. 2016a. Food mechanical properties and dietary ecology. Am J Phys Anthropol, 159: 79–104.

Berthaume, M.A. 2016b. On the relationship between tooth shape and masticatory efficiency: A finite element study. Anat Rec., 299: 679–687.

Berthaume, M.A., Lazzari, V., & Guy. F. 2020. The landscape of tooth shape: Over 20 years of dental topography in primates. Evolutionary Anthropology, 29(5): 245-262. doi: 10.1002/evan.21856

Bezzobs, T., & Sanson, G. 1997. The effects of plant and tooth structure on intake and digestibility in two small mammalian herbivores. Physiological Zoology, 70: 338–351. doi: 10.1086/639612

Boyer, D.M. 2008. Relief index of second mandibular molars is a correlate of diet among prosimian primates and other euarchontan mammals. Journal of Human Evolution, 55: 1118–1137.

Blomberg, S.P., Garland, T., & Ives, A.R., 2003. Testing for phylogenetic signal in comparative data: behavioral traits are more labile. Evolution, 57(4): 717–745.

Claude, J. 2013. Log-shape ratios, Procrustes superimposition, elliptic Fourier analysis: three worked examples in R. Hystrix, It. J. Mamm. 24: 94–102.

Cox, P.G., & Baverstock, H. 2016. Masticatory muscle anatomy and feeding efficiency of the American beaver, *Castor canadensis* (Rodentia, Castoridae). J. Mamm. Evol. 23: 191–200.

Crompton, A.W., Owerkowicz, T., & Skinner, J. 2010. Masticatory motor pattern in the koala (Phascolarctos cinereus): a comparison of jaw movements in marsupial and placental herbivores. J. Exp. Zool. A Ecol. Genet. Physiol. 313: 564–578.

D'Elía, G., & Pardiñas, U.F.J. 2015. Tribe Akodontini Vorontsov 1959. In: Patton JL, Pardiñas UFJ, D'Elía G (eds) Mammals of South America, vol 2. Chicago University Press, Chicago, pp 140–144.

Dumont, E.R., Davalos, L.M., Goldberg, A., Santana, S.E., Rex, K., & Voigt, C.C. 2012. Morphological innovation, diversification and invasion of a new adaptive zone. Proceedings of the Royal Society B: Biological Sciences, 279(1734): 1797–1805. doi: 10.1098/rspb.2011.2005

Drummond, A.J., & Rambaut, A. 2007. BEAST: Bayesian evolutionary analysis by sampling trees. BMC Evolutionary Biology; 7: 214.

Evans, A.R., & Pineda-Munoz, S. 2018. Inferring mammal dietary ecology from dental morphology. In D.A. Croft, D.F. Su, & S.W. Simpson (Eds.), *Methods in paleoecology: Reconstructing Cenozoic terrestrial environments and ecological communities* (pp. 37–51). Springer International Publishing.

Evans, A.R., Wilson, G. P., Fortelius, M., & Jernvall, J. 2007. High-level similarity of dentitions in carnivorans and rodents. Nature, 445: 78–81.

Fabre, P.H., Herrel, A., Fitriana, Y., Meslin, L., & Hautier, L. 2017. Masticatory muscle architecture in a water-rat from Australasia (Murinae, Hydromys) and its implication for the evolution of carnivory in rodents. Journal of Anatomy, 231(3): 380–397. doi: 10.1111/joa.12639

Fedorov, A., Beichel, R., Kalpathy-Cramer, J., Finet, J., Fillion-Robin, J.C., Pujol, S., Bauer, C., Jennings, D., Fennessy, F., Sonka, M. & Buatti, J. 2012. 3D Slicer as an image computing platform for the Quantitative Imaging Network. Magnetic resonance imaging, 30(9): 1323–1341.

Felsenstein, J. 1985. Phylogenies and the comparative method. The American Naturalist, 125(1): 1–15.

Greaves, W.S. 2012. The mammalian jaw: A mechanical analysis. Cambridge University Press.

Grossnickle, D.M. 2017. The evolutionary origin of jaw yaw in mammals. Sci. Rep. 7:45094.

Grossnickle, D.M., & Polly, P.D. 2013. Mammal disparity decreases during the Cretaceous angiosperm radiation. Proc. R. Soc. B Biol. Sci. 280:20132110.

Grossnickle, D.M. 2020. Feeding ecology has a stronger evolutionary influence on functional morphology than on body mass in mammals. Evolution, 74: 610-628. doi: 10.1111/evo.13929

Grossnickle, D.M., Sadier, A., Patterson, E., Cortés-Viruet, N.N., Jimenez Rivera, S., Sears, K.E.; & Santana, S.E. 2023. On the cusp of adaptive change: the hierarchical radiation of phyllostomid bats. bioRxiv 2023.05.23.541856; doi: 10.1101/2023.05.23.541856

Guindon, S., Dufayard, J.-F., Lefort, V., Anisimova, M., Hordijk, W., & Gascuel, O. 2010. New algorithms and methods to estimate maximum-likelihood phylogenies: Assessing the performance of PhyML 3.0. Systematic Biology, 59: 307–321. doi: 10.1093/sysbio/syq010

Hershkovitz, P. 1966. South American swamp and fossorial rats of the scapteromyine group (Cricetinae, Muridae) with comments on the glans penis in murid taxonomy. Z Säugetierkd., 31: 81–149.

Hoang, D.T., Chernomor, O., von Haeseler, A., Minh, B.Q., & Vinh, L.S. 2018. UFBoot2: Improving the ultrafast bootstrap approximation. Molecular Biology and Evolution, 35: 518–522. doi: 10.1093/molbev/msx281

Hulsey, C.D., & Wainwright, P.C. 2002. Projecting mechanics into morphospace: Disparity in the feeding system of labrid fishes. Proceedings of the Royal Society of London. Series B: Biological Sciences, 269(1488): 317–326. doi: 10.1098/rspb.2001.1874

IUCN. 2024. IUCN Redlist of Threatened Species. Version 2024.2. Available at www.iucnredlist.org. Accessed July 01, 2024.

Jeuniaux, C. 1961. Chitinase: an addition to the list of hydrolases in the digestive tract of vertebrates. Nature, 192 (4798).

Kalyaanamoorthy, S., Minh, B.Q., Wong, T.K. F., von Haeseler, A., & Jermiin, L.S. 2017. ModelFinder: Fast model selection for accurate phylogenetic estimates. Nature Methods, 14: 587–589. doi: 10.1038/nmeth.4285

Kassambara, A. 2023. _ggpubr: 'ggplot2' Based Publication Ready Plots_. R package version 0.6.0, <https://CRAN.R-project.org/package=ggpubr>.

Katoh, K., & Standley, D.M. 2013. MAFFT Multiple sequence alignment software version 7: Improvements in performance and usability. Molecular Biology and Evolution, 30: 772–780. doi: 10.1093/molbev/ mst010

Konow, N., Bellwood, D.R., Wainwright, P.C., & Kerr, A.M. 2008. Evolution of novel jaw joints promote trophic diversity in coral reef fishes. Biological Journal of the Linnean Society, 93(3): 545–555. doi: 10.1111/j.1095-8312.2007.00893.x

López-Aguirre, C., Hand, S.J., Simmons, N.B., & Silcox, M.T., 2022. Untangling the ecological signal in the dental morphology in the bat superfamily Noctilionoidea. Journal of Mammalian Evolution, 29(3): 531-545.

Lucas, P.W. 1979. The dental-dietary adaptations of mammals. Neues Jahrbuch fur Geologie und Palaontologie Monatshefte 8: 486–512.

Lucas, P.W., Teaford, M.F. 1994. The functional morphology of colobine teeth. In: Oates, J., Davies, A.G. (Eds.), Colobine Monkeys: Their Evolutionary Ecology. Cambridge University Press, Cambridge, pp. 173–203.

Lucas, P.W. 2004. Dental functional morphology: how teeth work, Cambridge: Cambridge University Press.

Maestri, R., Monteiro, L.R., Fornel, R., Upham, N.S., Patterson, B.D., & de Freitas, T.R. O. 2017. The ecology of a continental evolutionary radiation: Is the radiation of sigmodontine rodents adaptive? Evolution, 71(3): 610–632.

Martins, E.P., & Hansen, T.F. 1997. Phylogenies and the comparative method: A general approach to incorporating phylogenetic information into the analysis of interspecific data. The American Naturalist, 149(4): 646–667. doi: 10.1086/286013

Martin, C.H., & Wainwright, P.C. 2011. Trophic novelty is linked to exceptional rates of morphological diversification in two adaptive radiations of Cyprinodon pupfish. Evolution: International Journal of Organic Evolution, 65(8): 2197–2212. doi: 10.1111/j.1558-5646.2011.01294.x

Martin, S.A., Alhajeri, B.H., & Steppan S.J. 2016. Dietary adaptability in the teeth of murine rodents (Muridae): a test of biomechanical predictions. Biological Journal of the Linnean Society, 199: 766–784.

Maynard Smith, J., & Savage, R.J.G. 1959. The mechanics of mammalian jaws. School Sci. Rev. 141: 289–301.

Mehta, R.S. 2009. Ecomorphology of the moray bite: Relationship between dietary extremes and morphological diversity. Physiological and Biochemical Zoology, 82(1): 90–103. doi: 10.1086/594381

Minh, B.Q., Schmidt, H.A., Chernomor, O., Schrempf, D., Woodhams, M.D., von Haeseler, A., & Lanfear, R. 2020. IQ-TREE 2: New models and efficient methods for phylogenetic inference in the genomic era. Molecular Biology and Evolution, 37: 1530–1534. doi: 10. 1093/molbev/msaa015

Misonne, X. 1969. African and Indo-Australian Muridae. Evolutionary trends. Musee Royal de l'Afrique Centrale, Tervuren, Belgique. Science Zoology, 173: 1–219.

Missagia, R.V., Patterson, B.D., Krentzel, D., & Perini, F.A. 2020. Insectivory leads to functional convergence in a group of Neotropical rodents. Journal of Evolutionary Biology, 34(2): 391–402. doi: 10.1111/jeb.13748

Mosimann, J.E. 1970. Size allometry: size and shape variables with characterizations of the lognormal and generalized gamma distributions. J. Am. Stat. Assoc. 65: 930–945.

Navalón, G., Bright, J.A., Marugán-Lobón, J., & Rayfield, E.J. 2019. The evolutionary relationship among beak shape, mechanical advantage, and feeding ecology in modern birds. Evolution, 73(3): 422–435. doi: 10.1111/evo.13655

Orme, D., Freckleton, R., Thomas, G., Petzoldt, T., Fritz, S., Isaac, N., & Pearse, W. 2023. _caper: Comparative Analyses of Phylogenetics and Evolution in R_. R package version 1.0.3, <https://CRAN.R-project.org/package=caper>.

Pampush, J.D., Winchester, J.M., Morse, P.E., Vining, A.Q., Boyer, D.M., & Kay, R.F. 2016. Introducing molaR: a New R Package for Quantitative Topographic Analysis of Teeth (and Other Topographic Surfaces). Journal of Mammalian Evolution, 23(4): 397–412.

Pampush, J.D., Morse, P.E., Fuselier, E.J., Skinner, M.M. and Kay, R.F. 2022. Sign-oriented Dirichlet normal energy: aligning dental topography and dental function in the R-package molaR. Journal of Mammalian Evolution, 29(4): 713–732.

Pampush, J., Morse, P., Vining, A., & Fuselier, E. 2023. _molaR: Dental Surface Complexity Measurement Tools_. R package version 5.3, <https://CRAN.R-project.org/package=molaR>.

Pardiñas, U.F.J., Myers, P., León-Paniagua, L., Ordóñez-Garza, N., Cook, J., Kryštufek, B., Haslauer, R., Bradley, R., Shenbrot, G., & Patton, J. 2017. Family cricetidae. In D. E. Wilson, R. A. Mittermeier, & T. E. Lacher (Eds.), Handbook of the mammals of the world, volume 7: Rodents II (pp. 204–279). Lynx Edicions.

Pardiñas, U.F.J., Cañón, C., Galliari, C.A., Brito, J., Hoverud, N.B., Lessa, G., & de Oliveira, J.A. 2020. Gross stomach morphology in akodontine rodents (Cricetidae: Sigmodontinae: Akodontini): a reappraisal of its significance in a phylogenetic context, Journal of Mammalogy, 101(3): 835–857. doi: 10.1093/jmammal/gyaa023

Price, S.A., Friedman, S. T., Corn, K.A., Martinez, C.M., Larouche, O., & Wainwright, P.C. 2019. Building a body shape morphospace of teleostean fishes. Integr. Comp. Biol. 59: 716–730.

R Core Team. 2024. _R: A Language and Environment for Statistical Computing_. R Foundation for Statistical Computing, Vienna, Austria. <https://www.R-project.org/>.

Radinsky, L.B. 1968. A new approach to mammalian cranial analysis, illustrated by examples of prosimian primates. J. Morphol. 124: 167–179.

Radinsky, L.B.1985. Approaches in evolutionary morphology: a search for patterns. Annu. Rev. Ecol. Syst. 16:1–14.

Rambaut, A., Drummond, A.J., Xie, D., et al. 2018. Posterior summarization in Bayesian phylogenetics using Tracer 1.7. Systematic Biology, 67: 901–4.

Reig, O.A. 1980. A new fossil genus of South American cricetid rodents allied to Wiedomys, with an assessment of the Sigmodontinae. J Zool. 192(2): 257–281.

Revell, L.J. 2009. Size-correction and principal components for interspecific comparative studies. Evolution 63:3258–3268.

Revell, L.J. 2024. phytools 2.0: an updated R ecosystem for phylogenetic comparative methods (and other things). PeerJ, 12, e16505.

Samuels, J.X. 2009. Cranial morphology and dietary habits of rodents. Zoological Journal of the Linnean Society, 156(4): 864–888. doi: 10.1111/j.1096-3642.2009.00502.x

Santana, S.E., Strait, S., & Dumont, E.R. 2011. The better to eat you with: functional correlates of tooth structure in bats. Functional Ecology, 25: 839–847. doi: 10.1111/j.1365-2435.2011.01832.x

Sanson, G. 2006. The biomechanics of browsing and grazing. American Journal of Botany, 93(10): 1531–1545.

Schenk, J.J., Rowe, K.C., & Steppan, S.J. 2013. Ecological opportunity and incumbency in the diversification of repeated continental colonizations by muroid rodents. Systematic biology, 62(6): 837-864. doi: 10.1093/sysbio/syt050

Spears, I.R., & Crompton, R.H. 1996. The mechanical significance of the occlusal geometry of great ape molars in food breakdown. Journal of Human Evolution, 31: 517–535. doi: 10.1006/jhev.1996.0077

Steppan, S.J., & Schenk, J.J. 2017. Muroid rodent phylogenetics: 900-species tree reveals increasing diversification rates. PLoS ONE, 12(8): e0183070

Strait, S.G. 1997. Tooth use and the physical properties of food. Evol. Anthropol. 5: 199–211.

Strait, S.G. 1993. Molar morphology and food texture among small-bodied insectivorous mammals. Journal of Mammalogy, 74: 391–402. doi: 10.2307/1382395

Suchard, M.A., Lemey, P., Baele, G., Ayres, D.L., Drummond, A.J., & Rambaut, A. 2018. Bayesian phylogenetic and phylodynamic data integration using BEAST 1.10 Virus Evolution 4, vey016. doi:10.1093/ve/vey016

van der Glas, H.W., van der Bilt, A., & Bosman, F. 1992. A selection model to estimate the interaction between food particles and post-canine teeth in human mastication. J. Theor. Biol., 155: 103–120.

Verde Arregoitia, L.D., & D'Elía, G., 2021. Classifying rodent diets for comparative research. Mammal Review, 51(1): 51-65.

Verde Arregoitia, L.D.V., Fisher, D.O., & Schweizer, M. 2017. Morphology captures diet and locomotor types in rodents. R. Soc. Open Sci. 4:160957.

Villalobos-Chaves, D., & Santana, S.E. 2021. Craniodental traits predict feeding performance and dietary hardness in a community of Neotropical free-tailed bats (Chiroptera: Molossidae). Functional Ecology, 36: 1690–1699. doi: 10.1111/1365-2435.14063

Westneat, M.W. 2003. A biomechanical model for analysis of muscle force, power output and lower jaw motion in fishes. Journal of Theoretical Biology, 223(3): 269–281. doi: 10.1016/S0022-5193(03)00058-4

Williams, S.H. & Kay, R.F. 2001. A comparative test of adaptive explanations for hypsodonty in ungulates and rodents. Journal of Mammalian Evolution, 8: 207–229.

Wilson, D.E., & Reeder, D.M. eds., 2005. Mammal species of the world: a taxonomic and geographic reference (Vol. 1). JHU press.

Wilson, D.E., Lacher, T.E. Jr., & Mittermeir, R.A. eds. 2016. Handbook of the Mammals of the World. Vol. 6. Lagomorphs and Rodents I. Lynx Edicions, Barcelona.

Winchester, J.M., Boyer, D.M., St Clair, E.M., Gosselin-Ildari, A.D., Cooke, S.B., & Ledogar, J.A. 2014. Dental topography of platyrrhines and prosimians: convergence and contrasts. Am J Phys Anthropol., 153: 29–44.

Yamaoka, K. 1983. Feeding behaviour and dental morphology of algae scraping cichlids (Pisces: Teleosti) in Lake Tanganyika. African Study Monographs, 4: 77–89. doi: 10.14989/ 68000

1.10 SUPPORTING TABLES AND FIGURES FOR CHAPTER 1

Table S1.1. Taxon coverage, number of aligned, conserved, variable, parsimony-informative sites, and singletons present in the alignments of mitochondrial and nuclear loci.

Loci	Genome	Coverage	Sites	Conserved	Variable	Pi	Singletons
Cyt-b	Mitochondrial	71 (100.0%)	1140	532	608	541	67
COI	Mitochondrial	33 (46.5%)	1545	965	580	514	66
Thr-Val block	Mitochondrial	24 (33.8%)	2790	1163	1416	882	455
Rbp3	Nuclear	60 (84.5%)	1266	786	480	264	216
RAG1	Nuclear	58 (81.7%)	2026	1263	759	383	376
GHR	Nuclear	56 (78.9%)	873	504	360	210	150
Acp5 (exon)	Nuclear	51 (71.8%)	243	190	53	29	24
Acp5 (intron)	Nuclear	50 (70.4%)	229	63	152	90	62
DMP1	Nuclear	37 (52.1%)	1188	690	480	236	244
THY (exon)	Nuclear	18 (25.4%)	122	118	4	2	2
THY (intron)	Nuclear	18 (25.4%)	451	433	18	10	8
-	**-**	**TOTAL**	**11873**	**6707**	**4910**	**3161**	**1670**

Table S1.2. Blomberg's K values and significance levels from the phylogenetic signal test. Significance codes: 0 '***' 0.001 '**' 0.01 '*' 0.05 '.' 0.1 ' ' 1

Variable (dental metrics)	***K-value***	***p*-value**
1) Convex portion of the DNE	1.04598	2e-04***
2) Concave portion of the DNE	0.493094	0.0274 .
3) Relief Index	0.663503	2e-04***
4) Orientation Patch Count	0.70161	9e-04***
Variable (mandibular morphology)		
1) Diastema length	0.740777	1e-04***
2) Jaw length	0.828939	1e-04***
3) m1 to post. jaw	0.787337	1e-04***
4) Joint elevation	0.484387	0.0111*
5) CPr elevation	0.507415	0.0068*
6) APr depth	0.37367	0.213
7) Corpus depth	0.760836	1e-04***
8) Jaw joint to m1	0.778283	2e-04***
9) JCPr length	0.376924	0.1302
10) JAPr posterior length	0.395404	0.2662
11) JAPr ventral length	0.678811	0.0012**
12) JAPr angle	0.948313	1e-04***

Table S1.3. Summary of the principal component analysis performed on dental topography metrics and mandibular measurements. Abbreviations: PC, loadings for each variable at each component; % variance, explained variance.

Variable (dental metrics)	PC1	PC2	PC3
Convex portion of the DNE	0.598447	-0.180298	-0.041970
Concave portion of the DNE	0.504364	-0.480572	0.542728
Relief Index	-0.269141	-0.827591	-0.492470
Orientation Patch Count	0.561285	0.227234	-0.67909
Eigenvalues	2.437515	1.086941	0.325571
% variance	60.93788	27.17352	8.139275
Variable (mandibular morphology)			
Diastema length	0.352343	-0.145069	-0.102705
Jaw length	0.427378	-0.12344	-0.125277
Joint elevation	-0.152303	0.502092	0.182482
CPr elevation	-0.052586	0.518057	-0.039024
APr depth	-0.278220	-0.396356	-0.305560
Corpus depth	-0.256765	-0.394949	-0.145807
Jaw joint to m1	0.402895	-0.037125	-0.102975
JCPr length	-0.117664	-0.197524	0.749941
JAPr posterior length	-0.130089	0.292928	-0.488056
JAPr ventral length	-0.385011	-0.062767	-0.105942
JAPr angle	-0.427293	-0.003643	-0.043219
Eigenvalues	5.000917	2.375601	1.198487
% variance	45.462884	21.596377	10.895339

Table S1.4. Summary statistics for bivariate phylogenetic generalized least squares (PGLS) regressions, which examine the relationship between diet (as a function of the percentage of plant matter) and mandibulo-dental traits in Akodontine rodents excluding herbivores species (i.e., *Kunsia tomentosus*). Significance codes: 0 '***' 0.001 '**' 0.01 '*' 0.05 '.' 0.1 ' ' 1

Dental traits	**Est.**	**SE**	***t*-stat**	***p*-value**	**AIC**	**delta**	***w***
1) Convex portion of the DNE	-0.0015241	0.0004498	-3.3885	0.001715 **	-12.539797	0.000000	0.22932747
2) Concave portion of the DNE	-0.00038718	0.00038178	-1.0141	0.317281	-9.513461	3.026335	0.05050050
3) Orientation Patch Count	-0.00078809	0.00085111	-0.9260	0.36063	-9.324356	3.215441	0.04594434
4) Relief Index	-1.09241	0.84526	-1.2924	0.20445	-9.903083	2.636714	0.06136221
Jaw traits							
1) Diastema length	-0.016742	0.584850	-0.0286	0.9773	-8.444910	4.094887	0.02959802
2) Jaw length	-0.044909	0.279316	-0.1608	0.8732	-8.459843	4.079954	0.02981984
3) m1 to post. jaw	-0.23899	0.36444	-0.6558	0.5161	-8.639461	3.900336	0.03262188
4) Joint elevation	-0.44224	0.92438	-0.4784	0.6352	-8.660151	3.879645	0.03296111
5) CPr elevation	-0.54759	0.66109	-0.8283	0.4130	-9.154358	3.385439	0.04220048
6) APr depth	0.4664502	0.6328646	0.7370	0.4659	-9.010806	3.528990	0.03927766
7) Corpus depth	2.07538	0.67360	3.0810	0.00394 **	-10.913570	1.626226	0.10170108
8) Joint to m1	-0.24955	0.36245	-0.6885	0.4955	-8.608899	3.930897	0.03212717
9) JCPr	0.92630	0.54496	1.6998	0.0978 .	-11.020099	1.519697	0.10726500
10) JAPr post.	-0.57202	1.00481	-0.5693	0.5727	-8.777274	3.762523	0.03494899
11) JAPr ventral	0.38179	0.76739	0.4975	0.6218	-8.672209	3.867587	0.03316044
12) JAPr angle	2.88441	0.94159	3.0633	0.004129 **	-10.822703	1.717094	0.09718381

Table S1.5. Summary statistics for bivariate phylogenetic generalized least squares (PGLS) regressions, which examine the relationship between diet (as a function of the percentage of plant matter) and mandibular traits in Akodontine rodents. In contrast to the analyses using log-shape ratios as size-corrected data (see Methods), here the data were size-corrected using regressions: measurements were log transformed and regressed (via PGLS) against jaw length, and residuals were used in subsequent PGLS regressions. Significance codes: 0 '***' 0.001 '**' 0.01 '*' 0.05 '.' 0.1 ' ' 1

Mandibular traits	Est.	SE	*t*-stat	*p*-value	AIC	delta	*w*
Diastema length	4.17122	5.02043	0.8308	0.411116	10.289756	11.316243	0.003043573
m1 to post. jaw	7.41972	7.97609	0.9302	0.357967	10.071388	11.097875	0.003394702
Joint elevation	4.41978	1.55353	2.8450	0.007041 **	3.777965	4.804452	0.078958906
CPr elevation	2.93026	1.83190	1.5996	0.117764	8.384134	9.410621	0.007891947
APr depth	2.91117	1.91835	1.5175	0.137195	8.600040	9.626527	0.007084363
Corpus depth	3.73993	2.33070	1.6046	0.11664	8.680661	9.707149	0.006804467
Joint to m1	8.04858	8.12573	0.9905	0.328033	9.963864	10.990351	0.003582203
JCPr	2.17854	1.85081	1.1771	0.246301	9.522826	10.549313	0.004466017
JAPr post.	2.26796	2.30597	0.9835	0.331417	9.952324	10.978811	0.003602932
JAPr ventral	3.36683	1.92391	1.7500	0.08798 .	8.154227	9.180714	0.008853355
JAPr angle	3.58731	0.98597	3.6383	0.0007938 ***	-1.026487	0.000000	0.872317536

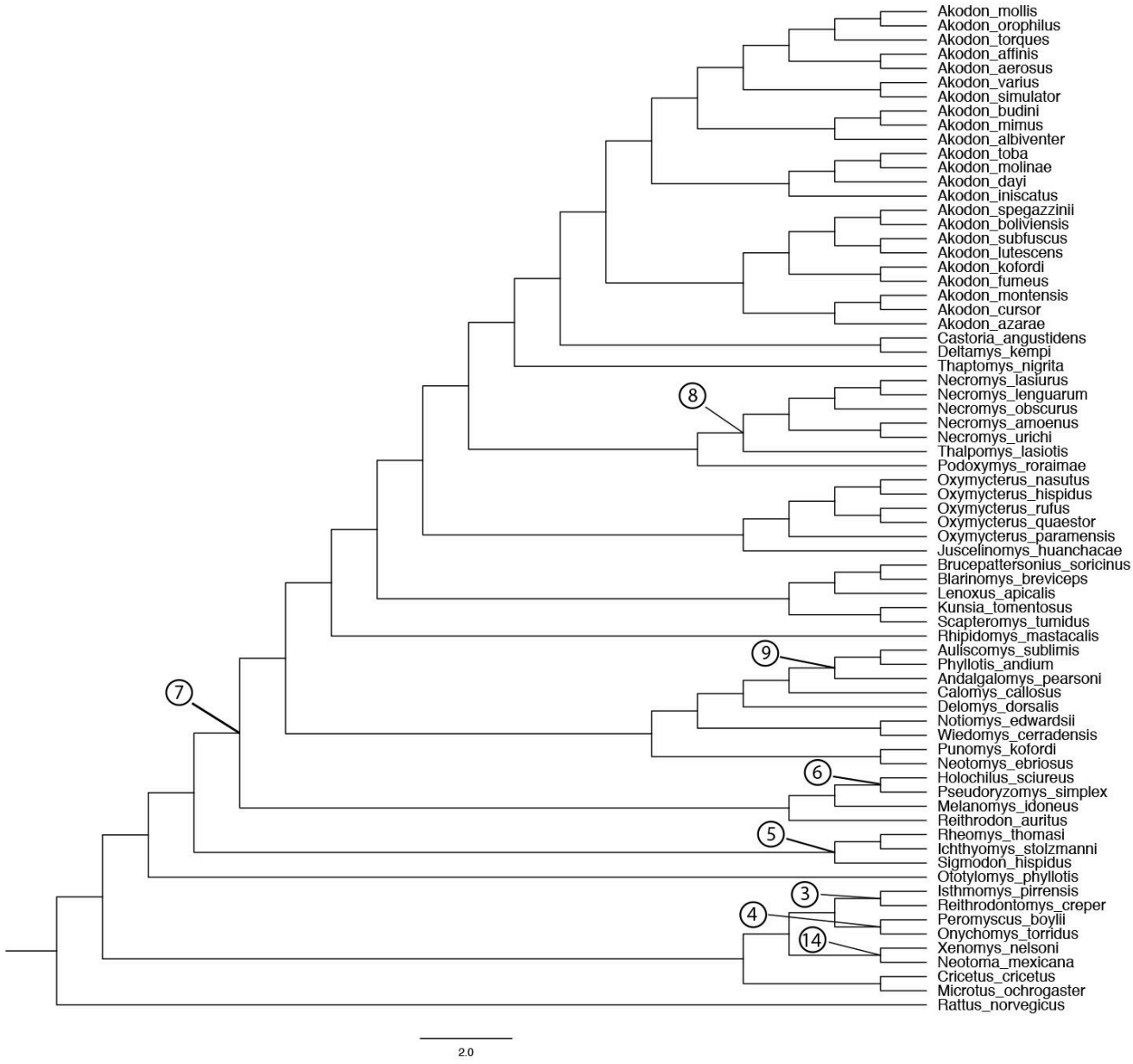

Figure S1.1. Time-calibrated ultrametric tree from the Beast analysis of the concatenated data. Nodes that were constrained in analyses based on fossil data are indicated with encircled numbers that correspond to specific fossils in Table1 from Steppan & Schenk (2017).

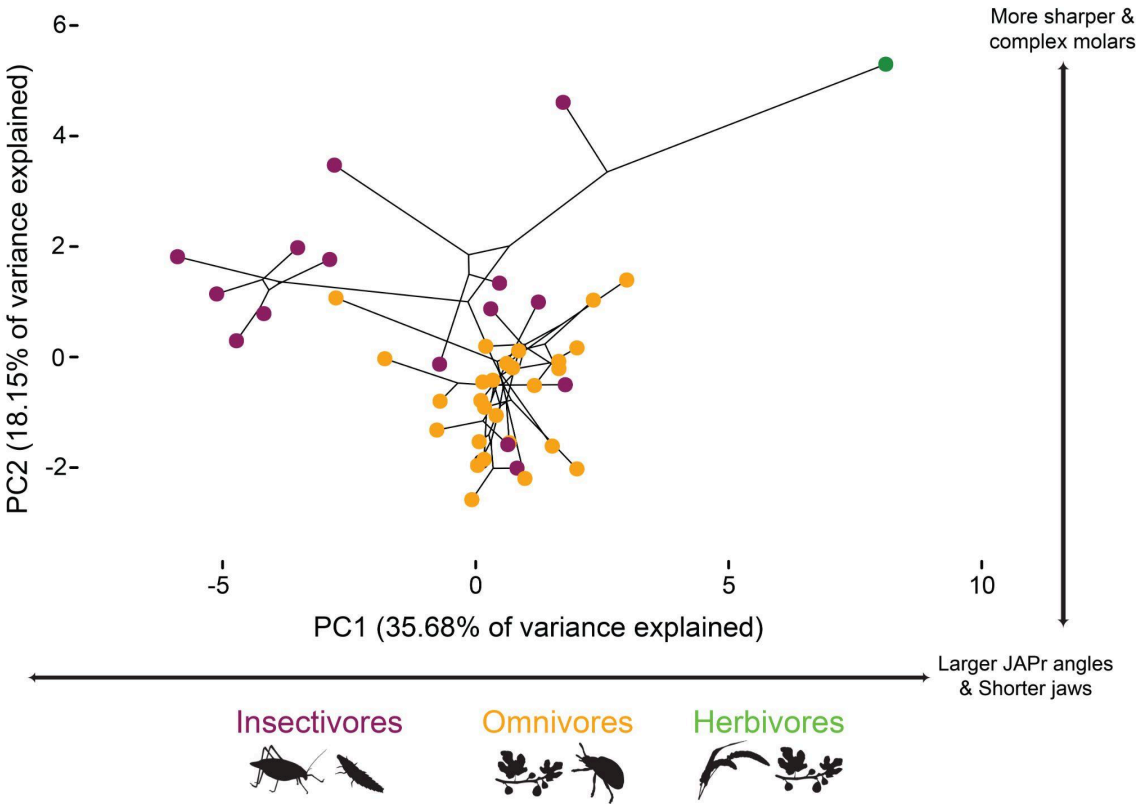

Figure S1.2. Phylomorphospace plot depicting Akodontini species on mandibulo-dental morphospace.

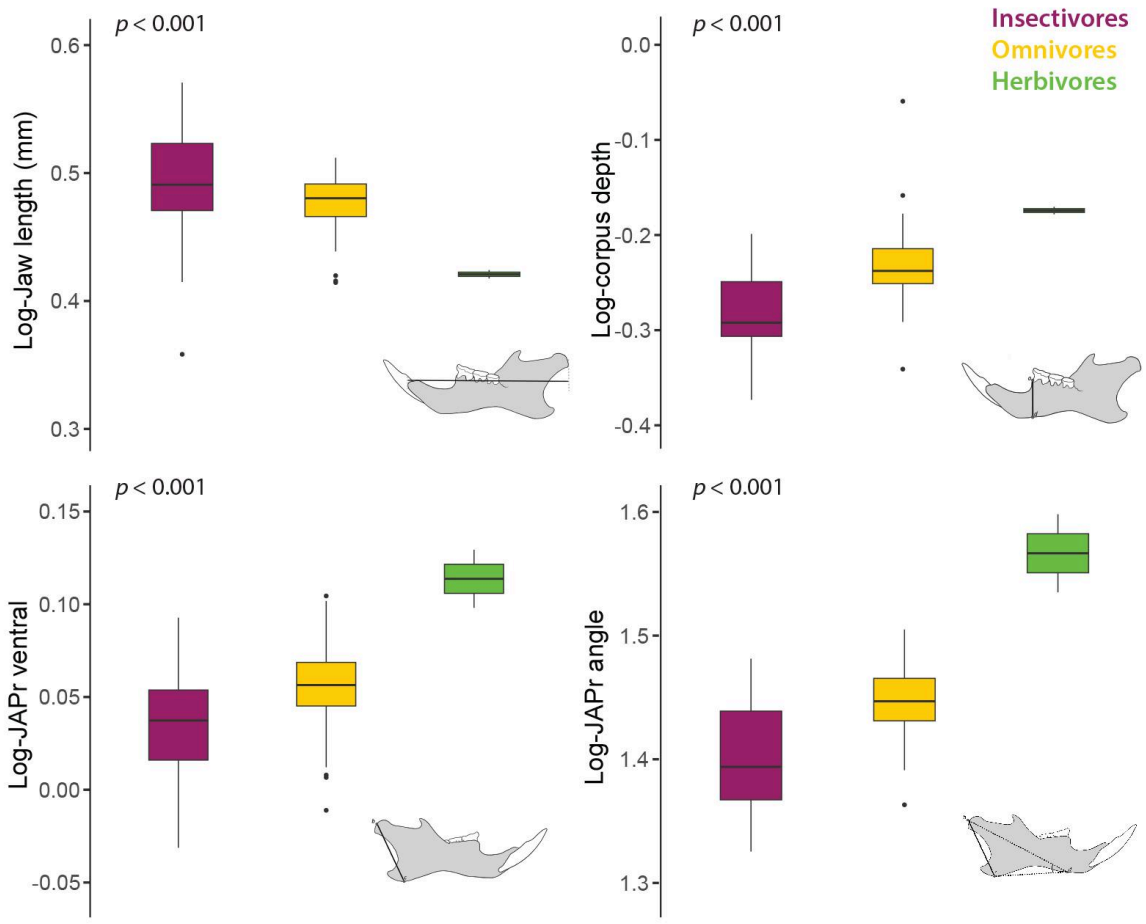

Figure S1.3. Schematic mandibular images displaying major morphological changes that are associated with differences in diet. The p-values in plots are from PGLS (Table 1). Box-and-whisker plots display medians, 25% to 75% quantiles (boxes), and ranges (whiskers).

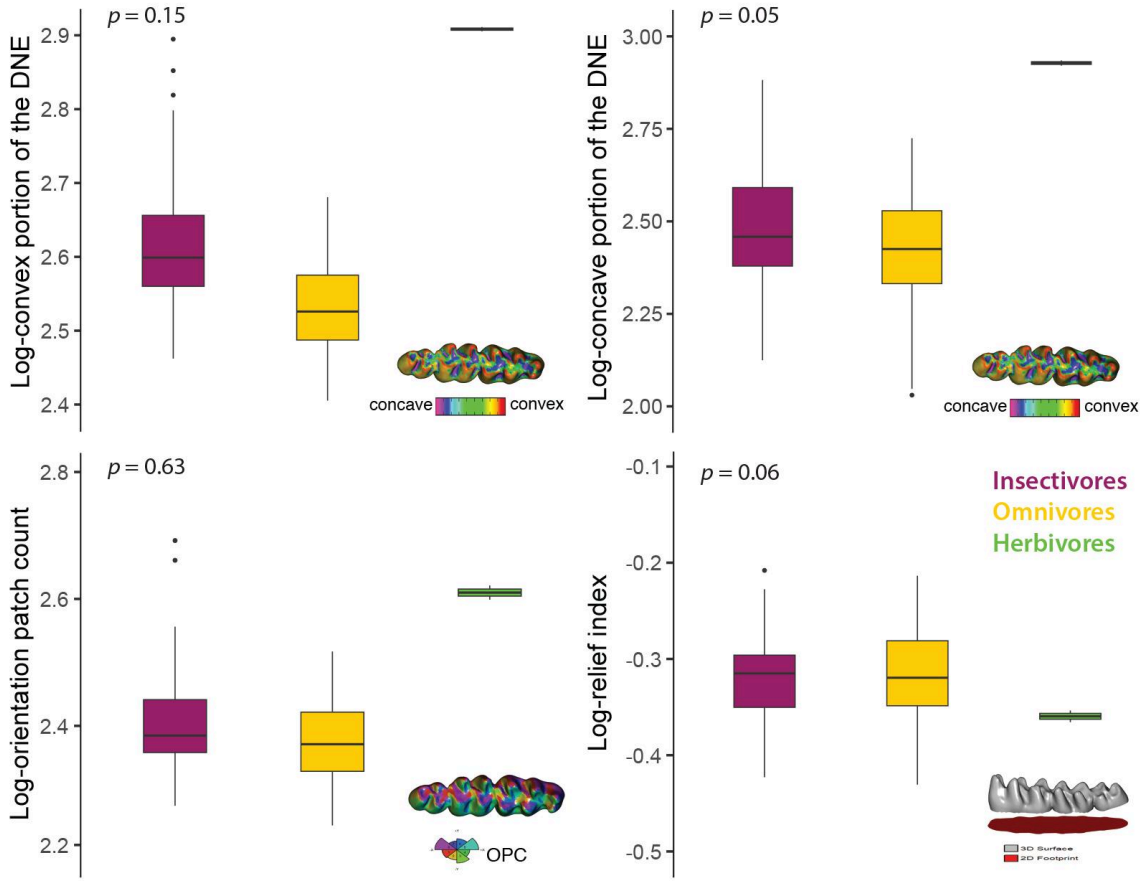

Figure S1.4. Schematic molar images displaying major morphological changes that are associated with differences in diet. The p-values in plots are from PGLS (Table 1). Box-and-whisker plots display medians, 25% to 75% quantiles (boxes), and ranges (whiskers).

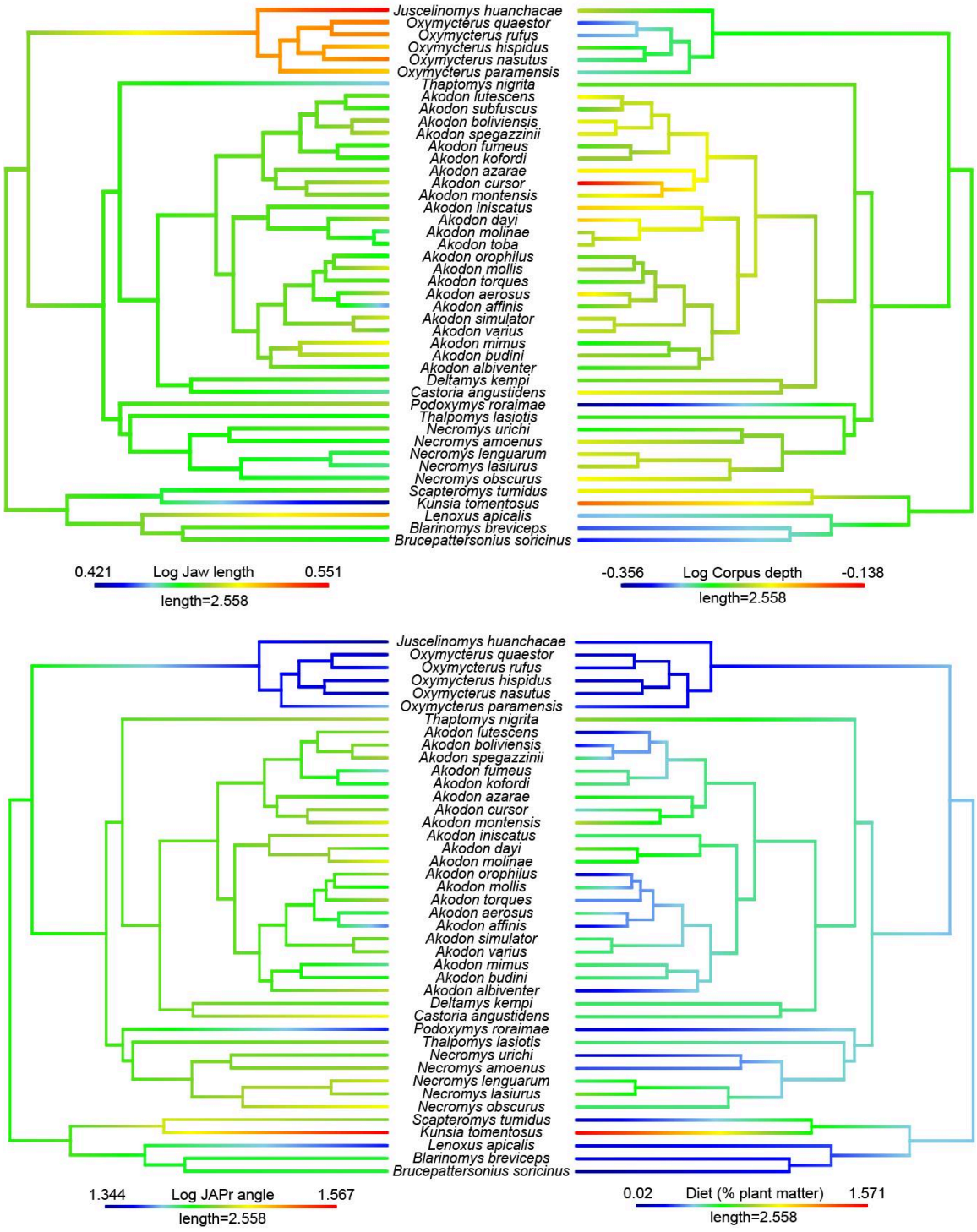

Figure S1.5. Mandibular traits (Jaw length, Corpus depth, JAPr angle) and dietary information (as arcsine-transformed proportion of dietary plant material) mapped onto the phylogeny of akodontine rodents.

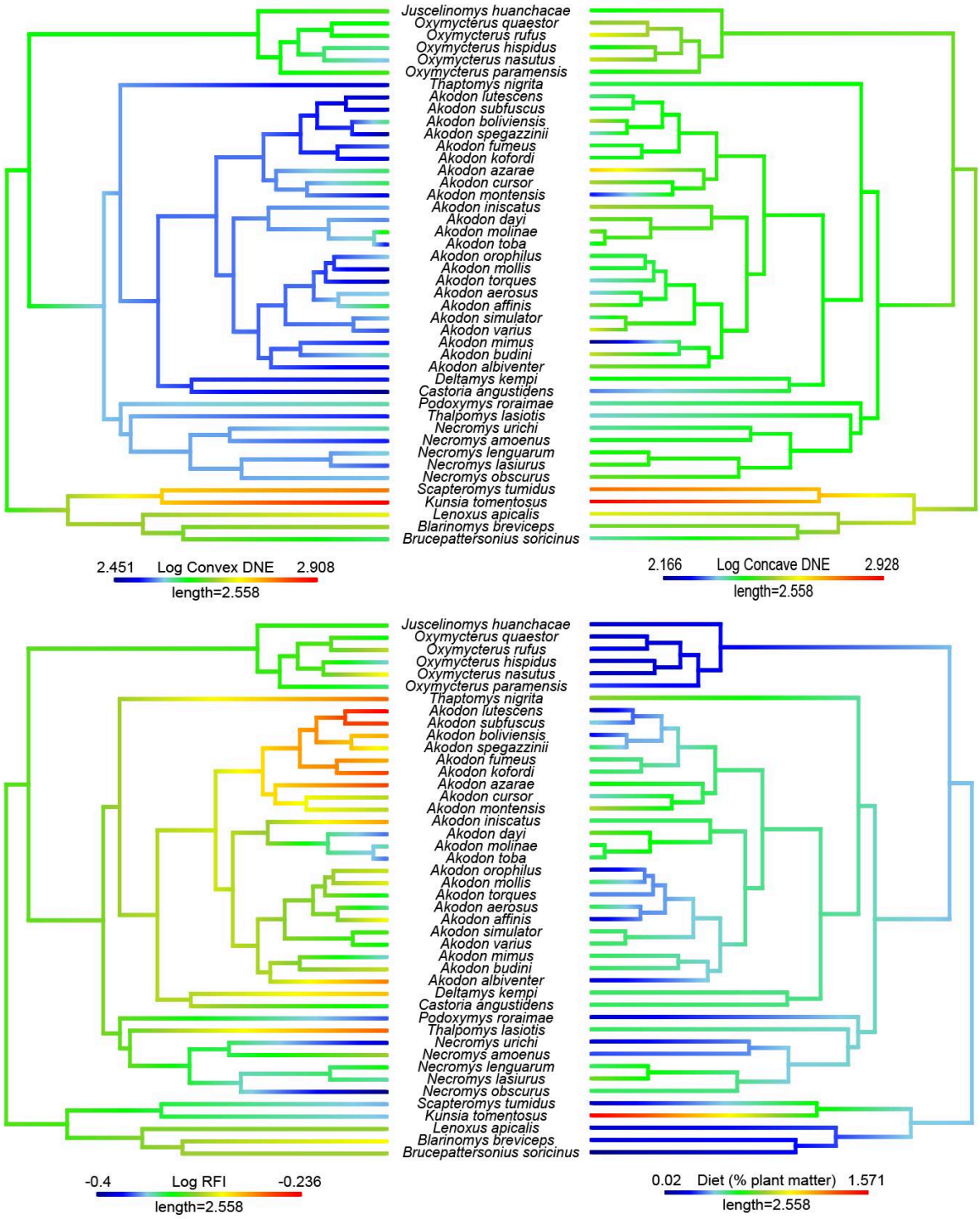

Figure S1.6. Dental topography metrics (Convex DNE, Concave DNE, RFI) and dietary information (as arcsine-transformed proportion of dietary plant material) mapped onto the phylogeny of akodontine rodents.

CHAPTER 2

Tiny mice tales in the cloud forest: Ecomorphological correlates of diet and feeding performance in a Neotropical rodent community

Drawing of a Short-tailed Singing Mouse, *Scotinomys irazu.*

2.1 ABSTRACT

Across animals, the shape and size of many morphological traits has been strongly linked to ecological selective pressures related to diet, with species evolving structures that optimize feeding function and maximize energy acquisition. However, trait morphology and size show great variation among taxa and are usually subject to functional tradeoffs, which can obscure our understanding on how natural selection has been shaping form-function-performance relationships across different animal lineages. For instance, myomorph rodents are within the most diverse and functionally versatile group of mammals, exhibiting unique morphological features that might be the result of diverse biotic and abiotic selective pressures. Here, we used this rodent group to investigate patterns of morpho-functional variation and elucidate performance differences that allow dietary specialization and trophic segregation among sympatric species inhabiting a Neotropical forest. We gathered data on the shape and size of external and craniodental anatomical structures in tandem with metrics of in-vivo feeding performance and dietary ecology. Our results revealed morphological traits that vary in tandem with the feeding ecology of the species, with extreme morphologies and performances corresponding to dietary habits that include greater amounts of either animal or plant matter. For instance, insectivorous species have, relatively, larger heads, shorter tails and longer jaws with shallower mandibular bodies; these trends that are correlated with a weaker bite force but larger mouth gapes. In contrast, the more herbivorous species have, relatively, smaller heads, longer tails and shorter jaws with deeper mandibular bodies, and these trends are correlated with stronger bite forces but smaller mouth gapes. Molar topography also varies significantly among species in relation to their feeding ecology, showing

contrasting morphologies that are directly linked to the mechanical properties of the species' preferred food items. Altogether, our study provides evidence on the relationship among form, function, and performance of morphological structures, and how these traits directly influence feeding ecology in sympatric myomorph rodent species. This highlights ecomorphological mechanisms that facilitate trophic segregation, and potential trade-offs resulting from ecological specialization.

Key words: bite force, Costa Rica, diet, gape, mandible, molars, resource partitioning.

2.2 INTRODUCTION

Trophic ecology is directly connected to morphological diversity in many species, in which distinct or similar dietary regimes diverge or converge on shapes that are functional and allow for optimal performance of feeding tasks (e.g., feeding — Dumont et al., 2012, Arbour et al., 2019; Leisler & Thaler 1982; Mares 1976; RÜber & Adams 2001; among others).

Understanding how morphology and ecology are intertwined is crucial and far from trivial, and these relationships provide strong clues of ecological pressures driving adaptive phenotypic changes (Grossnickle 2020). Within mammals, for instance, molar teeth exhibit highly diverse occlusal topographies and jaw sizes and jaw shapes that are strongly correlated with intra and/or interspecific dietary differences (Eisenberg 1981; Peters 1986; Evans & Pineda-Munoz 2018). Patterns in these traits have been detected and described in multiple taxa, particularly those in which the presence of foods with challenging mechanical properties (e.g., high fiber content, very hard items) seems to be

the main driver of size-form-and-function relationships (Berthaume et al., 2020). Outstanding examples can be found in some mammalian herbivores that exhibit overall larger body size, a larger angular process of the jaw and a molariform tooth row with higher complexity and larger occlusal area (Berthaume et al., 2020; Grossnickle 2020).

Nevertheless, although useful, our understanding of correlational relationships should also be informed with performance-based studies that could validate assumptions about how morphological and/or behavioral variation enables differential access to prey (Santana 2015). For example, variation in maximum bite force and gape among species, which are measures of whole-organism performance, is associated with specialization on food items with different mechanical properties and/or sizes (Binder & Valkenburgh 2000; Dumont & Herrel 2003; Norconk et al., 2009; Williams et al., 2009; Ross & Iriarte-Diaz 2014; Santana 2015). Altogether, these performance-morphology relationships play an important role in mechanisms that allow niche separation and diversification processes at broader (e.g., macroevolution) and finer (e.g., community ecology) scales (Aguirre et al., 2002).

With over 2, 200 species, rodents are among the most widespread, abundant and diverse group of living mammals in the world, directly influencing ecosystem health and functioning through their multiple roles as seed dispersers, pollinators, predators and prey (Wilson et al., 2016). All living rodents can be classified into four groups (i.e., the Protrogomorpha, the Sciuromorpha, the Hystricomorpha and the Myomorpha) based on the expansion of the masseter muscle from the zygomatic arch to the rostrum, which in turn has functional implications for their mandible biomechanics and the potential access to available food resources (Cox et al., 2012). For instance, in comparison with

sciuromophs and hystricomorphs, the biting efficiency and feeding behaviors of myomorph rodents have allowed them to invade multiple trophic niches (Cox et al., 2012). This functional versatility and, potentially, differences in performance, represents a unique and understudied opportunity to understand how subtle variations in the morphology of the rodent feeding apparatus may allow performance differences that are related to resource specialization and partitioning among species; this may hold true especially at small spatial scales where rodents are coexisting and might be subject to strong competition pressures.

In this context, in the present work we evaluated the relationship between ecomorphological and performance traits among the coexisting members of a community of myomorph rodents in Costa Rica to assess functional differences in resource use and explain mechanisms of trophic partitioning. Correspondingly, we hypothesize that if feeding ecology has influenced morphological evolution through selection on shapes that function better at processing food items with specific mechanical properties, evolved differences in morphological traits would facilitate performance variation among members of the community. Specifically, due to the tradeoffs associated with processing plant materials (e.g., tough stationary prey with usually low energy contents that need to be masticated thoroughly), we predict that more herbivorous species will have relatively larger body sizes and heads, and jaw traits that enable overall stronger bite forces even at the small gapes involved in mastication. On the other hand, as capturing and processing animal prey presents different challenges (e.g., mobile and soft prey that need to be captured), we predict that species with more insectivorous diets will have relatively smaller body sizes with head and jaw traits that would result in faster jaw movements, but

lower bite forces. Moreover, due to the potential advantages of having generalized morphologies to deal with food items of contrasting material properties (e.g., stiff vs pliant materials), we predict that species with duller, less complex (i.e., less tools) and smaller occlusal areas will tend towards omnivory, while higher topographic values will be found in species in which more animal matter or more plant matter is present in the diet. This would be due to the advantages of having sharper, heavily equipped (i.e., # tools) and larger occlusal areas to break down cuticles of varying stiffness with less bite force, or, on the other hand, mechanically process highly demanding plant material.

2.3 MATERIALS AND METHODS

2.3.1 Field work & taxonomic sample

To collect information on the morphology, dietary ecology and feeding performance of sympatric Neotropical rodents from Costa Rica, we performed field work at a locality of the Pacific slope of the Costa Rican Cordillera de Talamanca, namely Parque Nacional Tapantí (hereafter, Tapantí—9.7582 N, -83.7809 W). There, at three different areas within Tapantí (i.e., Los Maestros, Árboles caídos and Oropéndola) and during six independent visits, we used baited Sherman live-traps to sample the community of rodent species.

We captured a total of 191 individuals of 7 species (Table 2.1), and kept, curated and exported 47 non-pregnant adults as voucher specimens to the Burke Museum of Natural History and Culture with permission from the Sistema Nacional de Áreas de Conservación (SINAC-ACC-PI-LC-020-2021; SINAC-ACC-PI-re-082-2021 and PE-CUSBSE-109-2022) (Supporting information file 4 — Table S1, Table S2a and Table

S2b). All procedures involving live animals were approved by the University of Washington's Institutional Animal Care and Use Committee (protocol# 4307-01).

We used specimens to create digital 3D models of the skull of each voucher using a Skyscan 1172 µCT Scanner (Bruker MicroCT, Belgium). All scans were run at a 13.4 um image voxel size while keeping other scanning parameters consistent (Supporting information file 4 — Table S3). We then used NRecon (Microphotonics) to convert CT shadow images into image stacks ('slices'), which we imported into Mimics v. 22.0 (Materialise, Leuven, Belgium) to produce 3D surface (*.stl) files. Raw stl files were then manipulated with the help of Geomagic Studio v. 2019 (Geomagic Inc., Research Triangle Park, NC, USA) to select and isolate the morphological structures of interest for our analysis.

2.3.2 Morphological information

External traits —We collected data on the age (AG), sex (SX), reproductive stage (RS), body mass (BM), head-body length (HB), tail length (TL), hind foot length (HF), ear length (EL), head length (HL), head width (HW) and head height (HH) from live animals in the field with the help of direct observation (i.e., age and sex), a spring scale (i.e., BM), rulers and digital calipers (i.e., all other linear measurements) (Fig. 2.1 and Table 2.1). Specifications regarding age and reproductive stage classification, as well as descriptions of the measurements can be found in the Supporting information file 4 — Table S1.

Mandibular traits —We used scaled hemi-mandible pictures obtained from 3D mesh models to gather data on 10 linear measurements and one angle (Fig. 2.1; Supplementary information file 4 — Table S4a and Table S4b) (Grossnickle 2020) that are directly related to the ecology and evolution of morphological patterns and functional tradeoffs among feeding morphologies (Verde Arregoitia et al., 2017; Grossnickle 2020; and see Chapter 1). Scaled pictures were taken in 3D Slicer (Fedorov et al., 2012 — http://www.slicer.org) while only using the right hemi-mandible at lingual and labial views to facilitate the precision of the measurements, which were taken in ImageJ (National Institutes of Health, Bethesda, MD, USA). Detailed descriptions of each mandibular trait and how data were collected can be found in Supporting information file 4 — Table S1, in addition to Fig. 2.1.

Dental traits —We used our 3D mesh models to isolate the entire tooth crowns (i.e., above the enameled cervix) of each right mandibular molar tooth row (i.e., M1, M2, and M3) of our voucher specimens (Boyer 2008). After isolation and cropping to expose the occlusal plane, we oriented the models with the occlusal plane parallel to the X-axis, the Y-axis perpendicular to the occlusal plane, and the Z-axis pointing in the lingual direction (see Fig. S3.2 of the supporting table and figures for Chapter 3) following Pampush et al. (2016). Because tooth wear can affect dental topography metrics, we visually inspected the models, classified them into 5 categories (i.e., 4 = highly worn molars; 0 = unworn molars) (Supplementary information file 4 — Table S5), and discarded from further analysis those specimens with values corresponding to 4 and 3 (i.e., highly/moderate wear). The best models were then exported into Avizo Lite 9.2.0 (FEI Visualization

Sciences Group, Berlin, Germany) for simplification (25,000 faces) and smoothing (20 smoothing iterations; lambda of 0.6) (Pampush et al., 2016). Finally, we used the package molaR and its function molaR_Batch to calculate and gather data on the following dental metrics: the Dirichlet normal energy (hereafter: DNE), the convex portion of the Dirichlet normal energy (hereafter: Convex DNE), the concave portion of the Dirichlet normal energy (hereafter: Concave DNE) , the concave and the convex area, the 2D area, the Relief index (hereafter: RFI), the Orientation patch count rotated (hereafter: OPCR), the Orientation patch count (hereafter: OPC), and the Slope (Pampush et al., 2016) (Supplementary information file 4 — Table S5).

For RFI calculations, we used an alpha value of 0.075, as this was the minimum value allowed for us to keep the subscript inside the bounds (see details in Pampush et al., 2016). We performed OPCR calculations with a minimum of 3 faces and 8 steps, with a step size of 5.62. Further comparative analysis was performed using only a subset of all of these metrics (see details in the data analysis section), which were selected through Spearman correlations to evaluate similarities among the metrics.

2.3.3 Dietary information

Dietary data came from direct observation of the behavioral response of the focal species to specific food items offered to them (i.e., fruits, seeds and invertebrates), in addition to a literature review of all the information available for each species.

Behavioral observations were performed in the field in an enclosed glass terrarium where animals of each species were individually placed with at least two items of each food (i.e., two fruits, two seeds, and two invertebrates). Arrangement of the food

items was based mostly on availability (as these are native foods that were collected in the forest), nevertheless when available, food items were consistently presented to the rodents in pairs (i.e., two food items of the same species). Each individual rodent species was left alone with their food for about five hours (1:00-6:00 am), and after this time period, food remains were collected to document any trace of feeding activity. We only considered those food items that were completely predated upon (i.e., 100%) or almost entirely predated (i.e., 90%) to make our dietary classifications. Partially predated items might have included, for example, insects that due to the presence of wings (which rodents do not eat) were not completely consumed but were evidently predated.

According to our behavioral data and bibliographic information, rodent species were classified into one qualitative dietary scheme with three categories (i.e., insectivores, omnivores, and herbivores — Table 2.1) and one quantitative, continuous, dietary scheme based on the available and/or estimated amount of plant/animal material in each of their diets. We defined insectivores as species with diets consisting of 80–100% animal prey (or 0–20% plant material — n = 1), omnivores as 20–85% plant material (n = 4), and herbivores as 85–100% plant material (n = 2) (Supporting information file 4 — Table S6). These two classifications are probably an oversimplification of diet, and proposed thresholds are based on previous studies of diet in mammals (Verde Arregoitia & D'Elía 2021; Grossnickle 2020; Barbero et al., 2023) and my own subjective criteria based on the feeding behavior of the focal species. However, due to the scarcity of dietary information and the fact that the majority of mammalian species consume some amount of both plant and animal matter (Pineda-Munoz & Alroy 2014), we also used our quantitative dietary scheme to reduce

bias regarding strict definitions of dietary categories that can be subjective (e.g., omnivory), in addition to easing the computational complexity of regression and model fitting analyses (Grossnickle 2020).

2.3.4 Performance data

Rodents' voluntary bite force and maximum passive gape at the incisors (Table 2) was measured in the field from selected animals via a piezoelectric force transducer (Kistler, type 9203, range ± 500 N, accuracy 0.01–0.1 N; Amherst, NY, USA) attached to a handheld charge amplifier (Kistler, type 5995, Amherst, NY, USA) and a digital caliper, respectively (Supporting information file 4 — Table S7 and Table S8).

Because we also needed information on the maximum passive gape of each species to set up the piezoelectric force transducer at a distance (i.e., the distance between the plates that determines the gape) that could be compared across rodents of different sizes, we first obtained information on this metric by measuring the linear distance between the upper and lower incisor tip (i.e., the maximum passive gape) of multiple animals per species. Each maximum passive gape measurement was collected from sedated animals after carefully opening the jaw to the maximum point of slight resistance. Individual rodents used to collect data on maximum passive gape were later used to collect data on external morphology, kept as voucher specimens, or released back to the wild. However, they were never used for further data collection of bite force and/or diet, as these data could have been subject to biases caused by stress due to sedation.

Finally, each rodents' voluntary bite force was measured taking into account the average maximum passive gape value measured for each species (above), by setting the

distance between the bite force meter's biting plates at a distance that would result in a gape that was 45% of the average maximum passive gape. We selected this value because it seems to optimize bite force production at the incisors in rodents (Williams et al., 2009). In total, we recorded a maximum of eight bites from each individual using these criteria and used the highest measurement for each individual as the maximum bite force. Data for animals that were reluctant to bite the plates were removed from the analysis. The maximum bite force for each species was obtained by averaging the maximum bite forces among individuals of the species.

2.3.5 Phylogenetic relationships

We assembled a phylogenetic tree based on Cytochrome B sequences to account for the influence of phylogenetic relatedness among the rodent species from the Tapantí community. To do so, we used GenBank and the sequence alignment software MUSCLE (Edgar 2004) to collect and manipulate genetic information on cytochrome B sequences for the focal species and one outgroup (i.e., *Ctenomys boliviensis*: Ctenomydae). The taxonomy of the species included in these data was manually verified against available synonyms (i.e., Wilson & Reeder 2005; Paradiñas et al., 2017). We chose the cytochrome B gene due to its advantage in detecting interspecific differences due toits high sequence variation among species (Castresana 2001). In addition, the cytochrome b gene is also very well represented in gene repositories encompassing many mammal species including the ones included here (Castresana 2001).

Following alignment, we created and tested 286 DNA models using IQ-TREE software for phylogenetic inference (Minh et al., 2020). The best candidate model was

chosen based on the Akaike and the bayesian information criterion values. The best fitting model was then used to generate, by computing ML distances, 99 parsimony trees. We then used tree scores to select the more parsimonious topology representing the phylogenetic relatedness among our focal species (Fig. S2.1). The specific details regarding voucher information, modeling parameters and tree estimation can be found in the Supporting information file 4 — Table S9.

2.3.6 Data Analysis

To reduce bias in morphological and performance data due to size differences among the rodent species, all comparative analyses were performed with size-corrected measurements (except those including dental topography metrics, which are not influenced by these differences — Berthaume et al., 2020). Thus, prior to each subsequent comparative analysis, we divided the raw data of each trait by the geometric mean of each data set to obtain the estimated shape ratios of each morphological trait (Mosimann 1970; Claude 2013). Following this process, and because means of traits for species cannot be considered as statistically independent data points due to differing amounts of shared phylogenetic history (Felsenstein 1985), we used the Cyt b phylogeny to evaluate the influence of phylogenetic relatedness by calculating the phylogenetic signal of each trait using the package 'phytools' (Revell 2012) with the lambda (λ) method. However, due to lack of a significant phylogenetic signal (lambda = 0, $P > 0.05$) in our traits, further analyses were carried out without phylogenetic corrections.

In our first comparative analysis, we explored the differences in external, mandibular and molar traits among rodents with distinct dietary ecologies. To do this, we

used non-parametric multivariate analyses of variance (hereafter: MANOVAs) using the ‘adonis’ function from the ‘vegan’ package (Oksanen et al., 2024), in addition to post-hoc pairwise T-test comparisons using the Holm method.

In our second comparative analysis, we tested the relationships between our morphological traits and performance metrics. Due to the extensive number of traits being evaluated, we used Principal Component Analysis (hereafter: PCA) scores extracted from the first and second axes of two independent PCAs (one on external traits, and one on mandibular traits), to fit into linear regression models that used the performance metrics as response variables (i.e., either maximum bite force or maximum passive gape). PCAs were run in the ‘prcomp’ function from the ‘stats’ package (R Core Team 2023).

Finally, our third comparative analysis was aimed at understanding how morphology and performance interact and how strongly they can predict feeding ecology. Here, we used linear regression models with the first two PCA axes of each PCA (i.e., one from external and one from mandibular traits), the individual dental topography metrics and the gape and bite force as the predictor variables. Moreover, because the mechanical properties of challenging foods might give us better signals on morphological or performance differences associated with their processing, we used the percentage of plant matter for each rodent species as a response variable. We tested the assumptions of each regression model using the package ‘gvlma’ (Pena & Slate 2019). All statistical analyses were performed in R (R Core Team 2023).

2.4 RESULTS

Coexisting rodent species from the Tapantí community can be classified into omnivores (*Peromyscus nudipes*, *Oligoryzomys costaricensis*, *Reithrodontomys brevirostris* and *Handleyomys alfaroi*), herbivores (*Heteromys oresterus* and *Nephelomys devius*) and insectivores (i.e., *Scotinomys irazu*) based on the dietary information available and the behavioral data collected at the study site (Table 2.1). Comparative analyses of size-corrected data (i.e., shape ratio data) show that rodent species with different diets statistically differ in external (Table S 2.1 and Fig. 2.2) and mandibular (Table S 2.1 and Fig. 2.3) morphology (non-parametric MANOVA: $P < 0.0001$).

PCA's indicate that, within the set of external morphological traits, differences in PC1 (39.24% of variance explained) are mainly driven by variation in tail length and head measurements (i.e., head width, head height, and head length). PC2 (19.60% of the variance explained) differences, on the other hand, are mainly driven by head-body length variation (Fig. 2.3 and Table S 2.2). Here, *S. irazu* (an insectivorous which is the smallest species; Fig. S 2.2) have proportionately, wider, taller and longer heads, shorter tails and similar head-body dimensions than omnivores and herbivores (Fig. 2.2). Moreover, within the set of mandibular traits, PC1 loadings (33.09% of variance explained) revealed traits such as the depth of the mandibular corpus and the maximum depression of the angular process (i.e., APr depth) as the main contributors of the differentiation among feeding ecologies (Fig. 2.3 and Table S 2.2). In addition, PC2 loadings (23.83% of variance explained) highlight traits such as the jaw length and the distance between the jaw joint to the m1as the main drivers of separation within this axis (Fig. 2.3). Here, patterns on mandibular morphology indicate that herbivorous species

such as *N. devius* and *H. oresterus* have deeper mandibular corpora and angular processes, but overall, shorter jaws than omnivore and insectivore species (Fig. 2.3).

In addition to external and mandibular differences among dietary groups, rodent species with varying feeding ecologies also show significant variation in molar shapes (non-parametric MANOVA: $P < 0.0001$; Table S 2.1 and Fig. 2.4). For example, rodents with more herbivorous diets have molars with more (indicated by higher OPC values) and sharper (indicated by higher Convex DNE values) tools, but smaller occlusal areas (i.e., lower RFI values). In contrast, insectivorous rodents show the lowest OPC and convex DNE with the highest RFI values (Fig. 2.4). Omnivorous rodents, in contrast to the other two extreme morphologies, seem to have molars with less acute shapes but also with the greatest variation among all (Fig. 2.4)

Furthermore, regression models indicate that incisor bite force differences among sympatric species are better explained by external morphology (Table 2.3 and Table S2.3). For instance, despite having relatively smaller heads, herbivorous species show significantly (Kruskal-Wallis chi-squared = 17.138, df = 2, p-value = 0.0001899) higher bite forces than omnivorous and insectivorous species (Fig. 2.5). On the other hand, gape differences among species are also best predicted by differences in external (i.e., PC1) and mandibular traits (i.e., PC2) (Table 2.3 and Table S2.3). Here, species with relatively bigger heads and longer jaws (such as insectivores) tend to have significantly (Kruskal-Wallis chi-squared = 14.142, df = 2, p-value = 0.0008492) larger maximum passive gapes than species with relatively smaller heads and shorter jaws (i.e., omnivores and herbivores — Fig. 2.5).

Finally, among morphological and performance traits collected in this study, we detected that a combination of performance traits (i.e., incisor bite force), external (i.e., PC1 — tail length, head height and head width) and dental morphology (i.e., Convex DNE) are the best predictors of the feeding ecology of species (Fig. 2.5, Table 2.4 and S2.4, Fig S2.2). Correspondingly, species with higher incisor bite forces, relatively smaller heads and sharper molars (i.e., *N. devius* and *H. oresterus*) include more plant material in their diet than species with weaker incisor bite forces, relatively larger heads and duller molars (Fig. 2.5 and Fig S2.1). Among other traits explored, feeding ecology is also predicted (although to a lesser extent) by the length of the jaw (i.e., PC2), the maximum passive gape and the occlusal area of the molar row (i.e., the RFI). Here, species that include more animal materials in their diet (i.e., *S. irazu* and omnivores in general) have relatively larger jaws and gapes, and more chewing area available (Fig. 2.4, Table 2.4 and Fig S2.2).

2.5 DISCUSSION

Our results are consistent with ecomorphological patterns detected in other vertebrates and mammals, in which external morphological traits (Baeckens et al., 2016; Villalobos-Chaves & Santana 2021), mandibular morphology (Maynard Smith & Savage 1959; Turnbull 1970; Grossnickle & Polly 2013) and dental traits (Evans & Pineda-Munoz 2018; Winchester et al., 2014; Selig et al., 2019) are highly correlated with feeding ecology. Moreover, our data also reveal a strong connection among diet, morphology, and performance; this highlights a strong influence of dietary ecology on morphology and performance that goes beyond body size and phylogenetic relatedness.

Interestingly, our results highlight head measurements and tail length (major contributors of the PC1) as important traits that differentiate insectivorous and herbivorous species, and to some extent, these two dietary groups from omnivores (Table S2.2 and Fig. 2.2). For instance, our results reveal that *S. irazu*, which is a small (i.e., 11g — Fig. 2.2 and Table 2.1) diurnal species that is the only insect specialist of the community (feeding up to 80% of insects — Hooper & Carleton 1976), have relatively larger heads and shorter tails, in addition to other contrasting traits such as wider gapes, longer jaws and weaker incisor bite forces than the rest of the species in the community. These morphological and performance traits detected in *S. irazu* challenge positive head size and bite force correlations (Verwaijen et al., 2002; Nogueira et al., 2009; Rao et al., 2018) but support positive size-gape trends (Williams et al., 2009), supporting potential trade-offs in the evolution of anatomical configurations that favor larger gapes at the expense of bite force (Dumont & Herrel 2003; Santana 2015). Tail length variation, on the other hand, seems to be partially explained by dietary ecology at least indirectly. For instance, as animal prey is more concentrated in the canopy (Wells et al., 2004) and arboreal locomotion is positively correlated with tail length due to its role as a counterweight supporting changes in torque (Russo 2015, Mincer & Russo 2020; Sheard et al., 2024), the evolution of longer tails might be related with the locomotor performance advantages of moving and finding food in the forest canopy.

Overall, although our data is limited for generating interpretations about the adaptive significance of the extreme morphology and performance found in *S. irazu*, some of these patterns have converged in independent lineages of Old-World (i.e., muroids — Samuels 2009) and New-World (i.e., Sigmodontinae — Maestri et al., 2017;

Missagia et al., 2020) tropical rodents. This contributes to the idea that selective pressures related to faunivorous/insectivorous diets shaped form-function-performance relationships and trade-offs in rodent species that feed mostly on animal matter (Samuels 2009; Maestri et al., 2017; Missagia et al., 2020). Special caution, nevertheless, should be taken when interpreting this ecomorphological axis of variation, because peak bite forces can be produced at different gape sizes in different species (Kaczmarek & Gidmark 2020), and modifications of the jaw-muscle architecture of specialized species –which were not studied here– also contribute to differences in feeding performance (Williams et al., 2009).

In addition to the specialized form-function-performance relationships detected in the insectivorous species of the community, we also observed contrasting trends as species tend to include more plant matter in their diet (Fig. 2.5). Overall, as species increase the amount of plant foods (e.g., seeds, fruits, stems, leaves) they tend to have larger body sizes (i.e., body mass — Table 2.1 and Fig. 2.2), relatively smaller heads (Fig. 2.2), taller and shorter mandibles (Fig. 2.3), and stronger incisor bite forces and smaller gapes (Fig. 2.5). Considering the above trends, differences in these traits in omnivores, and specially, in herbivores, might reflect selective pressures related to procuring and processing food items with mechanical properties that differ from those of insect cuticle or other animal prey. For example, a potential biomechanical explanation for the importance of incisor bite force and external morphology (i.e., head size) on diet (Table 2.4) might be associated with the consumption of food items that require more force to be initially punctured. This holds especially true, for instance, for species of the genus *Peromyscus*, *Oligoryzomys*, *Heteromys* and *Reithrodontomys*, all of which have

been previously documented to feed on hard seeds of multiple plant species (Chinchilla 2009; Hafner 2016; Leiser-Miller et al., 2019)

Differences among guilds in mandibular traits such as an enlarged angular process (measurement 5) also suggest functional adaptations that are advantageous for plant matter consumption (Fig. 2.3). For instance, greater attachment areas for the superficial masseter and medial pterygoid muscles are highly correlated with an expanded angular process (Grossnickle 2020). These muscles are involved in transverse jaw movements for grinding occlusion (Maynard Smith & Savage 1959; Radinsky 1985; Crompton et al., 2010; Grossnickle 2017), which in many rodents, should help them to sustain forceful occlusal contact during extended power strokes (i.e., better grinding efficiency — Grossnickle 2020).

Moreover, important differences among species with contrasting feeding ecologies within the community are also reflected in the mandibular corpus depth (measurement 6), the jaw-joint-to-m1 length (measurement 7) and the jaw joint to the ventral-most point of the angular process (JAPr ventral) length (measurement 10) (Fig. 2.3, Table S2.1 and Fig. S2.3). Specifically, increases in the depth of the jaw body (e.g., corpus depth) are related to increased incisor size which might be advantageous for gnawing on harder objects (Radinsky 1968). Reduction of the jaw-joint-to-m1 distances on more herbivorous species might also be related to trade-offs regarding the mechanical advantage exerted while chewing; this distance approximates the outlever length for bites at the m1, which involve jaw rotation around an axis at the jaw joint, thus the mechanical advantage will increase with a shortened outlever if the in lever remains constant (Grossnickle 2020). Finally, differences observed in the JAPr distance (Fig. S2.3) among

insectivorous and more herbivorous species might also reflect functional trade-offs in gape and bite force among feeding ecologies. This is because JAPr distance influences the position of the superficial masseter and medial pterygoid muscles in relation to the jaw joint, influencing muscle stretch during jaw opening (Herring & Herring 1974). Therefore, selective pressures may have operated in favor of longer JAPr distances (i.e., bigger superficial masseter and medial pterygoid muscles) in herbivorous species to restrict gape opening while maintaining strong bite forces. On the other hand, because some JAPr distances result in muscle configurations that limit maximum gape and decrease bite force during wide gape (which may be especially detrimental to insectivores that consume large prey) insectivorous species are expected to show shorter JAPr distances and wider gapes, which are indeed the patterns observed in *Scotinomys irazu* (Fig. 2.5 and Fig. S2.3).

Lastly, strong functional relationships can also be found in the dental morphology of the species within the community (Fig. 2.4). In feeding ecology, dental morphology (and especially molar topography), underlie strong dietary signals (Evans & Pineda-Munoz 2018); as biting and chewing food is largely about fracture, it is expected that occlusal topographies evolved to efficiently break down of food items (Ungar 2010; Evans & Pineda-Munoz 2018). However, as the fracture of a material relates to its mechanical properties and the strain-stress responses of that material due to an applied force (Berthaume 2016), the topographic patterns observed in our community suggest potential trade-offs between food mechanical properties and occlusal topography.

For instance, higher convex DNE and OPC values with higher herbivory might increase the availability and sharpness of shearing surfaces on the molar rows. In

herbivorous mammals, a configuration such as this could be advantageous because the consumption of tissues with more fiber contents requires more efficient grinding surfaces to gain access to the cytosol and/or to expose more surface area of the plant cell wall for more rapid enzymatic hydrolysis in the gut (Sanson 2006). Interestingly, patterns on the convex DNE and orientation patch count values for insectivorous species suggest that selective pressures might have acted in the opposite direction, reducing complexity and sharpness of the shearing surfaces (Fig. 2.4). From a mechanical standpoint, these results might indicate that *S. irazu* is more suited to prey upon softer insects or invertebrates that are more efficiently comminuted with lower stresses distributed over larger contact areas (Strait 1993). This idea might also explain the truly exceptional size of the occlusal area in the molars of this species (Fig. 2.3). Considering the contrasting trends in dental topography metrics detected, we argue that potential trade-offs might be involved in the dynamic between availability/sharpness of shearing surfaces and occlusal area, with natural selection favoring one side or the other.

In conclusion, our results provide compelling evidence for interspecific differences in ecomorphological and performance traits among coexisting rodent species in a Neotropical forest, demonstrating how form-function-performance relationships might ultimately facilitate trophic resource partitioning among members of the community (Abrams 2022). Future steps might be focused on the collection and use of quantitative data on diet (e.g., mechanical properties), as well as studies of the functional trade-offs of specialized and generalized feeding morphologies (Huey & Hertz 1984; Roslin & Salminen 2008; Santana et al., 2011). Additional efforts should also be taken to understand the feeding behavior of species and its implication on feeding performance

(e.g., Santana & Dumont, 2009), as well as spatial and temporal differences that might be contributing to resource partitioning. Altogether, our study explores multiple layers of morphological and performance traits, which allowed us to elucidate functional links and trade-offs that underlie the feeding ecology and coexistence of rodent species.

2.6 ACKNOWLEDGMENTS

We appreciate the staff of the Sistema Nacional de Areas de Conservacion and the Parque Nacional Tapanti for providing research permits and support during fieldwork and data collection. The Museo de Zoología, Universidad de Costa Rica and the Burke Museum of Natural History and Culture, provided critical support to curate and store the voucher specimens for this research. DVC was supported by endowments from the Mammalogy Department at the Burke Museum of Natural History and Culture, the Department of Biology (WRF-Hall Fellowship) and the Graduate School (Boeing International Fellowship) from the University of Washington, in addition to the American Society of Mammalogist (Latin American Student Field Research Award). SES was supported by NSF grant # 2017738.

2.7 DATA AVAILABILITY STATEMENT

Curated data used for the analysis and scripts are archived here. 3D models (i.e., stl or ply files) will be available upon request.

2.8 TABLES AND FIGURES

Table 2.1. External ecomorphological traits of importance collected in this study. Results shown are mean ± SD.

Family	Subfamily	Species	Diet	Sample size (n)	Body mass (grams)	Head height (mm)	Head length (mm)	Head width (mm)
Cricetidae	Neotominae	*Peromyscus nudipes*	Omnivore	67	55.9 ± 6.8	13.6 ± 0.5	36.7 ± 1.3	15.5 ± 0.8
Cricetidae	Sigmodontinae	*Oligoryzomys costaricensis*	Omnivore	11	17.5 ± 4.9	10.4 ± 0.8	25.7 ± 1.3	11.9 ± 0.6
Cricetidae	Neotominae	*Scotinomys irazu*	Insectivore	18	11.3 ± 1.1	10.0 ± 0.3	24.9 ± 0.7	11.7 ± 0.5
Cricetidae	Neotominae	*Reithrodontomys brevirostris*	Omnivore	5	10.6 ± 1.8	9.8 ± 0.2	23.8 ± 0.8	11.4 ± 0.3
Cricetidae	Sigmodontinae	*Handleyomys alfaroi*	Omnivore	4	27.4 ± 4.1	12.0 ± 0.5	30.6 ± 0.4	13.7 ± 1.0
Heteromyidae	Heteromyinae	*Heteromys oresterus*	Herbivore	6	73.3 ± 6.0	15.1 ± 1.2	40.8 ± 1.0	17.2 ± 0.7
Cricetidae	Sigmodontinae	*Nephelomys devius*	Herbivore	9	95.1 ± 15.5	17.2 ± 0.5	42.5 ± 2.4	18.9 ± 0.9

Table 2.2. Performance traits collected for the species in this study. Results shown are mean ± SD.

Species	Sample size_bite force (n)	max. bite force (N)	Sample size_max. pass. gape (n)	max. passive gape (mm)
Peromyscus nudipes	19	13.34 ± 2.30	16	13.5 ± 1.3
Oligoryzomys costaricensis	2	7.82 ± 2.51	10	9.4 ± 2.9
Scotinomys irazu	4	5.98 ± 0.91	10	10.1 ± 0.8
Reithrodontomys brevirostris	3	7.05 ± 1.24	5	9.9 ± 0.6
Handleyomys alfaroi	3	11.59 ± 1.74	4	11.7 ± 0.8
Heteromys oresterus	3	18.99 ± 1.32	5	15.6 ± 1.6
Nephelomys devius	3	24.23 ± 1.46	8	16.3 ± 2.8

Table 2.3. Fit of the best performing regression models for bite force and maximum passive gape . *F* = F-statistic; R^2 = R squared; *p* = p-value. Models are ranked by R^2 values.

Model	*F*	R^2	*p*
Bite force ~ Ext. morphology (PC1) * Ext. morphology (PC2)	10.2	0.82	0.043*
Bite force ~ Ext. morphology (PC1) + Ext. morphology (PC2) + Mand. traits (PC2)	5.23	0.67	0.103
Bite force ~ Ext. morphology (PC2) + Mand. traits (PC1) + Mand. traits (PC2)	4.13	0.61	0.137
Bite force ~ Ext. morphology (PC1) + Ext. morphology (PC2) + Mand. traits (PC1) + Mand. traits (PC2)	2.68	0.52	0.289
Gape ~ Ext. morphology (PC1) + Mand. traits (PC2)	4.70	0.55	0.089
Gape ~ Ext. morphology (PC1)	6.60	0.48	0.050*
Gape ~ Ext. morphology (PC1) : Ext. morphology (PC2)	6.04	0.45	0.057
Gape ~ Ext. morphology (PC2) : Mand. traits (PC1)	5.89	0.44	0.059

Asterisks indicate statistical significance ($p < .05$). Signal '+' indicates the combination of variables, ':' indicates the interaction between variables, and 'x' indicates the combination of variables with the interactions between them.

Table 2.4. Fit of the five best performing regression models for feeding ecology. F = F-statistic; R^2 = R squared; p = p-value. Models are ranked by R^2 values.

Model	F	R^2	p
Diet ~ Bite force * Ext. morphology (PC1)	283.3	0.99	0.0003
Diet ~ Bite force + Ext. morphology (PC1) + Convex DNE	221.6	0.99	0.0005
Diet ~ Bite force + Ext. morphology (PC1) + Ext. morphology (PC2) + Convex DNE	1455	0.99	0.0006
Diet ~ Bite force + Gape + Ext. morphology (PC1) + Mand. traits (PC2)	187.6	0.99	0.0053
Diet ~ Bite force + Ext. morphology (PC1) + Convex DNE + RFI	179.4	0.99	0.0055

Asterisks indicate statistical significance ($p < .05$). Signal '+' indicates the combination of variables, ':' indicates the interaction between variables, and 'x' indicates the combination of variables with the interactions between them.

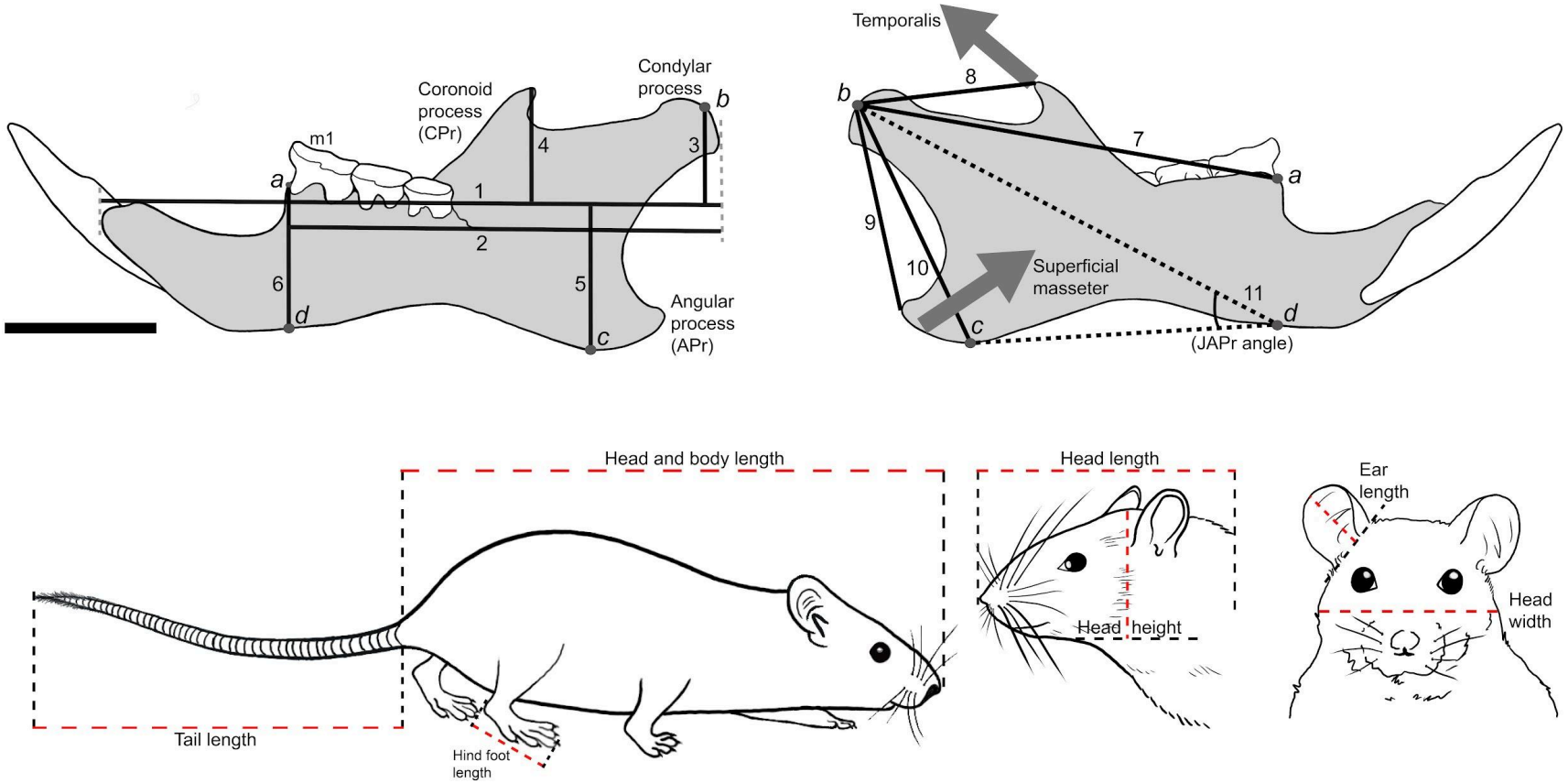

Figure 2.1. Mandibular and external measurements collected from each voucher specimen. Measurements on the top view, left (lingual position) were taken perpendicular or parallel to the jaw length line (measurement 1) which passes along the alveolar margin. The top view, right (labial position) shows measurements involving the articulation surface of the condylar process (point b). Measurements 8 and 10 approximate the moment arm lengths for the force vectors of the temporalis muscle and

superficial masseter muscle, respectively. Figure labels on the jaw correspond to: (1) jaw length, (2) M1 to posterior jaw length, (3) joint elevation, (4) coronoid process (CPr) elevation, (5) angular process (APr) depth, (6) mandibular corpus depth, (7) jaw joint to M1 length, (8) jaw joint to coronoid process (JCPr) length, (9) jaw joint to the posterior-most point of the angular process (JAPr posterior) length, (10) jaw joint to the ventral-most point of the angular process (JAPr ventral) length, and (11) jaw joint to the angular process angle (JAPr angle) (11). Detailed description of measurements are in Supporting information file 3, Table S1. Scale bar: 4cm.

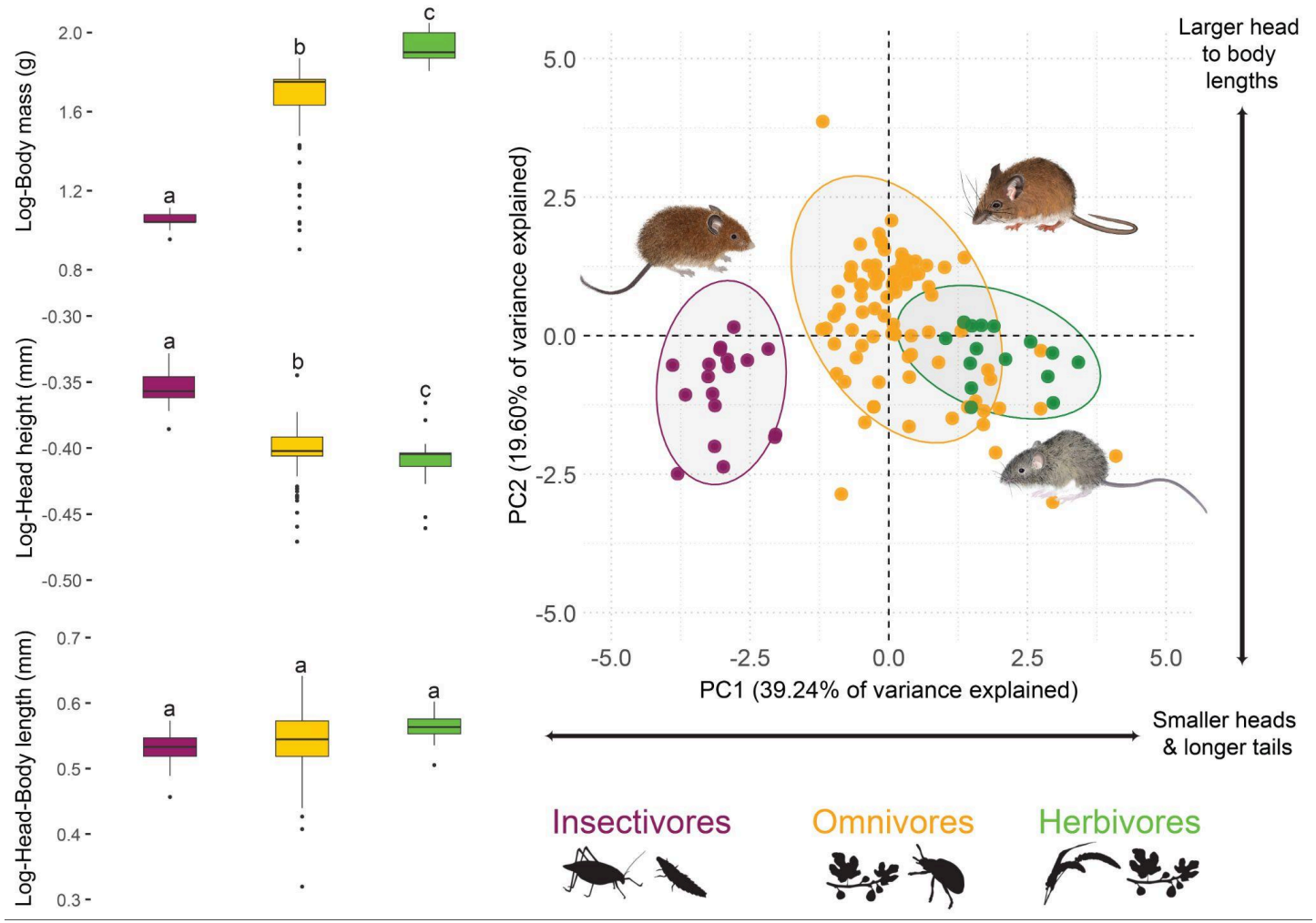

Figure 2.2. Differentiation among coexisting rodent species across major dietary classifications based on external morphological traits. Boxplots depict morphological variables with higher contribution among PCA axes. Different letters indicate significant variation of traits among dietary ecologies.

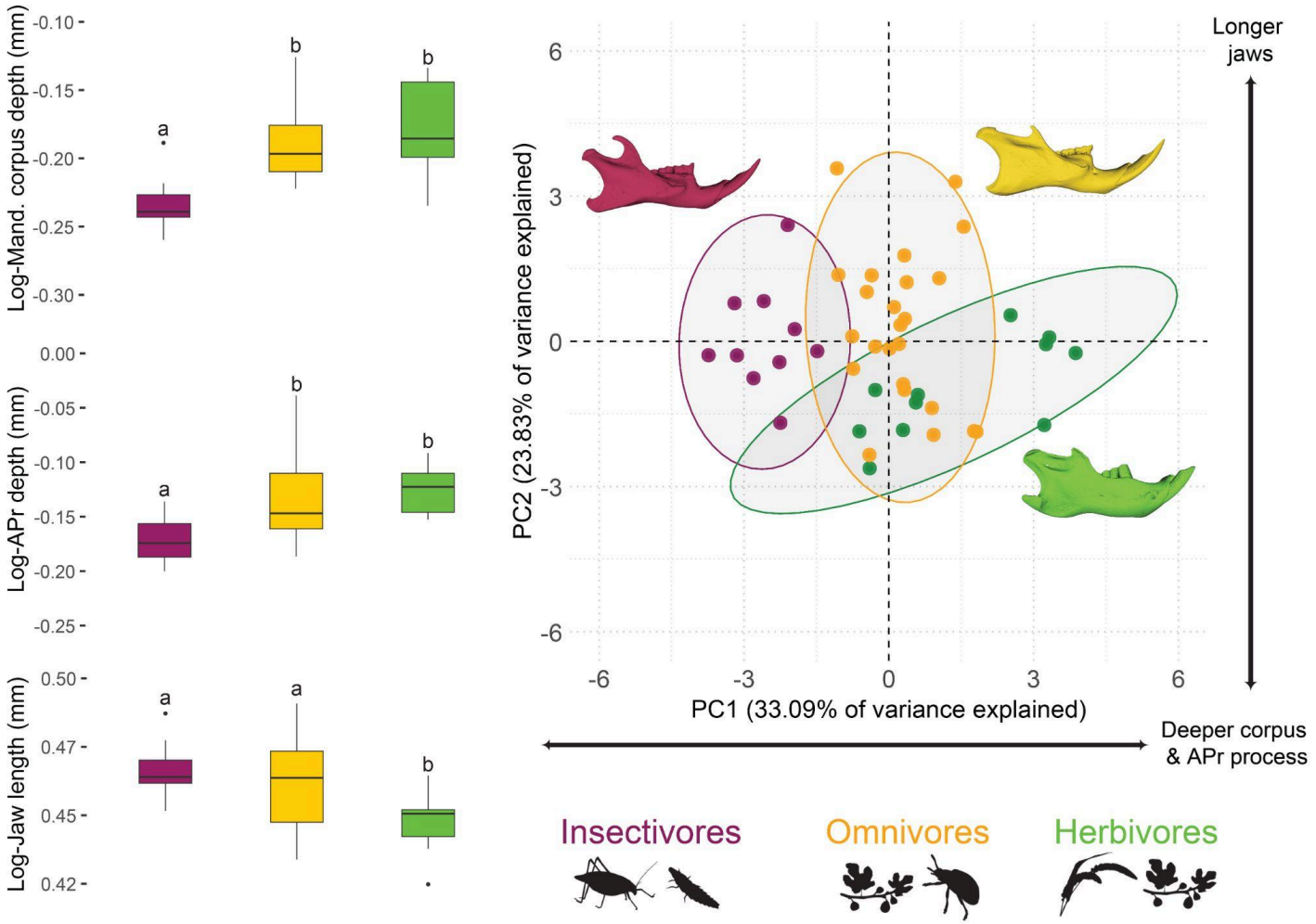

Figure 2.3. Differentiation among coexisting rodent species across major dietary classifications based on mandibular traits. Boxplots depict morphological variables with higher contribution among PCA axes. Different letters indicate significant variation of traits among dietary ecologies.

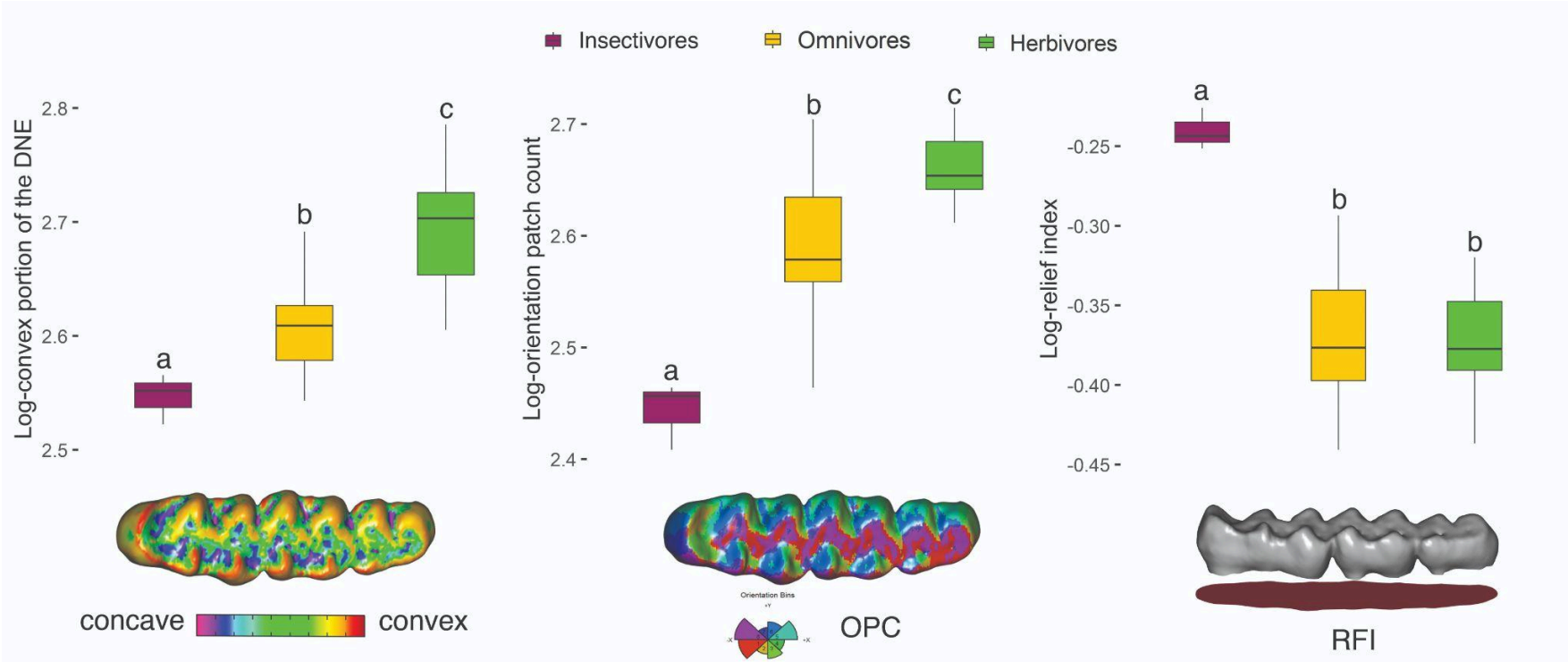

Figure 2.4. Trends in molar topography metrics among major dietary classifications. Different letters indicate significant variation of traits among dietary ecologies.

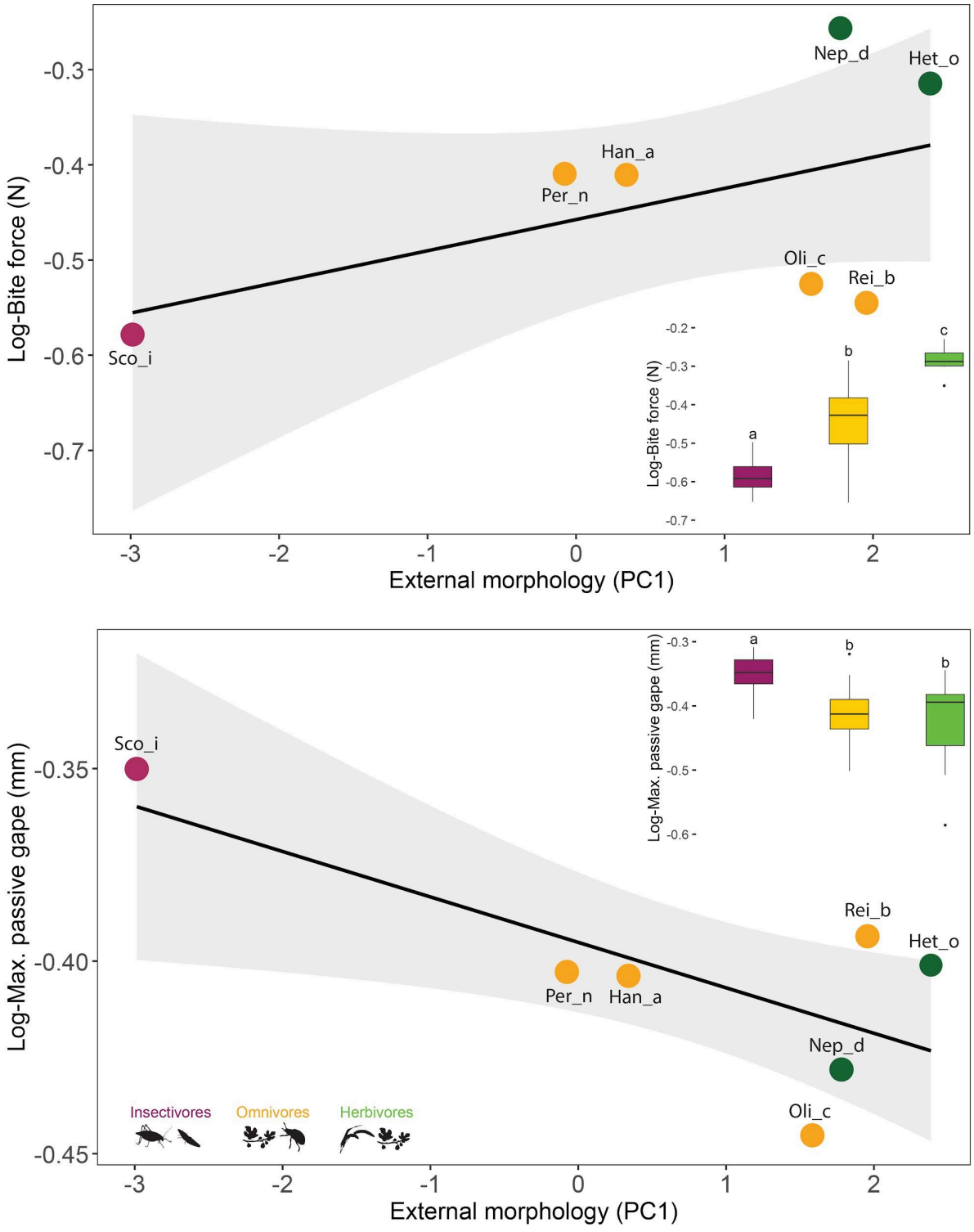

Figure 2.5. Graphical representation of the best fitting models depicting the relationships between performance metrics bite force (top) and maximum passive gape (bottom), and

external morphological traits (PC1) and feeding ecology. Boxplots within the plots show trends in bite force and maximum passive gape in relation to feeding ecology. Different letters indicate significant variation of traits among dietary ecologies. Sco_i: *Scotinomys irazu*; Han_a: *Handleyomys alfaroi*; Oli_c: *Oligoryzomys costaricensis*; Rei_b: *Reithrodontomys brevirostris*; Per_n: *Peromyscus nudipes*; Nep_d: *Nephelomys devius*; Het_o: *Heteromys oresterus*.

2.9 REFERENCES

Abrams, P.A. 2022. Competition Theory in Ecology. Oxford University Press, USA.

Aguirre L.F., Herrel, A., van Damme R., & Matthysen, E. 2002. Ecomorphological analysis of trophic niche partitioning in a tropical savannah bat communityProc. R. Soc. Lond. B.2691271–1278. doi: 10.1098/rspb.2002.2011

Arbour, J.H., Curtis, A.A., & Santana, S.E. 2019. Signatures of echolocation and dietary ecology in the adaptive evolution of skull shape in bats. Nat Commun 10, 2036. doi: 10.1038/s41467-019-09951-y

Baeckens, S., García-Roa, R., Martín, J., Ortega, J., Huyghe, K., & Van Damme, R. 2016. Fossorial and durophagous: implications of molluscivory for head size and bite capacity in a burrowing worm lizard. Journal of Zoology, 301(3): 193–205. https://doi.org/10.1111/jzo.12412

Barbero, S., Teta, P., & Cassini, G.H. 2023. An ecomorphological approach to the relationship between craniomandibular morphology and diet in sigmodontine rodents from central-eastern Argentina, Zoology, 156: 126066. https://doi.org/10.1016/j.zool.2022.126066.

Berthaume, M.A. 2016. Food mechanical properties and dietary ecology. American Journal of Physical Anthropology, 159: 79–104.

Berthaume, M.A., Lazzari, V., & Guy. F. 2020. The landscape of tooth shape: Over 20 years of dental topography in primates. Evolutionary Anthropology, 29(5): 245-262. doi: 10.1002/evan.21856

Binder, W.J. & Valkenburgh, B. 2000. Development of bite strength and feeding behaviour in juvenile spotted hyenas (Crocuta crocuta). Journal of Zoology, 252: 273–283.

Boyer, D.M. 2008. Relief index of second mandibular molars is a correlate of diet among prosimian primates and other euarchontan mammals. J. Human Evol., 55: 1118–1137.

Castresana, J. 2001. Cytochrome b Phylogeny and the Taxonomy of Great Apes and Mammals, Molecular Biology and Evolution, 18(4): 465–471. doi: 10.1093/oxfordjournals.molbev.a003825

Chinchilla, F.A. 2009. Seed predation by mammals in forest fragments in Monteverde, Costa Rica. Rev Biol Trop. 57(3): 865–77. doi: 10.15517/rbt.v57i3.5499. PMID: 19928478.

Crompton, A.W., Owerkowicz, T, & Skinner, J. 2010. Masticatory motor pattern in the koala (Phascolarctos cinereus): a comparison of jaw movements in marsupial and placental herbivores. J. Exp. Zool. A Ecol. Genet. Physiol. 313:564–578.

Claude, J. 2013. Log-shape ratios, Procrustes superimposition, elliptic Fourier analysis: three worked examples in R. Hystrix, It. J. Mamm., 24: 94–102.

Cox, P.G., Rayfield, E.J., Fagan, M.J., Herrel, A., Pataky, T.C., & Jeffery, N. 2012. Functional evolution of the feeding system in rodents. PLoS One, 7(4): p.e36299.

Dumont, E.R., Davalos, L.M., Goldberg, A., Santana, S.E., Rex, K., & Voigt, C.C. 2012. Morphological innovation, diversification and invasion of a new adaptive zone. Proceedings of the Royal Society B: Biological Sciences, 279(1734): 1797–1805. doi: 10.1098/rspb.2011.2005

Dumont, E.R. & Herrel, A. 2003. The effects of gape angle and bite point on bite force in bats. Journal of Experimental Biology, 206: 2117–2123.

Edgar, R.C. 2004. MUSCLE: multiple sequence alignment with high accuracy and high throughput. Nucleic acids research, 32(5): 1792–1797. doi: 10.1093/nar/gkh340

Eisenberg, J.F. 1981. The mammalian radiations: an analysis of trends in evolution, adaptation, and behaviour. Chicago Univ. Press, Chicago.

Evans, A.R., & Pineda-Munoz, S. 2018. Inferring mammal dietary ecology from dental morphology. In D.A. Croft, D.F. Su, & S.W. Simpson (Eds.), Methods in paleoecology: Reconstructing Cenozoic terrestrial environments and ecological communities (pp. 37–51). Springer International Publishing.

Fedorov, A., Beichel, R., Kalpathy-Cramer, J., Finet, J., Fillion-Robin, J.C., Pujol, S., Bauer, C., Jennings, D., Fennessy, F., Sonka, M. & Buatti, J. 2012. 3D Slicer as an image computing platform for the Quantitative Imaging Network. Magnetic resonance imaging, 30(9): 1323–1341.

Felsenstein, J. 1985. Phylogenies and the Comparative Method. The American Naturalist, 125(1): 1–15.

Grossnickle, D.M., & Polly, P.D. 2013. Mammal disparity decreases during the Cretaceous angiosperm radiation. Proc. R. Soc. B Biol. Sci. 280: 20132110.

Grossnickle, D.M. 2017. The evolutionary origin of jaw yaw in mammals. Sci. Rep. 7:45094.

Grossnickle, D.M. 2020. Feeding ecology has a stronger evolutionary influence on functional morphology than on body mass in mammals. Evolution, 74: 610-628. doi: 10.1111/evo.13929

Hafner, D.J. 2016. Family Heteromyidae (Pocket mice, Kangaroo mice and Kangaroo rats). Pp. 170–234 in. Wilson, D.E., Lacher, T.E., Jr & Mittermeier, R.A. eds (2016). Handbook of the Mammals of the World. Vol. 6. Lagomorphs and Rodents I. Lynx Edicions, Barcelona.

Herring, S.W., & Herring, S.E. 1974. The Superficial Masseter and Gape in Mammals. The American Naturalist, 108(962), 561–576.

Huey, R.G., & Hertz, P.E. 1984. Is a Jack-of-All-Temperatures a Master of None?. Evolution, 38: 441–444. doi: 10.2307/2408502

Hooper, E.T., & Carleton, M.D. 1976. Reproduction, growth and development in two contiguously allopatric rodent species, genus Scotinomys. Misc. Publ. Mus. Zool., Univ. Michigan, 151: 1–52.

ImageJ (U.S. National Institutes of Health, Bethesda, MD, 1997–2014). 26.

Kaczmarek, E.B., & Gidmark, N.J. 2020. The bite force–gape relationship as an avenue of biomechanical adaptation to trophic niche in two salmonid fishes. Journal of Experimental Biology, 223(20): jeb223180.

Leiser‐Miller, L.B., Kaliszewska, Z.A., Villalobos‐Chaves, D., & Santana, S.E. 2019. A pygmy rice rat eats a peppery snack. Frontiers in Ecology & the Environment, 17(7).

Leisler, B., & Thaler, E. 1982. Differences in morphology and foraging behaviour in the goldcrest *Regulus regulus* and firecrest *R. ignicapillus*. Annales Zoologici Fennici, 19(4): 277–284.

Maestri, R., Monteiro, L.R., Fornel, R., Upham, N.S., Patterson, B.D., & de Freitas, T.R. O. 2017. The ecology of a continental evolutionary radiation: Is the radiation of sigmodontine rodents adaptive? Evolution, 1–56. doi: 10.1111/evo.13155

Mares, M.A. 1976. Convergent evolution of desert rodents: multivariate analysis and zoogeographic implications. Paleobiology, 2(1): 39–63. doi:10.1017/S0094837300003298

Maynard Smith, J., & R. J. G. Savage. 1959. The mechanics of mammalian jaws. School Sci. Rev., 141: 289–301.

Mincer, S.T. & Russo, G.A. 2020. Substrate use drives the macroevolution of mammalian tail length diversity. Proceedings of the Royal Society B, 287(1920), p.20192885.

Minh, B.Q., Schmidt, H.A., Chernomor, O., Schrempf, D., Woodhams, M.D., von Haeseler, V., & Lanfear, R. 2020. IQ-TREE 2: New Models and Efficient Methods for Phylogenetic Inference in the Genomic Era, Molecular Biology and Evolution, 37(5): 1530–1534. doi: 10.1093/molbev/msaa015

Missagia, R.V., Patterson, B.D., Krentzel, D., & Perini, F.A. 2020. Insectivory leads to functional convergence in a group of Neotropical rodents. Journal of Evolutionary Biology, 34(2): 391–402. doi: 10.1111/jeb.13748

Mosimann, J.E. 1970. Size allometry: size and shape variables with characterizations of the lognormal and generalized gamma distributions. J. Am. Stat. Assoc., 65: 930–945.

Nogueira, M.R., Peracchi, A.L., & Monteiro, L.R. 2009. Morphological correlates of bite force and diet in the skull and mandible of phyllostomid bats. Functional Ecology, 23(4): 715–-723.

Norconk, M.A., Wright, B.W., Conklin-Brittain, N.L. & Vinyard, C.J. 2009. Mechanical and nutritional properties of food as factors in Platyrrhine dietary adaptations. South American Primates (eds. P. Garber, A. Estrada, J. Bicca-Marques, E. Heymann & K. Strier kbstrier), pp. 279–319. Springer New York, New York.

Oksanen. J., Simpson, G., Blanchet, F., Kindt, R., Legendre, P., Minchin, P., O'Hara, R., Solymos, P., Stevens, M., Szoecs, E., Wagner, H., Barbour, M., Bedward, M., Bolker, B., Borcard, D., Carvalho, G., Chirico, M., De Caceres, M., Durand, S., Evangelista, H., FitzJohn, R., Friendly, M., Furneaux, B., Hannigan, G., Hill, M., Lahti, L., McGlinn, D., Ouellette, M., Ribeiro Cunha, E., Smith, T., Stier, A., Ter Braak, C., & Weedon, J. 2024. _vegan: Community Ecology Package_. R package version 2.6-6.1, <https://CRAN.R-project.org/package=vegan>.

Pampush, J.D., Winchester, J.M., Morse, P.E., Vining, A.Q., Boyer, D.M., & Kay, R.F. 2016. Introducing molaR: a new R package for quantitative topographic analysis of teeth (and other topographic surfaces). Journal of Mammalian Evolution, 23: 397–412. doi: 10.1007/s10914-016-9326-0

Paradiñas, U.F.J., Myers, P., León-Paniagua, L., Ordóñez Garza, N., Cook, J.A., Kryštufec, B., Hauslauer, R., Bradley, R.D., Shenbrot, G.I., & Patton, J.L. 2017. Family Cricetidae (True Hamsters, Voles, Lemmings and New World Rats and Mice). PP: 204–535. In: Wilson, D. E.., Lacher, T. E., Jr & Mittermeier, R. A. eds. (2017). *Handbook of the Mammals of the World*. Vol. 7. Rodents II. Lynx Edicions, Barcelona.

Pena, E.A., & Slate, E.H. 2019. _gvlma: Global Validation of Linear Models Assumptions_. R package version 1.0.0.3, <https://CRAN.R-project.org/package=gvlma>.

Peters, R.H. 1986. The ecological implications of body size.Vol. 2. Cambridge Univ. Press, Cambridge, UK.

Pineda-Munoz, S., & Alroy, J. 2014. Dietary characterization of terrestrial mammals. Proc. R. Soc. B. 28120141173. doi: 10.1098/rspb.2014.1173

R Core Team. 2023. R: A Language and Environment for Statistical Computing_. R Foundation for Statistical Computing, Vienna, Austria. <https://www.R-project.org/>.

Radinsky, L.B. 1968. A new approach to mammalian cranial analysis, illustrated by examples of prosimian primates. J. Morphol. 124:167–179.

Radinsky, L.B. 1985. Approaches in evolutionary morphology: a search for patterns. Annu. Rev. Ecol. Syst. 16:1–14.

Rao, X., Yang, C., Ma, L., Zhang, J., Liang, W., & Møller, A.P. 2018. Comparison of head size and bite force in two sister species of parrotbills. Avian Research, 9: 1–6.

Revell, L.J. 2012. phytools: an R package for phylogenetic comparative biology (and other things). Methods Ecol. Evol., 3: 217–223.

Roslin, T., & Salminen, J.P. 2008. Specialization pays off: contrasting effects of two types of tannins on oak specialist and generalist moth species. Oikos, 117: 1560–1568. doi: 10.1111/j.0030-1299.2008.16725.x

Ross, C.F. & Iriarte-Diaz, J. 2014. What does feeding system morphology tell us about feeding? Evolutionary Anthropology: Issues, News, and Reviews, 23: 105–120.

RÜber, L., & Adams, D.C. 2001. Evolutionary convergence of body shape and trophic morphology in cichlids from Lake Tanganyika, Journal of Evolutionary Biology, 14(2): 325–332. doi: 10.1046/j.1420-9101.2001.00269.x

Russo, G.A. 2015. Postsacral vertebral morphology in relation to tail length among primates and other mammals. The Anatomical Record, 298: 354–375.

Samuels, J.X. 2009. Cranial morphology and dietary habits of rodents. Zoological Journal of the Linnean Society, 156(4): 864–888. doi: 10.1111/j.1096-3642.2009.00502.x

Sanson, G. 2006. The biomechanics of browsing and grazing. American Journal of Botany, 93(10): 1531–1545.

Santana, S.E. & Dumont, E.R. 2009. Connecting behaviour and performance: the evolution of biting behaviour and bite performance in bats. Journal of Evolutionary Biology, 22: 2131–2145. doi: 10.1111/j.1420-9101.2009.01827.x

Santana, S.E., Strait, S., & Dumont, E.R. 2011. The better to eat you with: functional correlates of tooth structure in bats. Functional Ecology, 25: 839–847. doi: 10.1111/j.1365-2435.2011.01832.x

Santana, S.E. 2015. Quantifying the effect of gape and morphology on bite force: biomechanical modeling and in vivo measurements in bats. Functional Ecology, 30: 557–565. doi: 10.1111/1365-2435.12522

Selig, K.R., Sargis, E.J., & Silcox, M.T. 2019. The frugivorous insectivores? Functional morphological analysis of molar topography for inferring diet in extant treeshrews (Scadentia). Journal of Mammalogy, 100: 1–17. doi: 10.1093/jmammal/gyz151

Sheard, C., Skinner, N., & Caro, T. 2024. The Evolution of Rodent Tail Morphology. The American Naturalist, 203(6), pp.629-643.

Strait, S.G. 1993. Molar morphology and food texture among small-bodied insectivorous mammals. Journal of Mammalogy, 74: 391–402. doi: 10.2307/1382395

Turnbull, W.D. 1970. Mammalian masticatory apparatus. Fieldiana Geol. 18:149–356.

Ungar, P.S. 2010. Mammal teeth: origin, evolution, and diversity. JHU Press.

Verde Arregoitia, L.D.V., Fisher, D.O., & Schweizer, M. 2017. Morphology captures diet and locomotor types in rodents. R. Soc. Open Sci. 4:160957.

Verde Arregoitia, L.D., & D'Elía, G. 2021. Classifying rodent diets for comparative research. Mammal Review, 51(1): 51-65.

Verwaijen, D., Van Damme, R., & Herrel, A. 2002. Relationships between head size, bite force, prey handling efficiency and diet in two sympatric lacertid lizards. Functional Ecology, 16(6): 842–850.

Villalobos-Chaves, D., & Santana, S.E. 2021. Craniodental traits predict feeding performance and dietary hardness in a community of Neotropical free-tailed bats (Chiroptera: Molossidae). Functional Ecology, 36: 1690–1699. doi: 10.1111/1365-2435.14063

Wells, K., Pfeiffer, M., Lakim, M. B., & Linsenmair, K. E. 2004. Use of arboreal and terrestrial space by a small mammal community in a tropical rainforest in Borneo, Malaysia. Journal of Biogeography, 31(4): 641–652.

Williams, S.H., Peiffer, E., & Ford, S. 2009. Gape and bite force in the rodents *Onychomys leucogaster* and *Peromyscus maniculatus*: Does jaw-muscle anatomy predict performance?. J. Morphol., 270: 1338–1347. doi: 10.1002/jmor.10761

Wilson, D.E., & Reeder, D.M. eds., 2005. Mammal species of the world: a taxonomic and geographic reference (Vol. 1). JHU press.

Winchester, J.M., Boyer, D.M., St. Clair, E.M., Gosselin-Ildari, A.D., Cooke, S.B., & Ledogar, J.A. 2014. Dental topography of platyrrhines and prosimians: Convergence and contrasts. American Journal of Physical Anthropology, 153: 29–44. doi: 10.1002/ajpa.22398

2.10 SUPPORTING TABLES AND FIGURES FOR CHAPTER 2

Table S2.1. Results (p-values) from the post-hoc pairwise T-test comparisons using the Holm method on molar, external and mandibular traits in relationship with diet categories.

Molar traits	Convex DNE	Relief Index	Orientation Patch Count							
Herbivores-Insectivores	**1.3e-05**	**2.5e-05**	**5.9e-06**							
Omnivores-Insectivores	**0.049**	**2.5e-05**	**0.00041**							
Omnivores-Herbivores	**3.9e-06**	0.62	**0.00284**							
External traits	Body mass	Head-body length	Tail length	Hind-foot length	Ear length	Head width	Head length	Head height		
Herbivores-Insectivores	**< 2e-16**	0.10	**< 2e-16**	**0.013**	**1.7e-08**	**< 2e-16**	**3.5e-06**	**2.5e-15**		
Omnivores-Insectivores	**1e-15**	0.44	**< 2e-16**	0.097	**0.015**	**< 2e-16**	**0.0021**	**1.5e-15**		
Omnivores-Herbivores	**1e-14**	0.11	**1e-06**	**5.9e-06**	**3.2e-07**	**0.0068**	**0.0021**	0.22		
Mandibular traits	Jaw length	Joint elevation	Cpr elevation	Apr elevation	Corpus depth	Joint to M1 distance	JCPr distance	JAPr posterior	JAPr ventral	JAPr angle
Herbivores-Insectivores	**0.012**	0.484	**0.00058**	**0.0045**	**3.1e-05**	**2.4e-05**	**0.00650**	0.140	**0.00064**	**9.5e-06**
Omnivores-Insectivores	0.404	0.097	**1.4e-06**	**0.0045**	**0.00018**	**0.0026**	**0.00039**	0.140	0.07585	**0.0039**
Omnivores-Herbivores	**0.015**	0.316	0.18216	0.4701	0.12509	**0.0140**	0.56003	**0.001**	**0.00889**	**0.0039**

Table S2.2. Summary of the principal component analysis performed on external morphological traits and mandibular measurements. Abbreviations: PC, loadings for each variable at each component; % variance, explained variance.

Variable (external morphology)	PC1	PC2	PC3
Head and body length	-0.05388	0.608305	0.590504
Tail length	0.522227	0.041098	0.040667
Hind foot length	0.152528	-0.4398	0.677516
Ear length	-0.33572	0.253022	-0.32091
Head width	-0.45952	-0.34552	0.071713
Head length	-0.40565	0.37157	0.247693
Head height	-0.46119	-0.33672	0.145423
Eigenvalues	2.746777	1.371829	0.960725
% variance	39.23967	19.59756	13.72464
Variable (mandibular morphology)			
Jaw length	-0.11176	0.602735	0.11597
joint elevation	-0.25413	-0.02841	0.50547
CPr elevation	-0.32924	-0.17314	0.386218
APr depth	0.433044	0.113234	0.149918
Corpus depth	0.484273	0.152301	-0.00156
jaw joint to M1	-0.24888	0.518786	0.094064
JCPr length	0.239207	0.346628	-0.21332
JAPr posterior length	-0.13042	0.262471	0.319524
JAPr ventral length	0.373078	0.16271	0.435179
JAPr angle	0.342235	-0.29198	0.462145
EVL	3.309217	2.383361	1.571648
% variance	33.09217	23.83361	15.71648

Table S2.3. Fit of regression models for bite force and maximum passive gape estimates. F = F-statistic; R^2 = R squared; p = p-value. Models are ranked by R^2 values.

#	Models (bite force)	F	R^2	p
1	Bite force ~ External morphology (PC1) * External morphology (PC2)	10.2	0.82	**0.043**
2	Bite force ~ External morphology (PC1) + External morphology (PC2) + Mandibular traits (PC2)	5.23	0.67	0.103
3	Bite force ~ External morphology (PC2) + Mandibular traits (PC1) + Mandibular traits (PC2)	4.13	0.61	0.137
4	Bite force ~ External morphology (PC1) + External morphology (PC2) + Mandibular traits (PC1) + Mandibular traits (PC2)	2.68	0.52	0.289
5	Bite force ~ Mandibular traits (PC1) * Mandibular traits (PC2)	2.89	0.48	0.203
6	Bite force ~ External morphology (PC2) * Mandibular traits (PC2)	2.80	0.47	0.209
7	Bite force ~ External morphology (PC1) * Mandibular traits (PC2)	2.71	0.46	0.216
8	Bite force ~ External morphology (PC2) + Mandibular traits (PC2)	3.05	0.40	0.156
9	Bite force ~ External morphology (PC1) + Mandibular traits (PC2)	2.64	0.35	0.185
10	Bite force ~ External morphology (PC1) + External morphology (PC2)	2.54	0.34	0.193
11	Bite force ~ External morphology (PC2) + Mandibular traits (PC1)	2.43	0.32	0.203
12	Bite force ~ External morphology (PC2) * Mandibular traits (PC1)	1.86	0.30	0.319
13	Bite force ~ Mandibular traits (PC1) + Mandibular traits (PC2)	2.25	0.29	0.221
14	Bite force ~ External morphology (PC1) : Mandibular traits (PC2)	3.39	0.28	0.124
15	Bite force ~ Mandibular traits (PC2)	3.09	0.25	0.138
16	Bite force ~ External morphology (PC1) + External morphology (PC2) + Mandibular traits (PC1)	1.36	0.15	0.403
17	Bite force ~ External morphology (PC1) + Mandibular traits (PC1) + Mandibular traits (PC2)	1.32	0.13	0.411
18	Bite force ~ External morphology (PC2)	1.81	0.11	0.235
19	Bite force ~ External morphology (PC1) : Mandibular traits (PC1) : Mandibular traits (PC2)	1.80	0.11	0.237
20	Bite force ~ External morphology (PC1)	1.56	0.08	0.265
21	Bite force ~ Mandibular traits (PC1)	1.40	0.06	0.290
22	Bite force ~ Mandibular traits (PC1) : Mandibular traits (PC2)	0.68	-0.0	0.446
23	Bite force ~ External morphology (PC2) : Mandibular traits (PC1)	0.71	-0.0	0.437
24	Bite force ~ External morphology (PC2) : Mandibular traits (PC2)	0.53	-0.0	0.496
25	Bite force ~ External morphology (PC1) : External morphology (PC2) : Mandibular traits (PC2)	0.55	-0.0	0.489
26	Bite force ~ External morphology (PC1) : External morphology (PC2) : Mandibular traits (PC1)	0.48	-0.0	0.516
27	Bite force ~ External morphology (PC1) : External morphology (PC2) : Mandibular traits (PC1) : Mandibular traits (PC2)	0.47	-0.0	0.523
28	Bite force ~ External morphology (PC1) : Mandibular traits (PC1)	0.06	-0.1	0.807
29	Bite force ~ External morphology (PC1) + Mandibular traits (PC1)	0.65	-0.1	0.567
30	Bite force ~ External morphology (PC1) : External morphology (PC2)	0.11	-0.1	0.750
31	Bite force ~ External morphology (PC2) : Mandibular traits (PC1) : Mandibular traits (PC2)	0.03	-0.1	0.868
32	Bite force ~ External morphology (PC1) * Mandibular traits (PC1)	0.32	-0.5	0.807

#	**Models (maximum passive gape)**			
1	Gape ~ External morphology (PC1) + Mandibular traits (PC2)	4.70	0.55	0.089
2	Gape ~ External morphology (PC1)	6.60	0.48	**0.050**
3	Gape ~ External morphology (PC2) * Mandibular traits (PC1)	2.86	0.48	0.205
4	Gape ~ External morphology (PC1) : External morphology (PC2)	6.04	0.45	**0.057**
5	Gape ~ External morphology (PC2) : Mandibular traits (PC1)	5.89	0.44	**0.059**
6	Gape ~ External morphology (PC1) * Mandibular traits (PC1)	2.57	0.44	0.228
7	Gape ~ External morphology (PC1) + Mandibular traits (PC1) + Mandibular traits (PC2)	2.60	0.44	0.226
8	Gape ~ External morphology (PC1) * Mandibular traits (PC2)	2.53	0.43	0.232
9	Gape ~ External morphology (PC1) + External morphology (PC2) + Mandibular traits (PC2)	2.40	0.41	0.245
10	Gape ~ External morphology (PC1) + External morphology (PC2)	2.74	0.36	0.177
11	Gape ~ External morphology (PC1) + Mandibular traits (PC1)	2.75	0.36	0.177
12	Gape ~ Mandibular traits (PC1)	2.83	0.23	0.153
13	Gape ~ Mandibular traits (PC1) + Mandibular traits (PC2)	1.88	0.22	0.264
14	Gape ~ External morphology (PC1) * External morphology (PC2)	1.55	0.21	0.362
15	Gape ~ Mandibular traits (PC1) * Mandibular traits (PC2)	1.53	0.21	0.366
16	Gape ~ External morphology (PC1) : External morphology (PC2) : Mandibular traits (PC1)	2.43	0.19	0.179
17	Gape ~ External morphology (PC1) : Mandibular traits (PC1)	2.30	0.17	0.189
18	Gape ~ External morphology (PC1) + External morphology (PC2) + Mandibular traits (PC1)	1.42	0.17	0.389
19	Gape ~ External morphology (PC1) + External morphology (PC2) + Mandibular traits (PC1) + Mandibular traits (PC2)	1.32	0.17	0.473
20	Gape ~ External morphology (PC1) : External morphology (PC2) : Mandibular traits (PC1) : Mandibular traits (PC2)	2.13	0.15	0.203
21	Gape ~ External morphology (PC2) + Mandibular traits (PC1)	1.18	0.05	0.395
22	Gape ~ External morphology (PC1) : Mandibular traits (PC1) : Mandibular traits (PC2)	1.36	0.05	0.295
23	Gape ~ Mandibular traits (PC2)	1.15	0.02	0.331
24	Gape ~ External morphology (PC2) : Mandibular traits (PC1) : Mandibular traits (PC2)	1.02	0.00	0.357
25	Gape ~ External morphology (PC1) : Mandibular traits (PC2)	0.81	-0.0	0.408
26	Gape ~ External morphology (PC2) : Mandibular traits (PC2)	0.88	-0.0	0.390
27	Gape ~ Mandibular traits (PC1) : Mandibular traits (PC2)	0.68	-0.0	0.446
28	Gape ~ External morphology (PC2) + Mandibular traits (PC1) + Mandibular traits (PC2)	0.95	-0.0	0.513
29	Gape ~ External morphology (PC1) : External morphology (PC2) : Mandibular traits (PC2)	0.49	-0.0	0.511
30	Gape ~ External morphology (PC2)	0.00	-0.1	0.958
31	Gape ~ External morphology (PC2) * Mandibular traits (PC2)	0.46	-0.2	0.659
32	Gape ~ External morphology (PC2) * Mandibular traits (PC2)	0.24	-0.6	0.864

Bold numbers indicate statistical significance ($p < .05$). Signal '+' indicates the combination of variables, ':' indicates the interaction between variables, and 'x' indicates the combination of variables with the interactions between them.

Table S2.4. Fit of regression models for dietary ecology. F = F-statistic; R^2 = R squared; p = p-value. Models are ranked by R^2 values.

#	Models (Diet)	F	R^2	p
1	Diet ~ Bite force * External morphology (PC1)	283.3	0.99	**0.0003**
2	Diet ~ Bite force + External morphology (PC1) + Convex_DNE	221.6	0.99	**0.0005**
3	Diet ~ Bite force + External morphology (PC1) + External morphology (PC2) + Convex_DNE	1455	0.99	**0.0006**
4	Diet ~ Bite force + Gape + External morphology (PC1) + Mandibular traits (PC2)	187.6	0.99	**0.0053**
5	Diet ~ Bite force + External morphology (PC1) + Convex_DNE + RFI	179.4	0.99	**0.0055**
6	Diet ~ Bite force + External morphology (PC2) + Mandibular traits (PC1) + RFI	178.3	0.99	**0.0055**
7	Diet ~ Bite force + External morphology (PC1) + Convex_DNE + OPC	159.8	0.99	**0.0062**
8	Diet ~ Gape + External morphology (PC1) + External morphology (PC2) + Mandibular traits (PC2)	151.9	0.99	**0.0065**
9	Diet ~ Bite force + External morphology (PC1) + External morphology (PC2) + Mandibular traits (PC1) + Convex_DNE	5560	0.99	**0.0101**
10	Diet ~ Bite force + External morphology (PC2) + Mandibular traits (PC1) + Mandibular traits (PC2) + RFI	966.3	0.99	**0.0244**
11	Diet ~ Gape + External morphology (PC1) + Convex_DNE + RFI + OPC	660.1	0.99	**0.0295**
12	Diet ~ Bite force + Gape + External morphology (PC1) + External morphology (PC2) + Convex_DNE	584.6	0.99	**0.0313**
13	Diet ~ Bite force + Gape + External morphology (PC2) + Mandibular traits (PC1) + RFI	310.8	0.99	**0.0430**
14	Diet ~ Bite force + Gape + External morphology (PC1) + External morphology (PC2) + Mandibular traits (PC2)	236.5	0.99	**0.0493**
15	Diet ~ Bite force + External morphology (PC2) + Mandibular traits (PC1) + Mandibular traits (PC2) + OPC	173.2	0.99	**0.0576**
16	Diet ~ Bite force + Gape + External morphology (PC1) + Convex_DNE	110.9	0.98	**0.0089**
17	Diet ~ Bite force + External morphology (PC1) + RFI + OPC	110.9	0.98	**0.0089**
18	Diet ~ Bite force + External morphology (PC1) + External morphology (PC2) + Mandibular traits (PC1) + RFI	75.5	0.98	0.0871
19	Diet ~ Bite force + External morphology (PC1) + External morphology (PC2) + Mandibular traits (PC1) + OPC	71.31	0.98	0.0896
20	Diet ~ Bite force + External morphology (PC1) + Convex_DNE + RFI + OPC	77.92	0.98	0.0857
21	Diet ~ Gape + External morphology (PC1) + External morphology (PC2) + Mandibular traits (PC1) + Mandibular traits (PC2)	68.04	0.98	0.0917
22	Diet ~ Bite force + Gape + External morphology (PC1) + External morphology (PC2) + OPC	63.00	0.98	0.0953
23	Diet ~ Bite force + External morphology (PC1)	106.8	0.97	**0.0003**
24	Diet ~ Bite force + External morphology (PC1) + External morphology (PC2)	94.44	0.97	**0.0018**
25	Diet ~ Bite force + Gape + External morphology (PC1) + Mandibular traits (PC1)	73.82	0.97	**0.0026**
26	Diet ~ Bite force + Gape + External morphology (PC1)	71.21	0.97	**0.0027**
27	Diet ~ Bite force + External morphology (PC1) + RFI	68.46	0.97	**0.0029**
28	Diet ~ Bite force + Gape + External morphology (PC1) + External morphology (PC2)	68.27	0.97	**0.0144**
29	Diet ~ Bite force + External morphology (PC1) + External morphology (PC2) + Mandibular traits (PC1)	67.76	0.97	**0.0146**
30	Diet ~ Bite force + External morphology (PC1) + External morphology (PC2) + OPC	72.03	0.97	**0.0137**
31	Diet ~ Bite force + External morphology (PC2) + Mandibular traits (PC1) + OPC	60.72	0.97	**0.0162**
32	Diet ~ Bite force + External morphology (PC1) + External morphology (PC2) + Mandibular traits (PC2)	49.97	0.97	**0.0197**
33	Diet ~ Bite force + Gape + External morphology (PC1) + External morphology (PC2) + Mandibular traits (PC1)	40.51	0.97	0.1187

34	Diet ~ Bite force + External morphology (PC1) + Mandibular traits (PC2)	57.08	0.96	**0.0038**
35	Diet ~ Bite force + External morphology (PC1) + OPC	54.13	0.96	**0.0041**
36	Diet ~ Bite force + Gape + External morphology (PC1) + Mandibular traits (PC1)	48.73	0.96	**0.0202**
37	Diet ~ Bite force + Gape + External morphology (PC1) + RFI	44.58	0.96	**0.0220**
38	Diet ~ Bite force + External morphology (PC1) + External morphology (PC2) + RFI	48.47	0.96	**0.0203**
39	Diet ~ Bite force + Gape + External morphology (PC1) + OPC	35.72	0.95	**0.0274**
40	Diet ~ Bite force + External morphology (PC2) + Convex_DNE + RFI	29.88	0.95	**0.0326**
41	Diet ~ Bite force + Gape + External morphology (PC1) + External morphology (PC2) + RFI	29.49	0.95	0.1389
42	Diet ~ Bite force + Gape + External morphology (PC2) + Mandibular traits (PC1) + OPC	25.31	0.95	0.1497
43	Diet ~ Bite force + External morphology (PC1) + External morphology (PC2) + Mandibular traits (PC1) + Mandibular traits (PC2)	28.95	0.95	0.140
44	Diet ~ Bite force + External morphology (PC2) + OPC	34.8	0.94	**0.007**
45	Diet ~ Bite force + External morphology (PC2) + RFI	28.41	0.93	**0.010**
46	Diet ~ Bite force + Gape + Convex_DNE + RFI + OPC	18.2	0.93	0.176
47	Diet ~ Bite force + Mandibular traits (PC1)	39.02	0.92	**0.002**
48	Diet ~ Bite force + External morphology (PC2) + Mandibular traits (PC1)	25.71	0.92	**0.012**
49	Diet ~ Bite force + Mandibular traits (PC1) + RFI	25.92	0.92	**0.012**
50	Diet ~ Bite force + Mandibular traits (PC1) + OPC	25.33	0.92	**0.012**
51	Diet ~ Bite force + External morphology (PC2) + Convex_DNE + OPC	20.12	0.92	**0.047**
52	Diet ~ Bite force + Gape + Convex_DNE	23.95	0.91	**0.013**
53	Diet ~ Bite force * Mandibular traits (PC1)	22.04	0.91	**0.015**
54	Diet ~ Bite force + Gape + External morphology (PC2) + Mandibular traits (PC2)	17.64	0.91	0.054
55	Diet ~ Bite force + Gape + External morphology (PC2) + OPC	17.42	0.91	0.055
56	Diet ~ Bite force + Gape + External morphology (PC2) + Convex_DNE	16.36	0.91	0.058
57	Diet ~ Bite force + External morphology (PC2) + Mandibular traits (PC1) + Mandibular traits (PC2)	16.16	0.91	0.059
58	Diet ~ Bite force + External morphology (PC2) + RFI + OPC	17.62	0.91	0.054
59	Diet ~ Bite force + External morphology (PC2) + Convex_DNE + RFI + OPC	14.54	0.91	0.195
60	Diet ~ Bite force + Gape + Mandibular traits (PC1)	21.15	0.90	**0.016**
61	Diet ~ Bite force + Mandibular traits (PC1) + Mandibular traits (PC2)	19.61	0.90	**0.017**
62	Diet ~ Bite force + Mandibular traits (PC1) + Convex_DNE	19.92	0.90	**0.017**
63	Diet ~ Bite force + Gape + Mandibular traits (PC2) + Convex_DNE	15.96	0.90	0.059
64	Diet ~ External morphology (PC1) + External morphology (PC2) + RFI + OPC	15.44	0.90	0.061
65	Diet ~ External morphology (PC1) + Convex_DNE + RFI + OPC	15.05	0.90	0.063
66	Diet ~ Bite force + Gape + External morphology (PC2) + Mandibular traits (PC1) + Mandibular traits (PC2)	11.97	0.90	0.215
67	Diet ~ Bite force + Gape + External morphology (PC2) + Mandibular traits (PC1)	14.24	0.89	0.066
68	Diet ~ Bite force + Gape + External morphology (PC2) + RFI	14.21	0.89	0.066
69	Diet ~ Bite force + Gape + Mandibular traits (PC1) + Convex_DNE	13.48	0.89	0.070
70	Diet ~ Bite force + Mandibular traits (PC1) + Mandibular traits (PC2) + RFI	13.33	0.89	0.070
71	Diet ~ Bite force + Mandibular traits (PC1) + Convex_DNE + RFI	13.43	0.89	0.070
72	Diet ~ Gape + External morphology (PC1) + RFI + OPC	14.12	0.89	0.067

73	Diet ~ Bite force + Gape + Mandibular traits (PC1) + RFI	13.02	0.88	0.072
74	Diet ~ Bite force + Gape + Mandibular traits (PC1) + OPC	12.83	0.88	0.073
75	Diet ~ Bite force + Gape + Convex_DNE + RFI	12.22	0.88	0.077
76	Diet ~ Bite force + External morphology (PC2) + Mandibular traits (PC1) + Convex_DNE	13.03	0.88	0.072
77	Diet ~ Bite force + Mandibular traits (PC1) + Mandibular traits (PC2) + OPC	12.71	0.88	0.074
78	Diet ~ Bite force + Mandibular traits (PC1) + Convex_DNE + OPC	12.71	0.88	0.074
79	Diet ~ Bite force + Mandibular traits (PC1) + RFI + OPC	12.96	0.88	0.072
80	Diet ~ Bite force + Gape + Mandibular traits (PC1) + Mandibular traits (PC2)	11.09	0.87	**0.008**
81	Diet ~ Bite force + Gape + Convex_DNE + OPC	11.99	0.87	0.078
82	Diet ~ Bite force : External morphology (PC1) : Convex_DNE : RFI	42.07	0.87	**0.001**
83	Diet ~ Bite force : External morphology (PC1) : Convex_DNE : OPC	42.83	0.87	**0.001**
84	Diet ~ Bite force : External morphology (PC1) : RFI : OPC	41.47	0.87	**0.001**
85	Diet ~ Bite force : External morphology (PC1) : Convex_DNE : RFI : OPC	43.70	0.87	**0.001**
86	Diet ~ Bite force : Gape : External morphology (PC1) : Convex_DNE : RFI : OPC	43.76	0.87	**0.001**
87	Diet ~ External morphology (PC1) * External morphology (PC2)	13.86	0.86	**0.029**
88	Diet ~ Bite force : External morphology (PC1) : Convex_DNE	39.00	0.86	**0.001**
89	Diet ~ Bite force : External morphology (PC1) : RFI	39.61	0.86	**0.001**
90	Diet ~ Bite force : External morphology (PC1) : OPC	39.87	0.86	**0.001**
91	Diet ~ Bite force : Gape : External morphology (PC1) : RFI	39.09	0.86	**0.001**
92	Diet ~ Bite force : External morphology (PC1)	36.04	0.85	**0.001**
93	Diet ~ External morphology (PC1) * OPC	13.19	0.85	**0.031**
94	Diet ~ Mandibular traits (PC1) * Mandibular traits (PC2)	12.53	0.85	**0.033**
95	Diet ~ Bite force + Mandibular traits (PC1) + Mandibular traits (PC2) + Convex_DNE	9.99	0.85	0.092
96	Diet ~ Bite force : Gape : External morphology (PC1) : Convex_DNE	35.77	0.85	**0.001**
97	Diet ~ Bite force : Gape : External morphology (PC1) : OPC	36.86	0.85	**0.001**
98	Diet ~ Bite force + Convex_DNE	17.28	0.84	**0.010**
99	Diet ~ RFI * OPC	12.11	0.84	**0.034**
100	Diet ~ Bite force + External morphology (PC2) + Convex_DNE	12.12	0.84	**0.034**
101	Diet ~ Bite force * Convex_DNE	11.85	0.84	**0.035**
102	Diet ~ Bite force : Gape : External morphology (PC1)	33.05	0.84	**0.002**
103	Diet ~ Bite force + Gape + Mandibular traits (PC2) + Convex_DNE	7.53	0.84	0.269
104	Diet ~ Convex_DNE : OPC	31.65	0.83	**0.002**
105	Diet ~ External morphology (PC2) + Mandibular traits (PC2)	11.38	0.83	**0.038**
106	Diet ~ Bite force + Convex_DNE + RFI	11.45	0.83	**0.037**
107	Diet ~ Bite force + Convex_DNE + OPC	10.97	0.83	**0.039**
108	Diet ~ Bite force + Gape + External morphology (PC2) + Mandibular traits (PC1) + Convex_DNE	7.28	0.83	0.273
109	Diet ~ Bite force + Gape + Mandibular traits (PC2) + Convex_DNE + RFI	6.98	0.83	0.279
110	Diet ~ Bite force + Gape + Mandibular traits (PC1) + Mandibular traits (PC2) + Convex_DNE	6.51	0.82	0.288
111	Diet ~ Bite force + External morphology (PC2) + Mandibular traits (PC1) + Mandibular traits (PC2) + Convex_DNE	6.48	0.82	0.289

112	Diet ~ External morphology (PC1) + External morphology (PC2) + Convex_DNE + RFI + OPC	6.82	0.82	0.282
113	Diet ~ RFI + OPC	14.32	0.81	**0.015**
114	Diet ~ Gape + Convex_DNE	14.18	0.81	**0.015**
115	Diet ~ External morphology (PC2) * OPC	10.09	0.81	**0.044**
116	Diet ~ Bite force + Gape + External morphology (PC2)	9.91	0.81	**0.045**
117	Diet ~ Bite force + External morphology (PC2)	13.68	0.80	**0.016**
118	Diet ~ Gape + External morphology (PC1) + Mandibular traits (PC2)	9.42	0.80	**0.048**
119	Diet ~ Bite force : Convex_DNE : OPC	25.99	0.80	**0.003**
120	Diet ~ Bite force : Convex_DNE	23.61	0.79	**0.004**
121	Diet ~ Bite force + OPC	12.9	0.79	**0.018**
122	Diet ~ Convex_DNE + OPC	12.6	0.79	**0.018**
123	Diet ~ Bite force + Mandibular traits (PC2) + Convex_DNE	8.73	0.79	0.054
124	Diet ~ Gape + Convex_DNE + OPC	8.73	0.79	0.054
125	Diet ~ Mandibular traits (PC1) + Mandibular traits (PC2) + OPC	8.99	0.79	0.052
126	Diet ~ Bite force + Mandibular traits (PC1) + Mandibular traits (PC2) + Convex_DNE	5.57	0.79	0.310
127	Diet ~ Bite force + Mandibular traits (PC1) + Convex_DNE + RFI + OPC	5.59	0.79	0.310
128	Diet ~ External morphology (PC1)+External morphology (PC2)+Mandibular traits (PC1) + Mandibular traits (PC2)+Convex_DNE	5.72	0.79	0.306
129	Diet ~ Mandibular traits (PC1) + OPC	12.6	0.78	**0.019**
130	Diet ~ External morphology (PC1) + Convex_DNE	11.79	0.78	**0.021**
131	Diet ~ Bite force + Gape	11.9	0.78	**0.020**
132	Diet ~ Gape * Convex_DNE	8.40	0.78	0.056
133	Diet ~ Gape + Mandibular traits (PC1) + Convex_DNE	8.29	0.78	0.057
134	Diet ~ Gape + RFI + OPC	8.37	0.78	0.057
135	Diet ~ External morphology (PC1) + External morphology (PC2) + Mandibular traits (PC2)	8.26	0.78	0.058
136	Diet ~ External morphology (PC1) + External morphology (PC2) + Convex_DNE	8.19	0.78	0.058
137	Diet ~ Bite force : Convex_DNE : RFI	22.94	0.78	**0.004**
138	Diet ~ Bite force : Convex_DNE : RFI : OPC	22.34	0.78	**0.005**
139	Diet ~ Bite force + Gape + Mandibular traits (PC1) + Mandibular traits (PC2) + RFI	5.37	0.78	0.315
140	Diet ~ Bite force + Mandibular traits (PC1) + Mandibular traits (PC2) + RFI + OPC	5.37	0.78	0.315
141	Diet ~ Bite force : OPC	21.49	0.77	**0.005**
142	Diet ~ Mandibular traits (PC1) * Convex_DNE	7.07	0.77	0.063
143	Diet ~ Bite force + RFI + OPC	7.92	0.77	0.061
144	Diet ~ Gape + External morphology (PC2) + Convex_DNE	7.96	0.77	0.061
145	Diet ~ External morphology (PC2) + Mandibular traits (PC1) + RFI + OPC	6.14	0.77	0.144
146	Diet ~ Bite force + Gape + Mandibular traits (PC1) + Mandibular traits (PC2) + OPC	5.13	0.77	0.322
147	Diet ~ Bite force + Mandibular traits (PC1) + Mandibular traits (PC2) + Convex_DNE + OPC	5.10	0.77	0.323
148	Diet ~ Bite force + Mandibular traits (PC2) + Convex_DNE + RFI + OPC	5.03	0.77	0.325
149	Diet ~ Mandibular traits (PC1) * OPC	7.45	0.76	0.066
150	Diet ~ Bite force + Gape + Mandibular traits (PC2)	7.66	0.76	0.064

151	Diet ~ Bite force + Gape + OPC	7.53	0.76	0.065
152	Diet ~ Gape + External morphology (PC1) + Convex_DNE	7.50	0.76	0.066
153	Diet ~ Gape + Mandibular traits (PC2) + Convex_DNE	7.42	0.76	0.066
154	Diet ~ Gape + Convex_DNE + RFI	7.65	0.76	0.064
155	Diet ~ Mandibular traits (PC2) + Convex_DNE + OPC	7.58	0.76	0.065
156	Diet ~ Convex_DNE + OPC + RFI	7.69	0.76	0.063
157	Diet ~ Bite force + Mandibular traits (PC2) + Convex_DNE + RFI	5.82	0.76	0.151
158	Diet ~ Bite force + Convex_DNE + RFI + OPC	5.86	0.76	0.150
159	Diet ~ Bite force	19.12	0.75	**0.007**
160	Diet ~ Bite force : RFI	19.15	0.75	**0.007**
161	Diet ~ External morphology (PC1) + OPC	10.3	0.75	**0.026**
162	Diet ~ External morphology (PC2) + OPC	10.05	0.75	**0.027**
163	Diet ~ Bite force + RFI	10.05	0.75	**0.027**
164	Diet ~ Mandibular traits (PC2) * Convex_DNE	7.18	0.75	0.069
165	Diet ~ Bite force * Gape	7.15	0.75	0.070
166	Diet ~ Bite force * External morphology (PC2)	7.29	0.75	0.068
167	Diet ~ Bite force * RFI	7.22	0.75	0.069
168	Diet ~ Mandibular traits (PC2) + Convex_DNE + RFI	7.26	0.75	0.068
169	Diet ~ Gape + External morphology (PC2) + RFI + OPC	5.53	0.75	0.158
170	Diet ~ Gape + Mandibular traits (PC1) + RFI + OPC	5.51	0.75	0.159
171	Diet ~ Gape + Mandibular traits (PC2) + RFI + OPC	5.69	0.75	0.155
172	Diet ~ Mandibular traits (PC1) + Convex_DNE + RFI + OPC	5.55	0.75	0.158
173	Diet ~ Bite force : Gape : Convex_DNE : RFI	19.46	0.75	**0.006**
174	Diet ~ Bite force : Gape : Convex_DNE : RFI : OPC	19.49	0.75	**0.006**

Asterisks indicate statistical significance ($p < .05$). Signal '+' indicates the combination of variables, ':' indicates the interaction between variables, and 'x' indicates the combination of variables with the interactions between them.

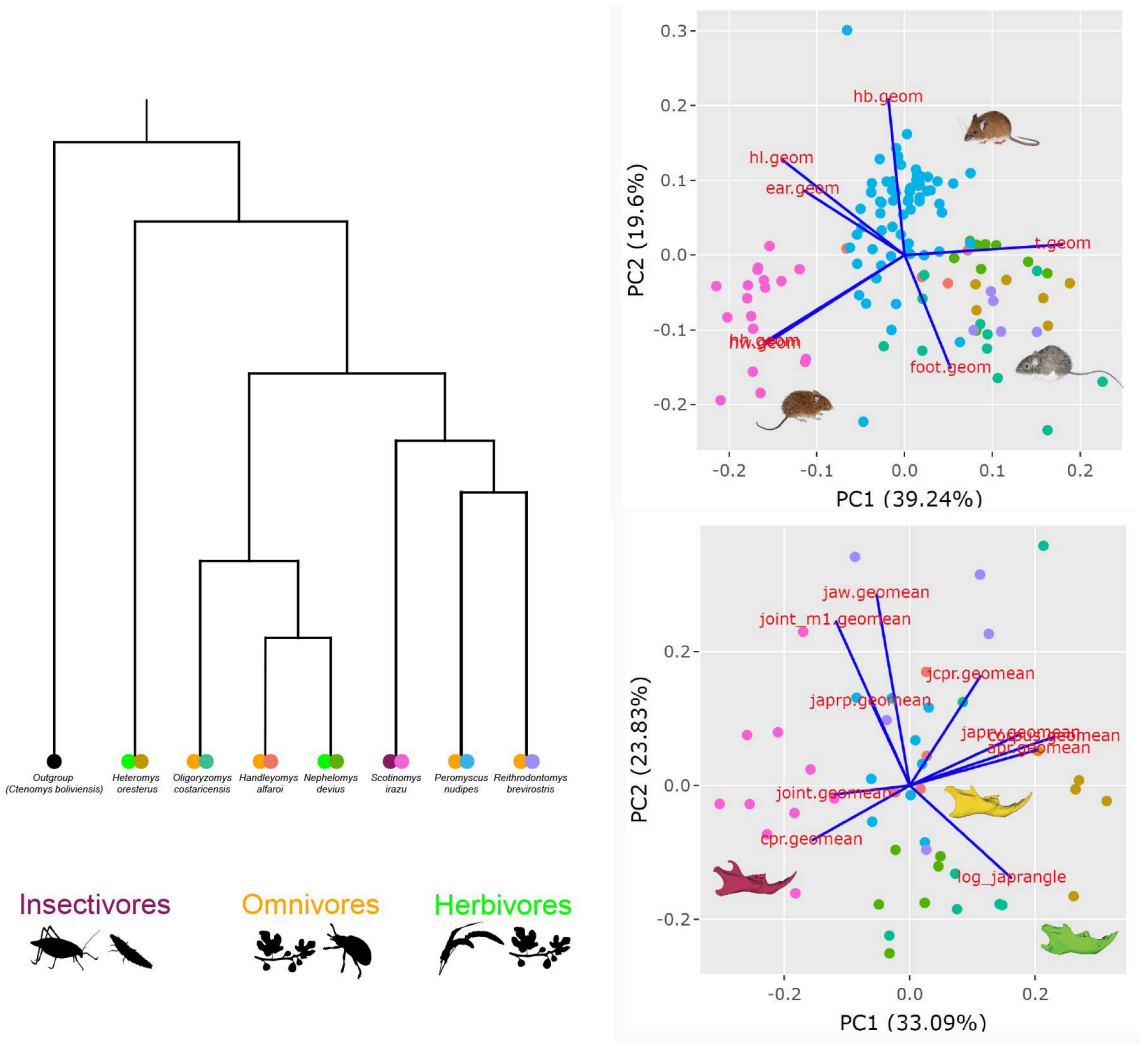

Figure S2.1. Most parsimonious tree topology (left) and PCA plots depicting the position of coexisting rodent species based on external morphological (upper right) and mandibular traits (lower right). Colors at the tip of the species at phylogeny indicate dietary ecology (left circle) and identity on the PCA's (right circle).

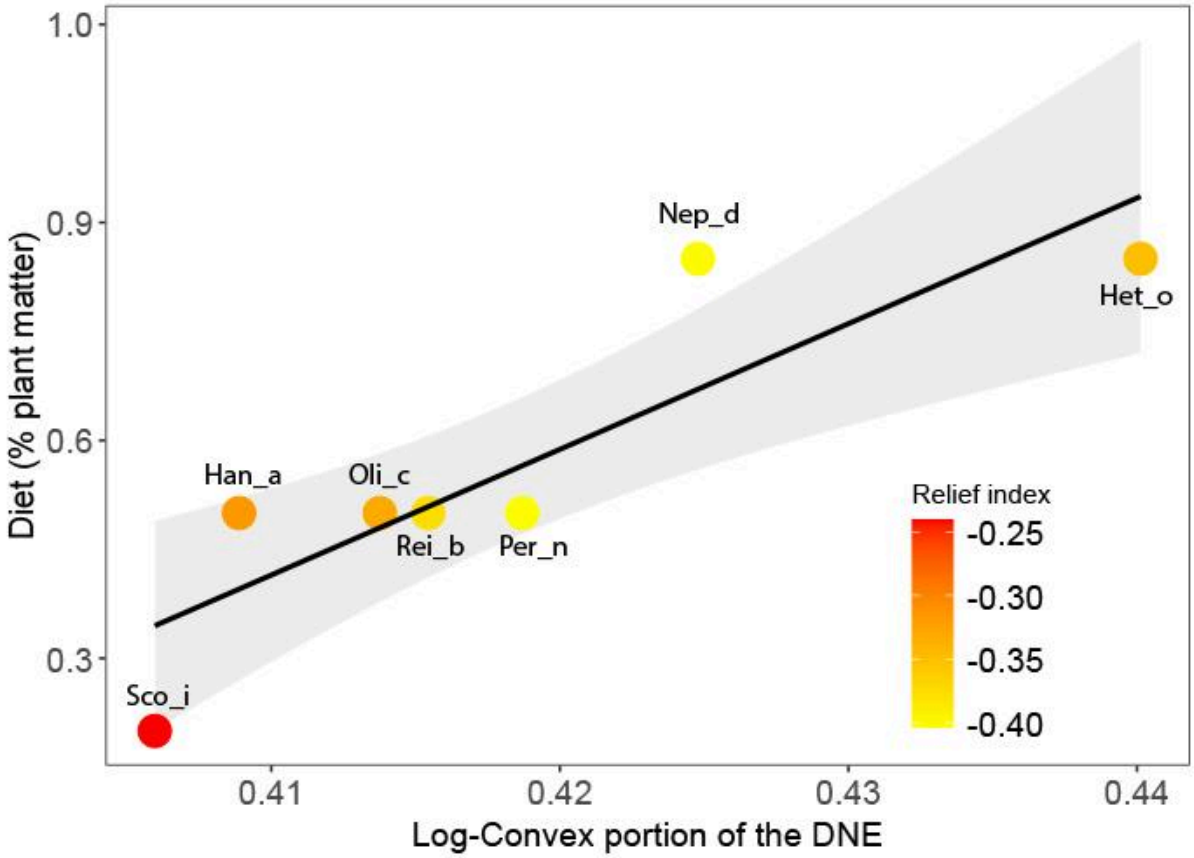

Figure S2.2. Graphical representation of the relationships between diet (as indicated by the percentage of plant matter) and dental metrics with high predictive power in the models. Sco_i: *Scotinomys irazu*; Han_a: *Handleyomys alfaroi*; Oli_c: *Oligoryzomys costaricensis*; Rei_b: *Reithrodontomys brevirostris*; Per_n: *Peromyscus nudipes*; Nep_d: *Nephelomys devius*; Het_o: *Heteromys oresterus*.

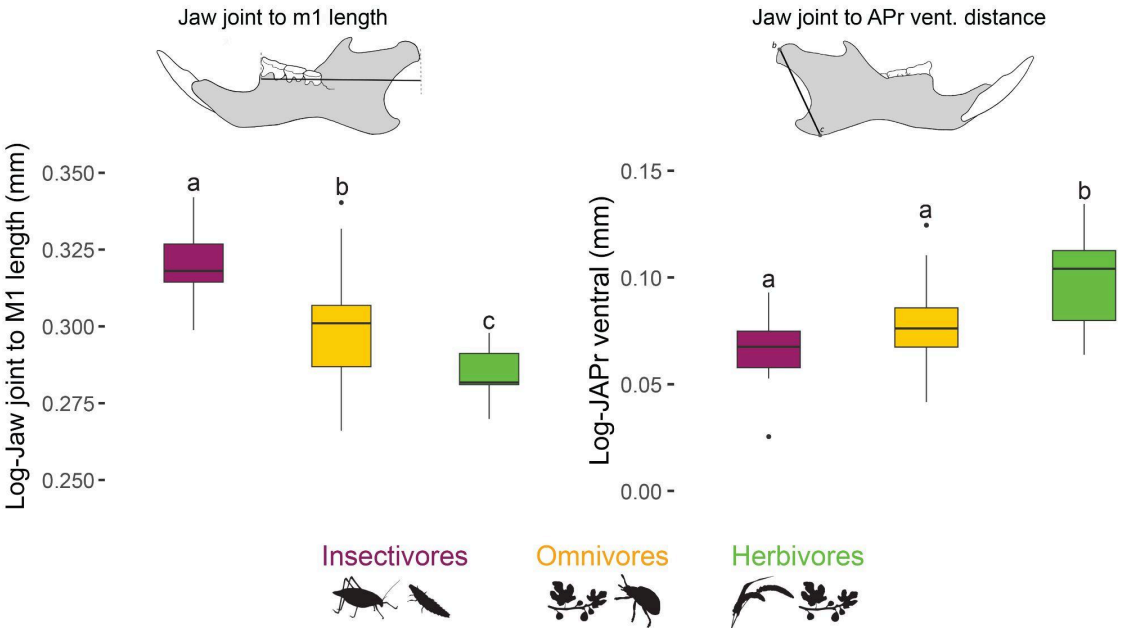

Figure S2.3. Patterns in mandibular morphology as indicated by important traits separating major dietary groups on the Principal Component Analysis. Different letters indicate significant variation of traits among dietary ecologies.

CHAPTER 3

How do you like your prey? Craniodental traits predict feeding performance and dietary hardness in a community of Neotropical free-tailed bats (Molossidae)*

Skulls of *Eumops underwoodi*, *Molossus molossus* and *E. nanus*

*Article published in the journal Functional Ecology, 2022, Vol. 36, Issue 7, pp. 1690-1699 (https://doi.org/10.1111/1365-2435.14063)

3.1 ABSTRACT

Form-function studies have established a strong link between dental morphology and the mechanical properties of food items, with animals evolving tooth shapes theoretically ideal for their diets. However, information on how teeth perform under natural conditions is rare, which limits our understanding of how dental morphology influences dietary ecology and niche partitioning within animal communities. Free-tailed bats (Molossidae) are a diverse clade of aerial insectivorous mammals that exhibit an outstanding variation in size and craniodental traits, which have been directly related to ecological segregation among sympatric species. We investigate the mechanisms that allow functional dietary specialization and trophic segregation among sympatric free-tailed bat species inhabiting a Neotropical forest. To do so, we coupled data on the shape and size of molar teeth and the feeding apparatus with in-situ collected measurements of feeding performance and dietary hardness. We found that evolved differences in molar topography and size vary in tandem with the mechanical demands of prey items naturally consumed by sympatric molossid species. This may be explained by feeding performance capabilities resulting from both molar shape and the overall size of the feeding apparatus, which seem to allow efficient processing of food items with specific mechanical properties. For instance, smaller bats with higher topographic values and more gracile heads mainly feed on softer prey items, whereas bigger bats with lower topographic values and more robust heads mostly feed on tougher prey items. Species with a broader range of sizes, craniodental morphologies, and prey hardness are also present in the community. Based on the extent of our results, our data provide compelling evidence on how the shape and size of feeding structures, in addition to how they perform, may facilitate trophic segregation among

sympatric free-tailed bat species. Similar mechanisms are thought to be driving the diversity of other present and even past bat and/or insectivorous communities, so correspondingly, we emphasize the value of gathering key information in order to better understand the functional significance of biological traits and ultimately the evolution of diverse communities. **Key words:** Costa Rica, molars, insectivory, diet, resource partitioning.

3.2 INTRODUCTION

The functional relationships between dental morphology and diet underlie ecological and evolutionary processes, including food niche partitioning and trophic radiation, across a wide array of vertebrate taxa (e.g., Primates — Kay & Hylander 1978; Lucas 1979; cichlids, Yamaoka 1983; carnivorans and rodents — Evans et al., 2007). This is because teeth are at the mechanical interface with food items, and therefore under strong selective pressures to perform efficiently at acquiring and breaking down foods with different mechanical properties (e.g., toughness — Ungar 2010; Evans & Pineda-Munoz 2018). In mammals, molar teeth exhibit highly diverse occlusal topographies and show a strong dietary signal (Evans & Pineda-Munoz 2018). Consequently, molars have been studied extensively to understand the trophic niches and diet in extinct and extant taxa (e.g., Strait 1993a; 1993b; Santana et al., 2011; Wilson 2013; Evans & Janis 2014; Martin et al., 2016; Selig et al., 2019). However, although there have been substantial advances in describing these form-function relationships, few studies have attempted to investigate how differences in molar morphology directly translate into variation in feeding

performance among sympatric species (but see Moore & Sanson 1995; Bezzobs & Sanson 1997; Santana et al., 2011).

Among mammals, there is evidence that rodent, primate, and marsupial species that have well developed shearing, crushing, and grinding molar cusps are more efficient at processing and digesting plant material (McArthur & Sanson 1988; Bezzobs & Sanson 1997). Similarly, it has been demonstrated that among bats, primates, and marsupials, certain molar morphologies (e.g., sharp crests/cusps) allow for high feeding performance while feeding on insects (i.e., finely comminuting exoskeleton — Moore & Sanson 1995; Kay & Sheine 1979; Santana et al., 2011). Therefore, incorporating performance estimates into form-function studies allows for a mechanistic understanding of the relationships between tooth morphology and diet, including the role of ecomorphological segregation (Wainwright 1994) in allowing some species to increase their masticatory and digestive efficiency, ultimately enhancing their feeding performance and fitness (Sheine & Kay 1977; Kay & Sheine 1979).

Free-tailed bats (Molossidae: Chiroptera; 110+ species) are small to medium-sized bats (2-220 g — Taylor 2019) that exhibit an outstanding range of skull and jaw morphologies within the aerial insectivorous niche (Freeman 1979; 1981). This morphological variation is thought to be related to specialization on different types of insects that are caught and processed in flight well above the canopy (Freeman 1981). Specifically, variation in body size, morphology of the skull (e.g., sagittal crest size), mandible (e.g., coronoid process size) and teeth (e.g., teeth number and size, height of the molar cusps) has been linked to trophic segregation of species throughout the Family; with molossids with robust skulls and thick jaws seem to specialize on hard-shelled

insects, whereas species with gracile skulls and thin jaws eat mostly soft-bodied insects (Freeman 1979; 1981; Swartz et al., 2003). These ecomorphological relationships are likely mediated by performance differences, which might in turn help understand ecological specialization, community structure, and diversification processes across this diverse mammalian clade.

Here, we investigate the relationships among size and craniodental traits, feeding performance and dietary hardness in sympatric Neotropical free-tailed bats in Costa Rica. We functionally link feeding performance (i.e., the ability to breakdown insect prey) and prey hardness estimates with craniodental traits and body size metrics (i.e., 3D DTMs, forearm length, head, and skull measurements). We test the hypothesis that evolved differences in molar topography and the overall size of the feeding apparatus enable differences in feeding performance and access to prey items with different mechanical properties, and subsequent functional dietary specialization and trophic segregation among free-tailed bat species. As exoskeleton thickness may affect which insect taxa molossid species can prey upon (Freeman 1979), and exoskeleton particle size indicates the degree of food processing (Santana et al., 2011), we predict that species with more robust (wider, taller) heads and lower molar topographic values specialize on harder prey (e.g., beetles) due their capacity to access and break down these mechanically challenging items more efficiently (e.g., due to higher bite force and blunter molars — Hepburn & Chandler 1976; Strait 1993b). Conversely, we predict that species with more gracile (narrower and shorter) heads and higher molar topographic values specialize on softer prey (e.g., moths) (Hepburn & Chandler 1976; Strait 1993b). Finally, across both guilds, we predict that as DTMs increase, so do the occlusal area and the number of tools

molars have for prey processing, leading to more efficient exoskeleton breakdown. Altogether, these ecomorphological differences may help explain the coexistence of molossid bats within this and other species-rich communities.

3.3 MATERIALS AND METHODS

3.3.1 Field work & data collection

Our study was conducted at Parque Nacional Diriá, Guanacaste, Costa Rica (hereafter Diriá; 10°10′25.8″ N, 085°35′46.3″ W, 128 m a.s.l.). Diriá is in the northwestern Pacific lowlands of Costa Rica and is characterized by the presence of a seasonal tropical dry forest and a river ca. 40 m wide (Río Enmedio) that is surrounded by a gallery forest (Pineda et al., 2008 — Fig. S3.1). Our sampling effort was focused on a subset of the insectivorous bats of the area (i.e., free-tailed bats — Family Molossidae). We captured bats during three consecutive nights in April 2014 and 2015 and May 2016 by placing three mist nets (12 x 3 m) across water ponds of the Río Enmedio (Fig. S3.1). During all sampling days, we set up mist nets in the same area and time frame (18:00h-21: 00h). Upon capture, we recorded each bat's species, age, sex, and reproductive status based on external traits (Brunet-Rossinni & Wilkinson 2009). We then kept each bat in an individual cloth bag for approximately 15 minutes to obtain fecal samples of their natural diet (Table 3.1). These bags were examined to obtain fecal pellets, which we carefully removed using fine tweezers and stored in Eppendorf centrifuges tubes. To obtain data about body size and dental topography traits of each bat species, we kept a subset of the captured animals as voucher specimens (N = 3 specimens; under permit ACT-OR-DR-147-14 and ACT-OR-DR-011-16; Supporting information file 5 — Table

S1), in addition to measuring forearm length (proxy for overall size) and head dimensions known to influence bite performance (head length, head width and head height — Santana et al., 2010) from live animals (Fig. S3.2 and Table 3.2). We augmented the morphological dataset with specimens from the Louisiana Museum of Natural Science (LSU) and Museum of Texas Tech University (TTU) mammal collections (Supporting information file 5 — Table S1), selecting Costa Rican specimens whenever possible (Total N = 31 specimens). All specimens used had minimal, if any, noticeable tooth wear.

3.3.2 Morphological information

Craniodental traits — We created digital 3D models of the skull of each voucher specimen using a Skyscan 1172 µCT Scanner (Bruker MicroCT, Belgium). All scans were performed at an 11.99 um image voxel size while keeping other scanning parameters consistent (Supporting information file 4 — Table S2). We used NRecon (Microphotonics) to convert CT shadow images into image stacks ('slices'), which we imported into Mimics v. 22.0 (Materialise, Leuven, Belgium) to segment the right upper and right lower molar rows of each specimen and produce 3D surface (*.stl) files. We imported raw stl files into Geomagic Studio v. 2019 (Geomagic Inc., Research Triangle Park, NC, USA) to select the entire tooth crown (i.e., above the enameled cervix) of premolars and molars of each specimen (Boyer 2008). We selected these teeth because premolars and molars are predominantly used by bats to process food items, including insect prey (Dumont 1999; Santana & Dumont 2009). We did not include vestigial premolars (PM^3) to avoid morphological variation of little functional importance (i.e., in *Eumops ferox*, *E. hansae*, *E. nanus*, *E. underwoodi* and *Promops centralis*—Freeman

1981). We oriented tooth row models with the occlusal plane parallel to the X-axis (which pointed anteriorly), the Y-axis perpendicular to the occlusal plane, and the Z-axis pointing in the lingual direction (Supporting information Figure 2a). We imported oriented models into Avizo Lite 9.2.0 (FEI Visualization Sciences Group, Berlin, Germany) for simplification to 40,000 faces and smoothing (100 iterations with a lambda of 0.6; Pampush et al., 2016). We then saved each tooth row as *.PLY files for subsequent analyses.

Following Freeman (1981), we collected a set of cranial and mandibular measurements of potential importance in determining the feeding performance of free-tailed bat species: Greatest skull length (GSL), Dentary thickness (DENT THIC) and Dentary length (DENT LEN), all measured from the 3D models of the skull and mandible (Fig. S3.2 and Supporting information file 5 — Table S3).

We calculated DTMs (DNE, RFI and OPCR) of the upper and lower molar tooth row of each specimen using tooth row models (*.stl flies) and the function molaR_Batch within the R package MolaR (Pampush et al., 2016). For RFI calculations, we used an alpha value between 0.4 and 0.6 for the upper molar rows, and an alpha value of 1.2 for the lower molar rows. These values correspond to the step size used for calculating the outline of the footprint and, contrary to the default setting (0.001), we assigned these values to our calculations as they allowed us to keep the subscript inside the bounds (see details in Pampush et al., 2016). We performed OPCR calculations with a minimum of 5 faces in each specimen following Winchester (2016). We used data across individuals to estimate the average value of each DTM across each molar row for each species.

3.3.3 Feeding performance & dietary hardness

From each fecal sample (Total N = 38), we randomly selected 1-2 g of fecal pellets, which we rehydrated for 24 hours in a Petri dish containing distilled water. Once exoskeleton pieces could be spread out by gently shaking the Petri dish, we placed a numbered grid under the Petri dish and used a random number generator to choose grid quadrants and select at least 20 exoskeleton particles from each fecal sample. As irregularly-shaped particles such as limb fragments or head capsules could introduce high variation to the data, we only selected flat cuticle pieces that were uniform in shape and thickness to collect diet and feeding performance data. Using fine tweezers, we collected and dried particles by placing them on a Kimwipe tissue.

We estimated feeding performance and dietary hardness by measuring the size and thickness, respectively, of each insect exoskeleton particle (Supporting information file 5 — Table S4 and Table S5).. Chitin is highly indigestible by mammals (Altman & Dittmer 1968); therefore, particle size is related to the ability to break down insect prey (i.e., feeding performance; Santana et al., 2011). Moreover, as exoskeleton thickness and insect hardness have been found to be positively correlated (Evans & Sanson 2005; Santana et al., 2011), variation in exoskeleton thickness reflects the physicals demands imposed by different insects or their body parts and may influence particle breakdown during feeding events (Santana et al., 2011). We measured exoskeleton particle size from digital pictures taken of each particle along with a millimetric scale under a binocular stereoscope (Leica M125 with attached camera, Leica Microsystems, Germany), using ImageJ (National Institutes of Health, Bethesda, MD, USA) to outline each particle's perimeter and calculate its corresponding area. We measured exoskeleton particle

thickness using a high precision micrometer with hemispherical attachments (Mitutoyo type 293-340-30CAL, range ± 25.4mm, resolution +/- 0.001 mm; Aurora, IL, USA). We averaged data on exoskeleton particle size and thickness within each sample and across individuals to obtain species means.

3.3.4 Data analysis

All variables used in our analyses were log transformed to ensure linearity assumptions of the parametric tests performed. When assumptions were still not met, we used non-parametric tests. We first employed Spearman's correlation tests to assess the relationship among body size metrics, among cranial and mandibular measurements, among DTMs of the lower and upper molar tooth rows, and between exoskeleton particle size and exoskeleton particle thickness.

To visualize interspecific patterns in body size and craniodental traits among bat species, we first classified free-tailed bat species into three dietary hardness categories based on dietary information available in the literature and our exoskeleton thickness data. Accordingly, *E. underwoodi* and *P. centralis* were classified as hard-insect eaters, *M. pretiosus*, *M. molossus* and *C. greenhalli* as intermediate, and *E. nanus*, *E. hansae* and *E. ferox* as soft-insect eaters. We centered all morphometric and dental variables by subtracting the mean from individual values and size-corrected these centered measurements using Burnaby's transformation (Burnaby 1966; Rohlf & Bookstein 1987; Claude 2008). We then performed Principal component analysis (PCA) on the size-corrected dental and morphometric data sets, respectively, using the 'prcomp' function, and corrplot (Wei et al., 2017) and factoextra (Kassambara & Mundt 2017)

packages. We plotted the first two PCs, which accounted for >70% of the total variance.

We evaluated the relationship between feeding performance and dietary hardness among species using two approaches. First, due to the lack of data for direct performance comparisons (i.e., exoskeleton particle sizes from bat species eating the same prey items) and the potential confounding effect of exoskeleton thickness on feeding performance, we plotted the particle size versus thickness data and fitted separate linear regression models for each of the diet hardness categories (hard, intermediate, soft) using the geom_smooth function (Wickham 2016). This allowed us to visualize if, for a given exoskeleton thickness, species within each of these categories produced particles that differed in size. Since this was the case (see Results), we used multivariate analyses of variance (MANOVA) to test for differences in DTMs, body size and cranial and mandibular traits among diet hardness categories (with the vegan package; Oksanen et al., 2017).

Second, we evaluated the relationship among feeding performance, dietary hardness, body size and craniodental traits without *a priori* groupings using linear regression models and phylogenetic generalized least squares (PGLS) regression models with a Brownian correlation. In these regressions, exoskeleton particle size and thickness were used as independent response variables, while DTMs (DNE, RFI, and OPCR), in addition to head length for the particle size analysis and head height for thickness analysis, were employed as the predictor variables. These specific head dimensions were selected among the multiple variables available (i.e., cranial, and mandibular measurements) because they were the most fitting predictors explaining the variation in feeding performance and dietary hardness, respectively. Assumptions of the regression

models were tested with package 'gvlma' (Pena & Slate 2019), and, since no phylogeny available includes all the species or has used the same molecular markers, we used phytools and ape (Revell 2012; Paradis & Schliep 2018) packages to run the PGLS with a tree topology based on published molecular relationships among molossid genera (Ammerman et al., 2012) and within *Eumops* (Bartlett et al., 2013), setting branch lengths to 1. Best fitting models were chosen based on the Akaike information criterion for small sample sizes (AIC_c), which considers the fit and complexity of the regressions (Schwarz 1978; Burnham & Anderson 2002). Models were ranked by AIC_c value (the lowest value of AIC_c has the most support from the data) and compared using AIC model weights (w_i). All statistical analyses were performed in R (R Core Team 2021).

3.4 RESULTS

Correlation analyses showed that DTMs between the upper and lower molar tooth rows were positively correlated. Body size, cranial and mandibular traits were also correlated with one another, as were exoskeleton particle size and thickness (Supporting information file 5 — Table S6)

When grouped into diet hardness categories, coexisting free-tailed bats differ in their DTMs ($F_{(2,31)} = 7.8$, $p = 0.001$), body size metrics ($F_{(2,44)} = 18.6$, $p < 0.001$) and cranial and mandibular traits ($F_{(2,39)} = 58.1$, $p < 0.001$). Principal component analyses indicate that all three DTM's (Fig 2a), forearm length and all three head dimensions (Fig. 3.2b), greatest skull length, and dentary thickness (Fig. 3.2c) contribute to the morphometric differences among dietary hardness groupings (Supporting information file 5 — Table S7). Species segregate into three morphotypes: (1) bigger species with more

robust (larger) heads/crania, thicker mandibles, and molariform dentitions that are flatter, with smaller occlusal surfaces and less complex topographies (i.e., lower DNE, RFI and OPCR — Fig. S3.5), (2) more generalized morphologies that exhibit greater variation in forearm length, head sizes and craniodental traits, and (3) smaller species with more gracile (smaller) heads/crania, thinner mandibles, and molariform dentitions with sharper/taller cusps, greater occlusal surfaces, and more complex topographies (i.e., higher DNE, RFI and OPCR — Fig. S3.5). These morphotypes differ in feeding performance (Fig. 3.2d); for a given particle thickness, bats from different dietary hardness groups produce exoskeleton particles of different sizes ($F_{(2,754)} = 63.5$, $p < 0.001$), with hard-insect eaters producing larger particles than soft-insect eaters, and intermediate species exhibiting large variation in feeding performance (Fig. 3.2d).

Across the community, regression models indicate that feeding performance and dietary hardness can be predicted by variations in DTMs and head length among the species (Table 3.2). Similar, PGLS analysis show that, independently of phylogenetic relationships, molossid species with narrower and more dorsoventrally flattened heads but high to intermediate DNE, RFI and OPCR values tend to prey upon less mechanically-demanding insects (i.e., with thinner exoskeleton) and are able to produce smaller exoskeleton particles (Supporting information file 5 — Table S8 and Table S9). Conversely to this trend, species with lower DNE, RFI and OPCR values and wider and taller heads prey upon more mechanically challenging insects (i.e., with thicker exoskeleton) and produce larger exoskeleton particles (Fig. 3.3).

3.5 DISCUSSION

Dental topography metrics have been successfully used as a proxy of dietary ecology in extant and extinct species (e.g., Evans 2013; Winchester et al., 2014; Selig et al., 2019; among others). Here, we expand upon this by examining the relationships among body size, craniomandibular and dental traits, feeding performance and dietary hardness in a community of closely-related, sympatric insectivorous bats. Altogether, our data are consistent with the idea that physical properties of the consumed food items are strongly tied to variation in shape, size, function and ultimately performance of the feeding apparatus of mammals (Spears & Crompton 1996; Freeman 1988; Herrel & Holanova 2008; Santana et al., 2011, Evans & Pineda-Munoz 2018). Available data on the interspecific variation in diet, body size, craniomandibular and dental morphology among insectivorous bats at large further supports that dental and size traits have been evolving in tandem with dietary ecology, allowing species to overcome potential challenges involved in the mechanical processing of insects (Freeman 1979, 1988; Strait 1993b).

From a mechanical standpoint, the interaction between molar topography, bite force, and the physical properties of the prey item will determine the extent to which the prey is broken down into pieces that are small enough for digestion (Sheine & Kay 1977; Berthaume 2016; Evans & Pineda-Munoz 2018). Our results indicate that free-tailed bat species that have sharper molars and more gracile heads and mandibles (*E. nanus*, *E. hansae,* and potentially *E. ferox*) are morphologically specialized to finely comminute softer insects (i.e., with thinner exoskeletons). As high stresses are not necessary to fracture the exoskeleton of soft insects (i.e., they are broken down via ductile fracture; Strait 1993b), these species are usually small and morphologically suited by having a

greater number of and sharper shearing features that allow the distribution of bite forces over larger contact areas (Strait 1993b). This is similar to other species of mammals that exhibit increased shearing surfaces and larger occlusal areas and feed on ductile foods (e.g., moles, primates, carnivorans, Strait 1993b; Evans et al., 2007). However, these molossid species may be functionally constrained by these adaptations (i.e., increased risks of tooth fracture and wear) when processing tougher food items (Freeman 1979; Strait 1993b).

In contrast to soft-insect eaters, a set of the molossid species in the community (*E. underwoodi* and *P. centralis*) appear to be occupying a more durophagous feeding niche (Freeman 1979; Strait 1993b). Specifically, our results suggest that these bigger bats with blunter molars and more robust heads and mandibles primarily feed and efficiently process prey items with thicker exoskeletons. By having fewer and smaller shearing features that can focus greater bite forces on small contact areas, these bats can concentrate stress on the prey item to produce brittle fracture, in a similar way that other durophagous mammals do (Fisher 1941; Strait 1993b; Kay 2017). Functional tradeoffs of these adaptations seem to be related with the production of larger particles for any given exoskeleton thickness (Fig. 3.2d).

In between specialized soft and hard insect eaters, several species in the community seem to occupy a more generalized morphospace and dietary niche (Fig. 3.2); *Molossus pretiosus*, *Cynomops greenhalli*, and potentially *M. molossus* are consuming prey items that vary highly in hardness (exoskeleton thickness). Therefore, these bats appear to be opportunistic feeders that consume prey of a wide range of physical properties but with overall lower feeding performance than specialized soft-insect eaters

(Fig 3.2d). These results support previously described functional trade-offs in feeding performance among vertebrates (e.g., Huey & Hertz 1984; Roslin & Salminen 2008; Santana et al., 2011).

Overall, our data on feeding performance and dietary hardness supports form-function-performance trends detected on the feeding ecology of mammals and other vertebrates (Strait 1993b, Kay & Hylander 1978; Lucas 1979; Yamaoka 1983; Evans et al., 2007, among others), highlighting how shape and size of key feeding structures as the molars, in addition to the total size of the feeding apparatus, have coevolve with the dietary ecology of bat species. Here, we also demonstrated how DTMs can be successfully employed in detailed comparative studies, and how matching data on diet and feeding performance can help to better understand the morphological evolution of biological structures.

Given our results, we encourage researchers to include feeding performance estimates and DTMs, or other informative metric of teeth morphology (see Strait 1993b) into form-function studies, as this combination may provide more cues on the functional understanding of the mechanisms driving dietary specialization and trophic segregation among sympatric species. Ultimately, and by gathering more detailed data on the natural history, morphology, and behavior of the species, we can better understand major patterns on ecomorphological diversification and community ecology.

In conclusion, our manuscript provides compelling evidence that explains the interspecific differences in the DTMs and size traits among free-tailed bats species coexisting in a Neotropical forest, demonstrating how these evolved differences in molar shape and feeding apparatus size translate into food resource use and feeding

performance in prey processing. Given the dietary, dental, craniomandibular and size differences described among other molossid species in other geographic areas (e.g., Freeman 1979, 1981; Giménez & Giannini 2016), similar trophic niche segregation mechanisms may operate in similar communities across the whole range of the Family (Ethiopian, Neotropical, and Indo-Australian species). Promising steps might be focused on investigating the functional trade-offs of specialized versus generalized feeding morphologies (Huey & Hertz 1984; Roslin & Salminen 2008; Santana et al., 2011), for example by conducting direct feeding performance comparisons (e.g., on the same prey items), detect and understand modulation of feeding behaviors (e.g., Santana & Dumont 2009), as well as by evaluating the spatio-temporal availability and the detailed mechanical properties of the insect prey on their natural environments.

3.6 ACKNOWLEDGMENTS

We thank the staff of Parque Nacional Diriá for providing facilities during fieldwork and data collection. The Museo de Zoología, Universidad de Costa Rica, the Burke Museum of Natural History and Culture, the Museum of Texas Tech University and the Louisiana Museum of National Science provided critical support and voucher specimens for this research. DVC was supported by the Mammalogy Department at the Burke Museum of Natural History and Culture, and SES was supported by NSF grant # 2017738.

3.7 DATA AVAILABILITY STATEMENT

Raw data are archived on Dryad Digital Repository https://doi.org/10.5061/dryad.j3tx95xgw (Villalobos-Chaves & Santana, 2022), and .stl files will be available upon request.

3.8 TABLES AND FIGURES

Table 3.1. Sample sizes, feeding performance and dietary hardness variation among the sympatric free-tailed bat species studied. Values are mean ± SD.

Species	N fecal samples	Exoskeleton particle size (mm)	Exoskeleton particle thickness (mm)
Molossus pretiosus	22	0.69 ± 0.54	0.12 ± 0.06
Molossus molossus	–	–	–
Eumops underwoodi	1	2.36 ± 2.67	0.13 ± 0.08
Promops centralis	–	–	–
Cynomops greenhalli	7	0.75 ± 0.79	0.08 ± 0.05
Eumops ferox	–	–	–
Eumops hansae	5	0.55 ± 0.32	0.08 ± 0.06
Eumops nanus	3	0.46 ± 0.34	0.08 ± 0.04

Table 3.2. Fit of the six best performing regression models based on exoskeleton particle size and thickness, respectively. df = degrees of freedom; *R2* = R squared; Loglik = Likelihood function; AIC_c = Akaike information criterion corrected for small sample size; Delta AICc = AIC_{ci} – minimum AIC_c; w_i = Akaike weights.

Model	***df***	***R2***	**Loglik**	**AIC_c**	**Delta AIC_c**	**w_i**
Particle size ~ RFI*Head length	5	0.99	14.84	-79.7	0.00	0.73
Particle size ~ DNE*OPCR	5	0.98	13.49	-77.0	2.70	0.19
Particle size ~ DNE*Head length	5	0.97	12.44	-74.9	4.80	0.06
Particle thickness ~ DNE*OPCR	5	0.99	26.97	-104.0	0.00	1.00
Particle thickness ~ DNE+RFI+OPCR	5	0.95	16.21	-82.40	21.53	0.00
Particle thickness ~ DNE+OPCR+Head height	5	0.79	12.57	-75.10	28.81	0.00

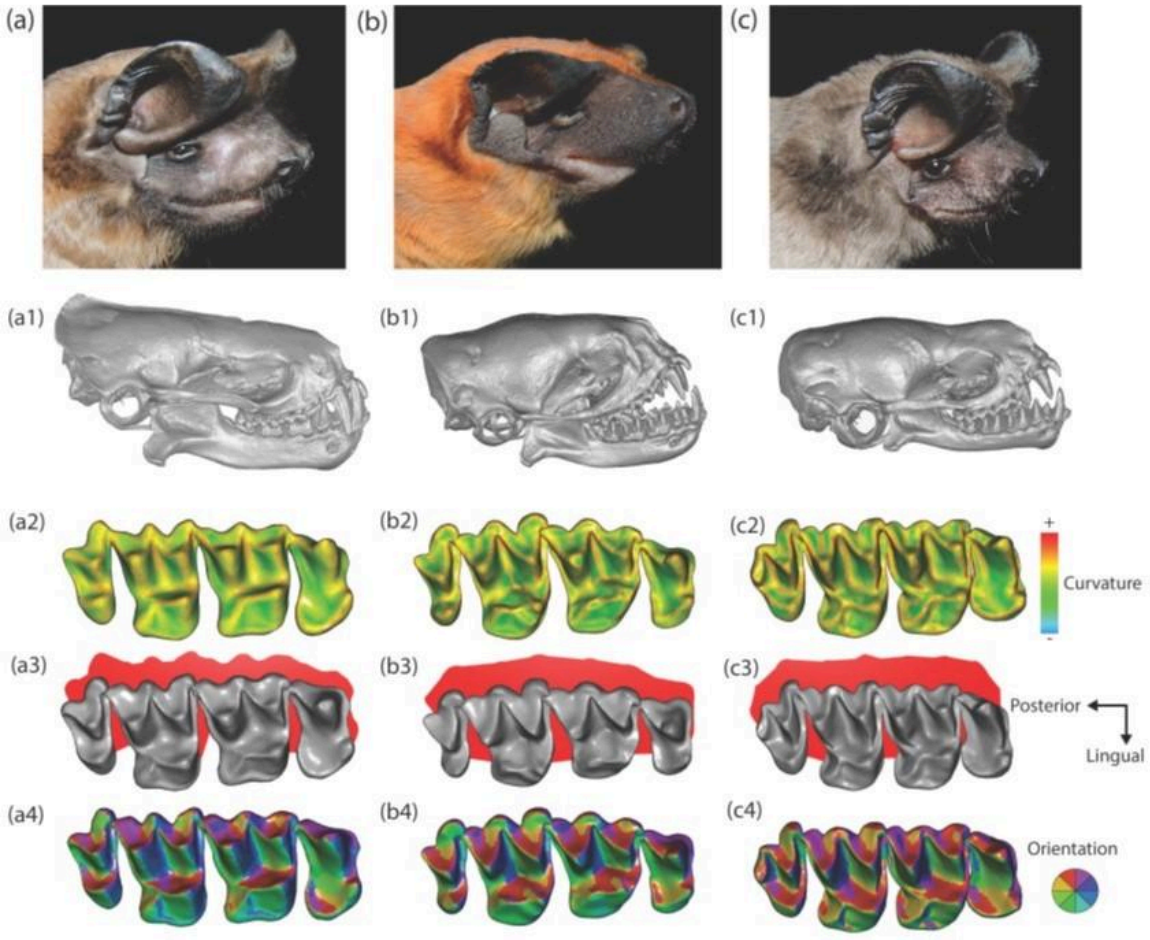

Figure 3.1. Three-dimensional reconstructions of two extreme (a, c), and one intermediate (b) skull and upper dentition morphologies found within the community of free-tailed bats studied. (a) *Eumops underwoodi*, (b) *Cynomops greenhalli*, (c) *Eumops nanus*. DNE (a2, b2, c2), RFI (a3, b3, c3) and OPCR (c4, b4, c4) maps are shown.

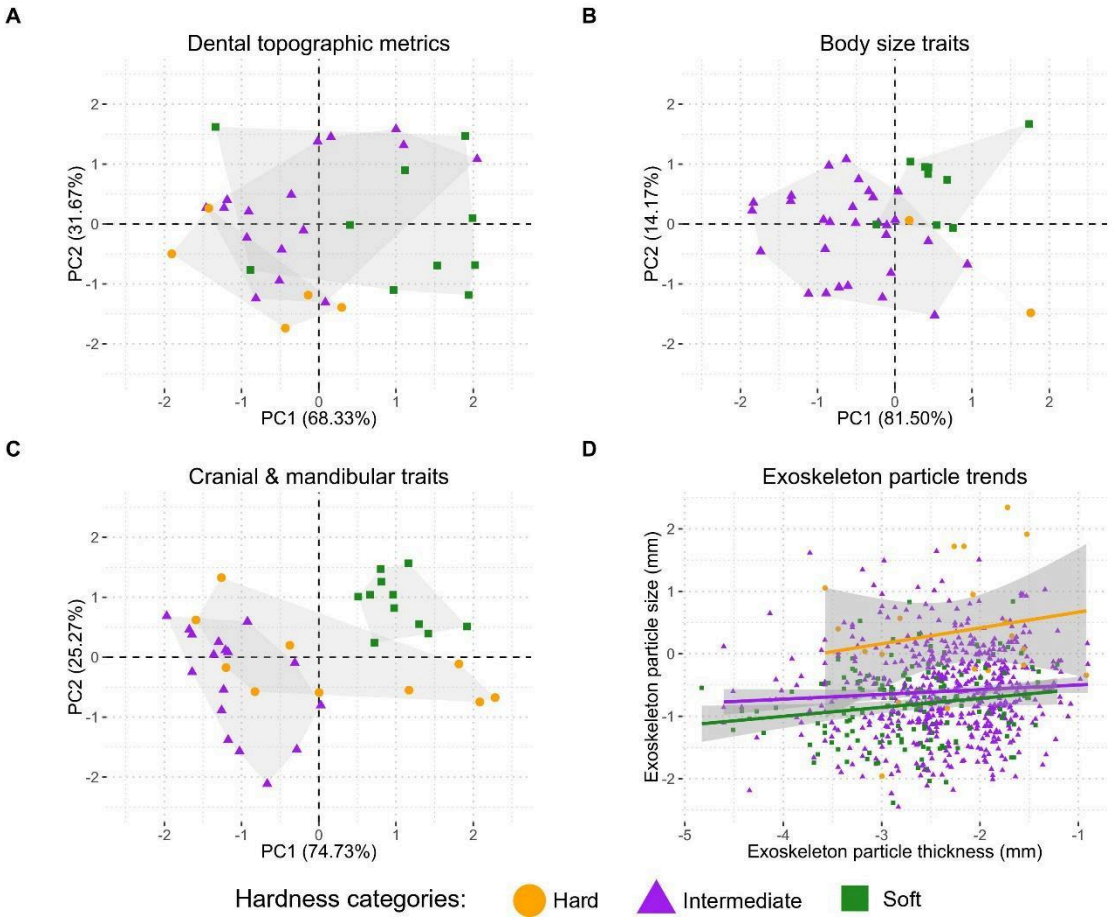

Figure 3.2. Principal Component (PC) analysis plots of dental topography and morphometric traits (A, B and C), and scatterplot showing the relationship between exoskeleton particle thickness and size among dietary hardness categories (D). See Supporting Information Table 5 for summary statistics.

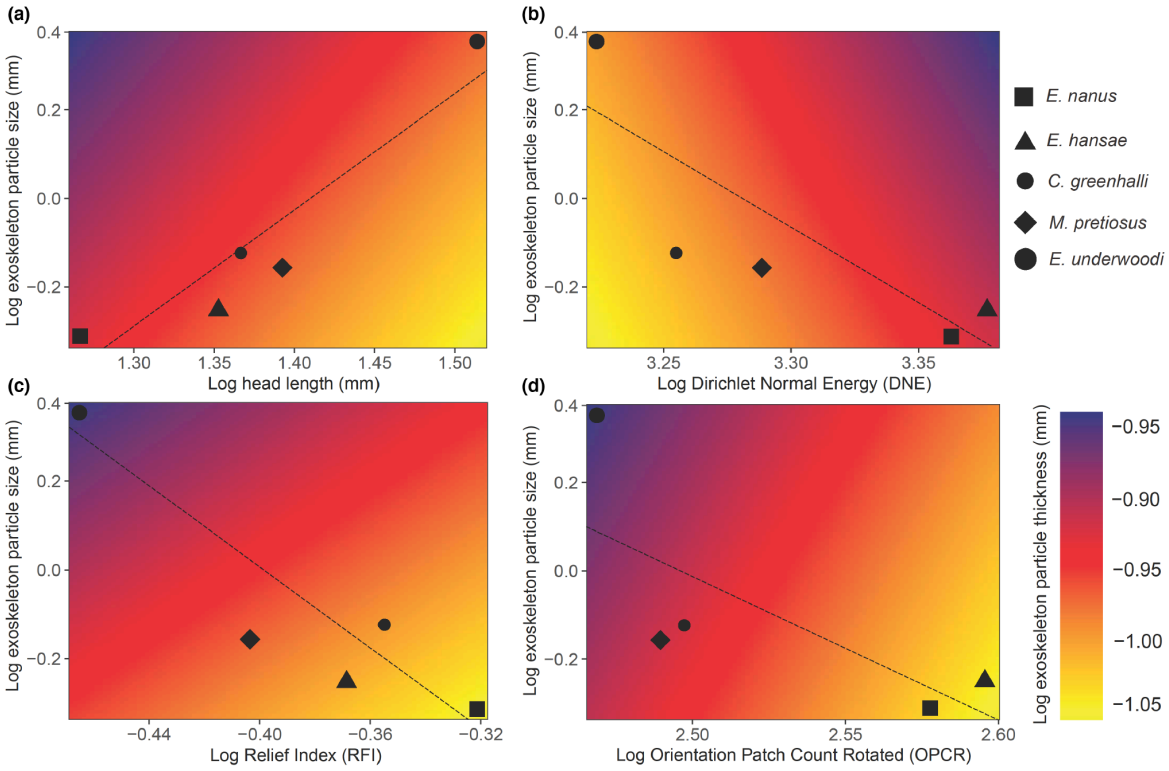

Figure 3.3. Graphical representation of the best fitting models illustrating the relationships between exoskeleton particle size and thickness and Head length (a), Dirichlet Normal Energy (b), Relief Index (c) and Orientation Patch Count Rotated (d).

3.9 REFERENCES

Ammerman, L.K., Lee, D.N., & Tipps, T.M. 2012. First molecular phylogenetic insights into the evolution of free-tailed bats in the subfamily Molossinae (Molossidae, Chiroptera). Journal of Mammalogy, 93: 12–28. doi: 10.1644/11-MAMM-A-103.1

Bartlett, S.N., McDonough, M.M., & Ammerman, L.K. 2013. Molecular systematics of bonneted bats (Molossidae: *Eumops*) based on mitochondrial and nuclear DNA sequences. Journal of Mammalogy, 94: 867–880. doi: 10.1644/12-MAMM-A-134.1

Berthaume, M.A. 2016. On the relationship between tooth shape and masticatory efficiency: A finite element study. Anatomical Records, 299: 679–687. doi: 10.1002/ar.23328

Bezzobs, T., & Sanson, G. 1997. The effects of plant and tooth structure on intake and digestibility in two small mammalian herbivores. Physiological Zoology, 70: 338–351. doi: 10.1086/639612

Boyer, D.M. 2008. Relief index of second mandibular molars is a correlate of diet among prosimian primates and other euarchontan mammals. Journal of Human Evolution, 55: 1118–1137. doi: 10.1016/j.jhevol.2008.08.002

Brunet-Rossinni, A.K., & Wilkinson, G.S. 2009. Methods for age estimation and the study of senescence in bats. In T.H. Kunz, & S. Parson (Eds.), *Ecological and Behavioral Methods for the Study of Bats* (pp. 315–323). Johns Hopkins University Press.

Bunn, J.M., Boyer, D.M., Lipman, Y., St. Clair, E. M, Jernvall, J., & Daubechies, I. 2011. Comparing Dirichlet normal surface energy of tooth crowns, a new technique of molar shape quantification for dietary inference, with previous methods in isolation and in combination. American Journal of Physical Anthropology, 145: 247–261. doi: 10.1002/ajpa.21489

Burnaby, T.P. 1966. Growth-Invariant Discriminant Functions and Generalized Distances. Biometrics, 22: 96–110. doi: 10.2307/2528217

Burnham, K.P., & Anderson, D.R. 2002. Model selection and inference: a practical information-theoretic approach. Springer-Verlag.

Claude, J. 2008. Morphometrics with R. Springer-Verlag.

Dumont, E.R. 1999. The effect of food hardness on feeding behaviour in frugivorous bats (Phyllostomidae): an experimental study. Journal of Zoology, 248: 219–229. doi: 10.1111/j.1469-7998.1999.tb01198.x

Evans, A.R. & Sanson, G.D. 2005. Biomechanical properties of insects in relation to insectivory: cuticle thickness as an indicator of insect 'hardness' and 'intractability'. Australian Journal of Zoology, 53: 9–19. doi: 10.1071/ZO04018

Evans, A.R., Wilson, G.P., Fortelius, M., Jernvall, J. 2007. High-level of similarity of dentitions in carnivorans and rodents. Nature, 445: 78–81. doi: 10.1038/nature05433

Evans, A.R., & Janis, C.M. 2014. The Evolution of High Dental Complexity in the Horse Lineage. Annales Zoologici Fennici, 51: 73–79. doi: 10.5735/086.051.0209

Evans, A.R., & Pineda-Munoz, S. 2018. Inferring mammal dietary ecology from dental morphology. In D.A. Croft, D.F. Su, & S.W. Simpson (Eds.), *Methods in*

paleoecology: Reconstructing Cenozoic terrestrial environments and ecological communities (pp. 37–51). Springer International Publishing.

Fisher, E.M. 1941. Notes on the Teeth of the Sea Otter. Journal of Mammalogy, 22: 428–433.

Freeman, P.W. 1979. Specialized Insectivory: Beetle-Eating and Moth-Eating Molossid Bats. Journal of Mammalogy, 60: 467–479. doi: 10.2307/1380088

Freeman, P.W. 1981. A Multivariate Study of the Family Molossidae Mammalia, Chiroptera): Morphology, Ecology, Evolution. Fieldiana Zoology, New Series, 7: 1–173. doi: 10.5962/bhl.title.3128

Freeman, P.W. 1988. Frugivorous and animalivorous bats (Microchiroptera): dental and cranial adaptations. Biological Journal of the Linnean Society, 33: 249–272. doi: 10.1111/j.1095-8312.1988.tb00811.x

Giménez, A.L., & Giannini, N.P. 2016. Morphofunctional segregation in Molossid bat species (Chiroptera: Molossidae) from the South American southern Cone. Hystrix Italian Journal of Mammalogy, 27: 170–180. doi: 10.4404/hystrix-27.2-11467

Hepburn, H.R., & Chandler, H.D. 1976. Material properties of arthropod cuticles: The arthrodial membranes. Journal of Comparative Physiology, 109: 177–198. doi: 10.1007/BF00689417

Herrel, A., & Holanova, V. 2008. Cranial morphology and bite force in Chamaeleolis lizards, adaptations to molluscivory?, Zoology, 111: 467–475. doi: 10.1016/j.zool.2008.01.002

Huey, R.G., & Hertz, P.E. 1984. Is a Jack-of-All-Temperatures a Master of None?. Evolution, 38: 441–444. doi: 10.2307/2408502

ImageJ (U.S. National Institutes of Health, Bethesda, MD, 1997–2014). 26.

Kay, R.F., & Hylander, W.L. 1978. The dental structure of mammalian folivores with special reference to Primates and Phalangeroidea (Marsupialia). In G. G. Montgomery (Ed.), *The biology of arboreal folivores* (pp. 173–191). Smithsonian Institution Press.

Kay, R.F., & Sheine, W.S. 1979. On the relationship between chitin particle size and digestibility in the primate *Galago senegalensis*. American Journal of Physical Anthropology, 50: 301–308. doi: 10.1002/ajpa.1330500303

Kay, R.F. 2017. The Nut-Crackers—A New Theory of the Adaptations of the Ramapithecinae. In R. L. Ciochan, & J. G. Fleagle (Eds.), *Primate Evolution and Human Origins* (pp. 230– 237). Routledge.

Kassambara, A., & Mundt, F. 2017. Package factoextra: Extract and visualize the Results of Multivariate Data Analyses. R Package Version 1.0. 7.

Martin, S.A., Alhajeri, B.H., & Steppan, S.J. 2016. Dietary adaptations in the teeth of murine rodents (Muridae): a test of biomechanical predictors. Biological Journal of the Linnean Society, 119: 766–784. doi: 10.1111/bij.12822

M'kirera, F., & Ungar, P.S. 2003. Occlusal relief changes with molar wear in *Pan troglodytes troglodytes* and *Gorilla gorilla gorilla*. American Journal of Primatology, 60: 31–41. doi: 10.1002/ajp.10077

Moore, S.J., & Sanson, G.D. 1995. A comparison of the molar efficiency of two insect-eating mammals. Journal of Zoology, 235: 175–192. doi: 10.1111/j.1469-7998.1995.tb05136.x

Lucas, P.W. 1979. The dental-dietary adaptations of mammals. *Neues Jahrbuch für Geologie und Paläontologie,* Monatshefte, 8: 486–512.

McArthur, C. & Sanson, G.D. 1988. Tooth wear in eastern grey kangaroos (*Macropus giganteus*) and western grey kangaroos (*Macropus fuliginosus*), and its potential influence on diet selection, digestion and population parameters. Journal of Zoology, 215: 491–504. doi: 10.1111/j.1469-7998.1988.tb02855.x

Oksanen, J., Guillaume Blanchet, F., Friendly, M., Kindt, R., Legendre, P., McGlinn, D., Minchin, P.R., O'Hara, R.B., Simpson, G.L., Solymos, P., et al. 2017. vegan: Community Ecology Package. R package version 2.4-3 [accessed 1 December 2021]. https://cran.rproject.org/ web/packages/vegan/index.html.

Pampush, J.D., Winchester, J.M., Morse, P.E., Vining, A.Q., Boyer, D.M., & Kay, R.F. 2016. Introducing molaR: a new R package for quantitative topographic analysis of teeth (and other topographic surfaces). Journal of Mammalian Evolution, 23: 397–412. doi: 10.1007/s10914-016-9326-0

Paradis, E., & Schliep, K. 2018. ape 5.0: an environment for modern phylogenetics and evolutionary analyses in R. Bioinformatics, 35: 526–528. doi: 10.1093/bioinformatics/bty633

Pena, E.A., & Slate, E.H. 2019. gvlma: Global Validation of Linear Models Assumptions. R package version 1.0.0.3. [accessed 1 March 2022]. https://cran.rproject.org/package=gvlma

Pineda, W., Rodríguez-Herrera, B., & Timm, R.M. 2008. Rediscovery, ecology, and identification of rare free-tailed bats (Chiroptera: Molossidae) in Costa Rica. Acta Chiropterologica, 10: 97–102. doi: 10.3161/150811008X331135

R Core Team. 2021. R: A language and environment for statistical computing. Vienna, Austria: R Foundation for Statistical Computing. Retrieved from https://www.R-project.org/

Revell, L.J. 2012. phytools: An R package for phylogenetic comparative biology (and other things). Methods in Ecology and Evolution, 3: 217–223. doi: 10.1111/j.2041-210X.2011.00169.x

Rohlf, J., & Bookstein, F.L. 1987. A Comment on Shearing as a Method for "Size Correction". Systematic Biology, 36: 356–367. doi: 10.2307/2413400

Roslin, T., & Salminen, J.P. 2008. Specialization pays off: contrasting effects of two types of tannins on oak specialist and generalist moth species. Oikos, 117: 1560–1568. doi: 10.1111/j.0030-1299.2008.16725.x

Santana, S.E. & Dumont, E.R. 2009. Connecting behaviour and performance: the evolution of biting behaviour and bite performance in bats. Journal of Evolutionary Biology, 22: 2131–2145. doi: 10.1111/j.1420-9101.2009.01827.x

Santana, S.E., Dumont, E.R., & Davis, J.L. 2010. Mechanism of bite force production and its relationship to diet in bats. Functional Ecology, 24: 776–784. doi: 10.1111/j.1365-2435.2010.01703.x

Santana, S.E., Strait, S., & Dumont, E.R. 2011. The better to eat you with: functional correlates of tooth structure in bats. Functional Ecology, 25: 839–847. doi: 10.1111/j.1365-2435.2011.01832.x

Schwarz, G. 1978. Estimating the Dimension of a Model. The Annals of Statistics, 6, 461–464.

Selig, K.R., Sargis, E.J., & Silcox, M.T. 2019. The frugivorous insectivores? Functional morphological analysis of molar topography for inferring diet in extant treeshrews (Scadentia). Journal of Mammalogy, 100: 1–17. doi: 10.1093/jmammal/gyz151

Sheine, W.S. & Kay, R.F. 1977. An analysis of chewed food particle size and its relationship to molar structure in the primates *Cheirogaleus medius* and *Galago senegalensis* and the insectivoran *Tupaia glis*. *A*merican Journal of Physical Anthropologists, 47: 15–20. doi: 10.1002/ajpa.1330470106

Spears, I.R., & Crompton, R.H. 1996. The mechanical significance of the occlusal geometry of great ape molars in food breakdown. Journal of Human Evolution, 31: 517–535. doi: 10.1006/jhev.1996.0077

Strait, S.G. 1993a. Differences in occlusal morphology and molar size in frugivores and faunivores. Journal of Human Evolution, 25: 471–484. doi: 10.1006/jhev.1993.1062

Strait, S.G. 1993b. Molar morphology and food texture among small-bodied insectivorous mammals. Journal of Mammalogy, 74: 391–402. doi: 10.2307/1382395

Swartz, S.M., Freeman, P.W., & Stockwell, E.F. 2003. Ecomorphology of bats: Comparative and experimental approaches relating structural design to ecology. In T. H. Kunz, & M. B. Fenton (Eds.), *Bat Ecology* (pp. 257–292). The University of Chicago Press.

Taylor, P.J. 2019. Family Molossidae (Free-tailed bats). In D. E. Wilson & R. A. Mittermeier (Eds.), *Handbook of the Mammals of the world. Vol. 9. Bats* (pp. 598–672). Lynx Edicions.

Ungar, P.S. 2010. Mammal Teeth: Origin, Evolution, and Diversity. Johns Hopkins University Press.

Ungar, P.S., & M'kirera, F. 2003. A solution to the worn tooth conundrum in primate functional anatomy. Proceedings of the National Academy of Sciences of the United States of America, 100: 3874–3877. doi: 10.1073/pnas.0637016100

Wainwright, P.C. 1994. Functional morphology as a tool in ecological research. In P. C. Wainwright & S. M. Reilly (Eds.), *Ecological morphology* (pp. 42–59). The University of Chicago Press.

Wei, T., Simko, V., Levy, M., Xie, Y., Jin, Y., & Zemla, J. 2017. Package 'corrplot'. Statistician, 56, e24.

Wickham, H. 2016. ggplot2: Elegant Graphics For Data Analysis. Springer-Verlag.

Wilson, G.P. 2013. Mammals across the K/Pg boundary in northeastern Montana, U.S.A.: dental morphology and body-size patterns reveal extinction selectivity and immigrant-fueled ecospace filling. Paleobiology, 39: 429–469. doi: 10.1666/12041

Winchester, J.M. 2016. MorphoTester: an open source application for morphological topographic analysis. PLoS ONE, 11, e0147649. doi: 10.1371/journal.pone.0147649

Winchester, J.M., Boyer, D.M., St. Clair, E.M., Gosselin-Ildari, A.D., Cooke, S.B., & Ledogar, J.A. 2014. Dental topography of platyrrhines and prosimians:

Convergence and contrasts. American Journal of Physical Anthropology, 153: 29–44. doi: 10.1002/ajpa.22398

Yamaoka, K. 1983. Feeding behaviour and dental morphology of algae scraping cichlids (Pisces: Teleosti) in Lake Tanganyika. African Study Monographs, 4: 77–89. doi: 10.14989/68000

3.10 SUPPORTING TABLES AND FIGURES FOR CHAPTER 3

Figure S3.1. Study locality at Parque Nacional Diriá, Guanacaste, Costa Rica. Pictures a to d represent different views of the Rio Enmedio. Red arrows in c and d indicate mist nets placed across water ponds of the river.

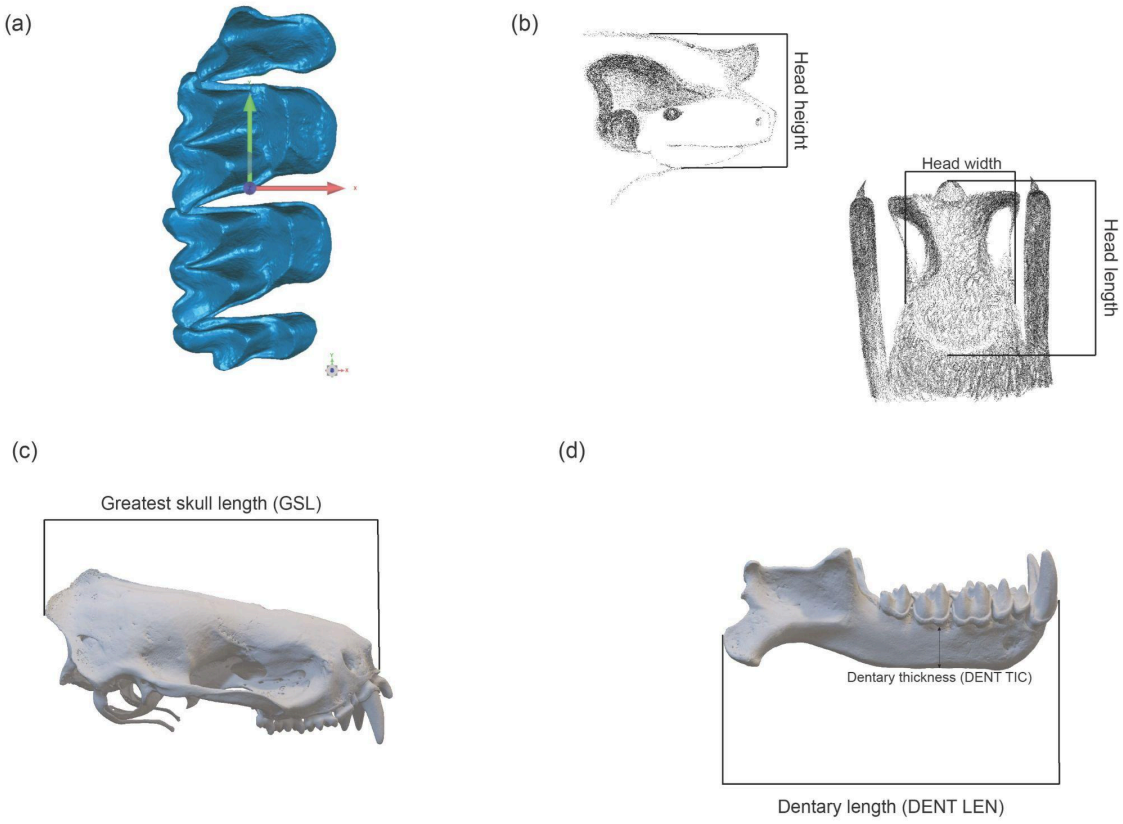

Figure S3.2. Orientation of the tooth crowns based on X, Y and Z axis (a); Head dimension measurements (b) and craniomandibular traits (c and d) across the sampled free-tailed bat species.

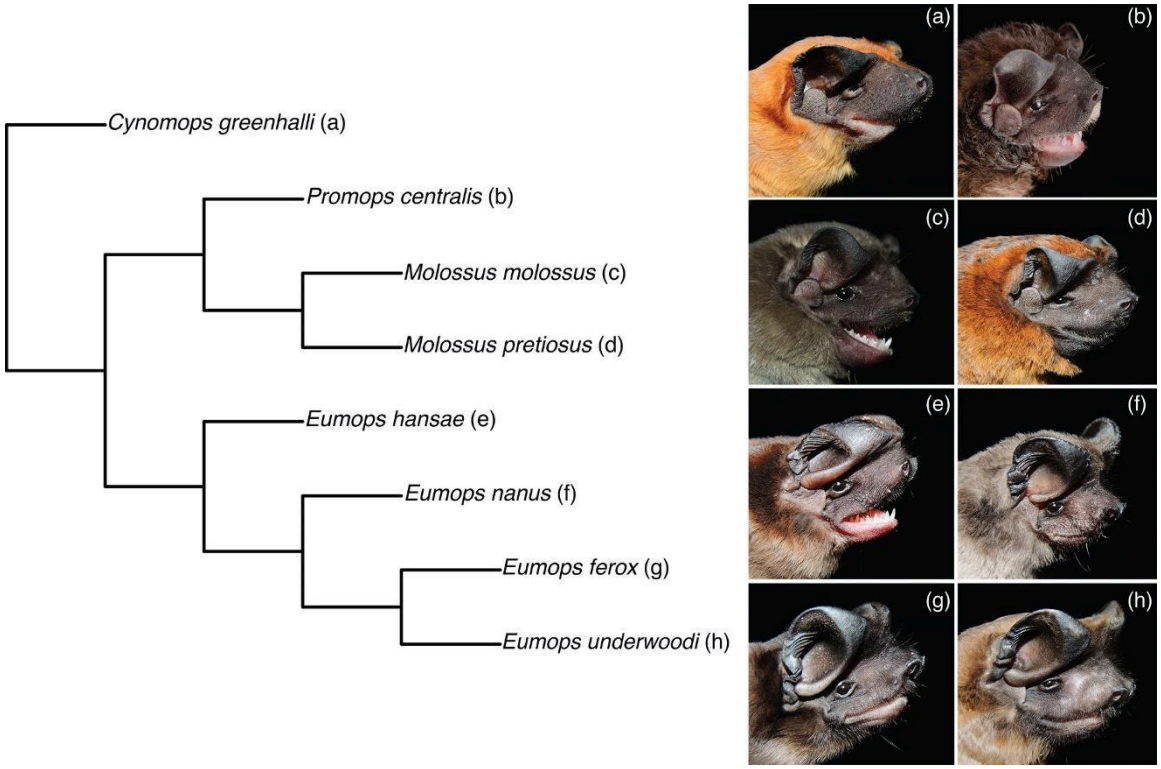

Figure S3.3. Tree showing the relationships among the free-tailed bat species included in this study (modified from Ammerman et al., (2012) and Bartlett et al., (2013)).

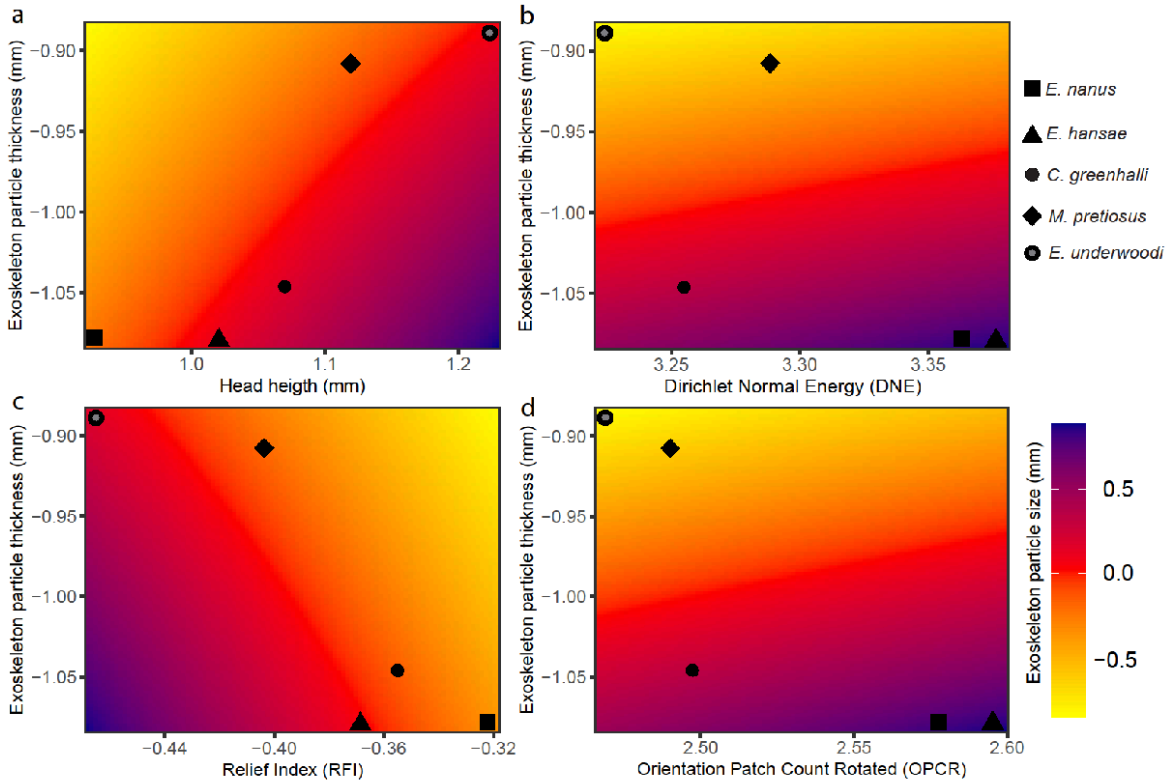

Figure S3.4. Graphical representation of the best fitting regressions models illustrating the interaction among exoskeleton particle thickness and size with head height (a), Dirichlet Normal Energy (b), Relief Index (c) and Orientation Patch Count Rotated (d) (predictive variables).

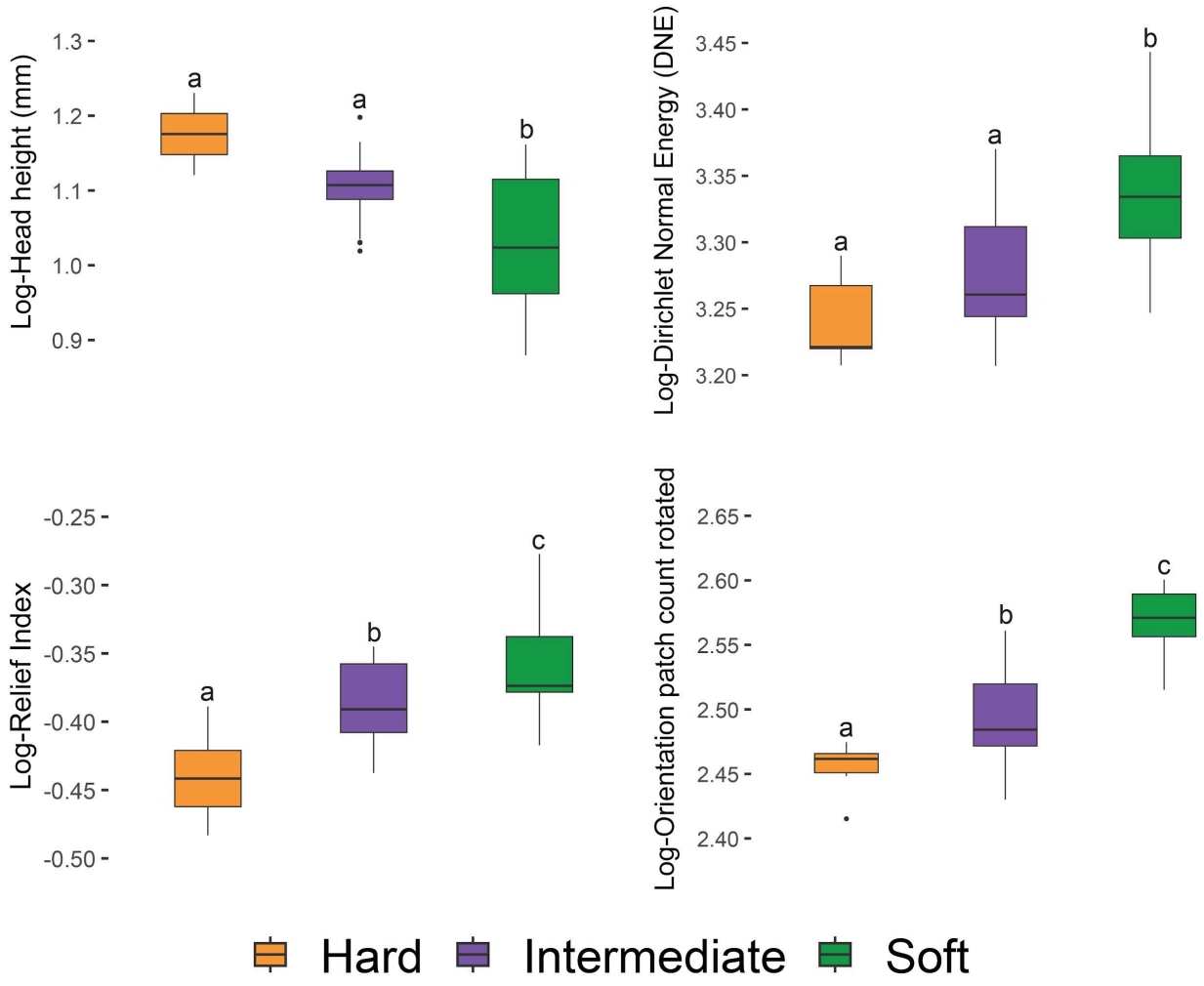

Figure S3.5. Patterns in head size and dental topography metrics among contrasting dietary hardness estimates. Different letters indicate significant variation of traits among hardness classifications.